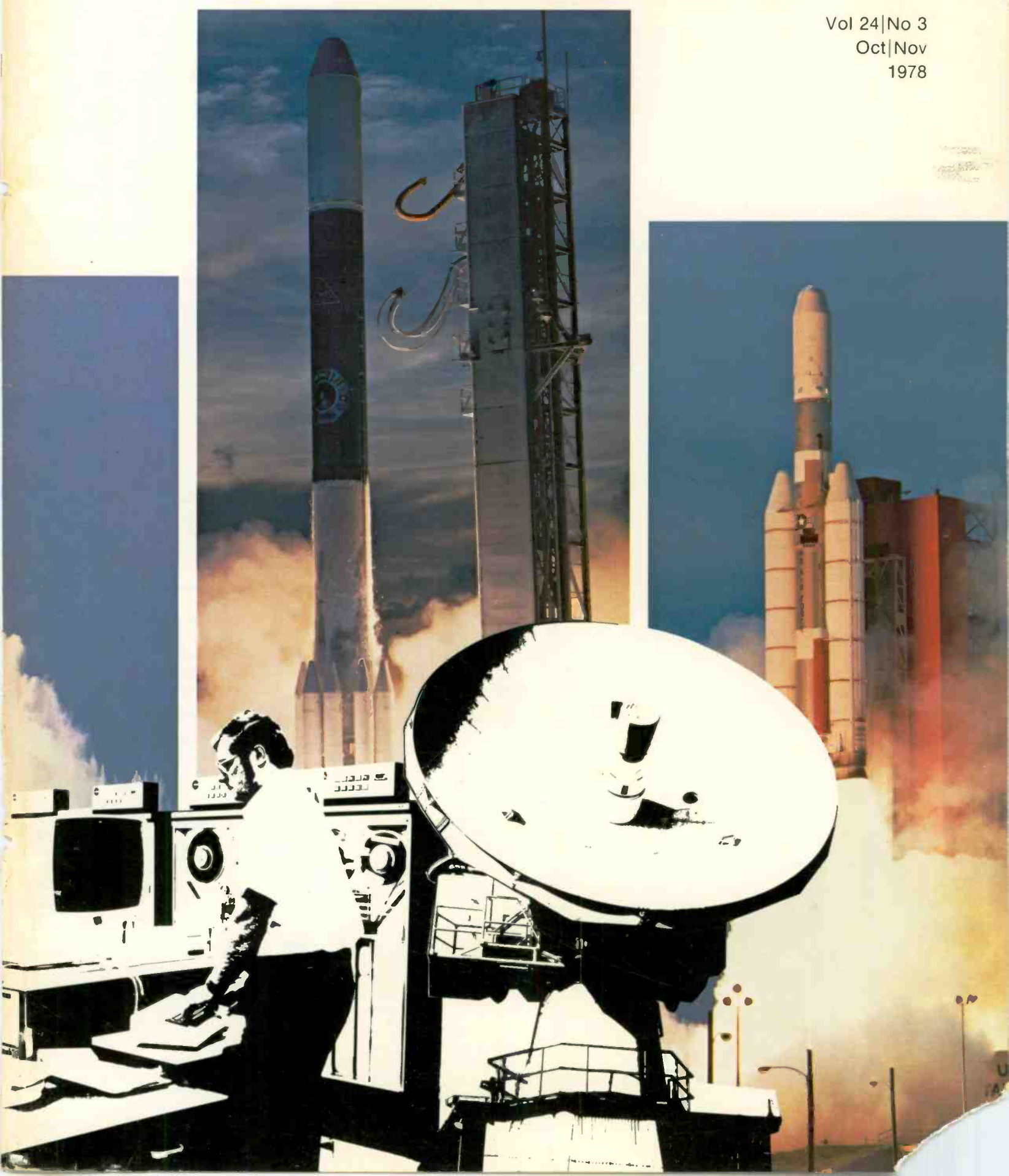


RCA Engineer

Vol 24|No 3
Oct|Nov
1978



RCA Engineer

A technical journal published by
RCA Research and Engineering
Bldg. 204-2
Cherry Hill, N.J. 08101
Tel. 222-4254 (609-338-4254)
Indexed annually in the Apr/May issue.

RCA Engineer Staff

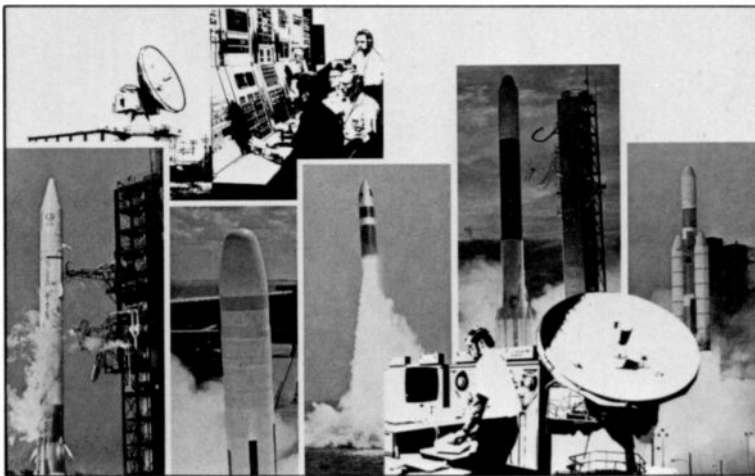
Mike Geverd	Editor
Bill Lauffer	Associate Editor
Joan Toothill	Art Editor
Frank Strobl	Contributing Editor
Betty Gutchigian	Composition
Dottie Snyder	Editorial Secretary

Editorial Advisory Board

Harry Anderson	Div. VP, Mfg. Operations, Consumer Electronics Div.
Jay Brandinger	Div. VP, Engineering, Consumer Electronics Div.
John Christopher	VP, Tech. Operations, RCA Americom
Bill Hartzell	Div. VP, Engineering, Picture Tube Division
Jim Hepburn	VP and Technical Director, RCA Globcom
Hans Jenny	Manager, Technical Information Programs
Arch Luther	Chief Engineer, Commercial Communications Systems Div.
Howie Rosenthal	Staff VP, Engineering
Carl Turner	Div. VP, Integrated Circuits, Solid State Division
Joe Volpe	Chief Engineer, Missile and Surface Radar
Bill Underwood	Director, Engineering Professional Programs
Bill Webster	VP, Laboratories

Consulting Editors

Ed Burke	Ldr., Presentation Services, Missile and Surface Radar
Walt Dennen	Mgr., News and Information, Solid State Division
Charlie Foster	Mgr., Scientific Publications, Laboratories
John Phillips	Mgr., Proposals and Publicity Automated Systems



Our cover shows launch action at the USAF Eastern Test Range and tracking by RCA's Missile Test Project. Starting on the back cover and moving left to right, the missiles are a NASA Atlas-Centaur, a Navy Trident, Poseidon, and Thor-Delta, and an Air Force Titan III. RCA is shown tracking these launches with an FPQ-6 radar and its control center at Patrick AFB, back cover, and a data-processing center at Cape Canaveral AFS and a TPQ-18 radar at Patrick AFB, front cover.

- To disseminate to RCA engineers technical information of professional value
- To publish in an appropriate manner important technical developments at RCA, and the role of the engineer
- To serve as a medium of interchange of technical information between various groups at RCA
- To create a community of engineering interest within the company by stressing the interrelated nature of all technical contributions
- To help publicize engineering achievements in a manner that will promote the interests and reputation of RCA in the engineering field
- To provide a convenient means by which the RCA engineer may review his professional work before associates and engineering management
- To announce outstanding and unusual achievements of RCA engineers in a manner most likely to enhance their prestige and professional status.

Missile Test Project— a quarter century of service and progress

This year the 1100 men and women of RCA Service Company's Government Services organization who are assigned at the Air Force Eastern Test Range mark completion of 25 consecutive years under contract there. In the highly competitive government support services industry, such longevity is rare and says much more than words can about the consistent quality of performance by the dedicated people of RCA through all those years.

At Eastern Test Range headquarters at Patrick Air Force Base, Cocoa Beach, Florida; at Cape Canaveral Air Force Station, 20 miles to the north; at downrange locations stretching from Grand Bahama Island to Ascension Island in the South Atlantic; and aboard missile tracking ships operating in the world's oceans, RCA Service Company managers, engineers, technicians, and support specialists have contributed to rapid and unprecedented technological developments leading to today's advanced state of the art in missile and spacecraft launching, tracking, and control.

Within RCA Service Company, our contract at the Eastern Test Range is known as the Missile Test Project. We have been associated with Pan American World Airways in this venture since the beginning in 1953, and the partnership has been fruitful and rewarding for both companies, as well as for the Air Force.

What of the people, the men and women of RCA who have invested many years of their working lives in our country's missile and space programs? In general, the work force at ETR has been stable; many employees have 20 or more years of RCA service. Individually, many RCA employees have significantly enhanced their careers, earned reputations for excellence, and received professional recognition, rewards, and opportunities for close and productive association with others in the vanguard of the aerospace industry. In addition, many engineering and management personnel have advanced from Missile Test Project assignments to positions of greater responsibility in other areas of Government Services, the Service Company, and RCA and, in fact, have contributed importantly to our ability to grow in a wide cross section of corporate technical endeavors.

The future offers further opportunity for individual and corporate growth as our national horizons in space are extended. For the present, the RCA team of professionals at the Eastern Test Range will continue to contribute to the success of the aerospace programs conducted there; they join me in welcoming readers of the *RCA Engineer* to an increased awareness of the Eastern Test Range and of RCA Service Company's key role in the fulfillment of the Department of Defense mission.



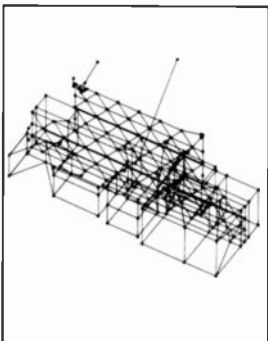
Joseph F. Murray
Division Vice President
Government Services
RCA Service Company
Cherry Hill, N.J.





RCA at the Missile Test Project

See how RCA can track missiles and satellites to within feet over thousands of miles of range.



solving the otherwise unsolvable

The finite-element method uses computers to solve structural problems that would take weeks by hand.

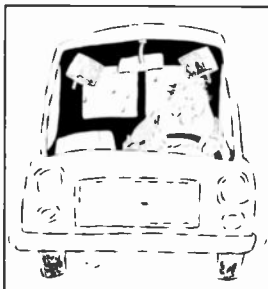
26



an environmental success story

An unusual "interview the fish" approach produced industry-government cooperation and cleaned up a formerly polluted stream.

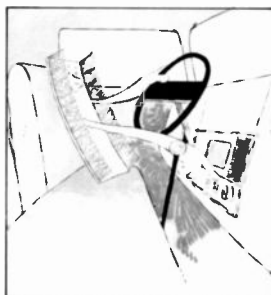
40



high-power auto stereo amp

The "phantom double bridge" puts sixty watts of stereo into your car or van. Build your own.

43



microprocessor-controlled radio

This am/fm auto radio has something extra—a COSMAC microprocessor tells time and displays and controls frequency.

52

coming up

Our next issue (Dec/Jan) centers around **manufacturing**. Following issues will cover **energy** (solar energy, fusion-power tubes, conservation) and the **color television receiver**.

RCA Engineer

Vol. 24|No. 3 Oct|Nov 1978

Missile Test Project

- | | | |
|--------------------------|----|---|
| T.E. Alman | 4 | RCA's Missile Test Project at the Eastern Test Range: an overview |
| J. Simpson | 6 | RCA's role in missile testing at the USAF's Eastern Test Range |
| M. Miller J. Burritt | 12 | Directing tracking instrumentation with microcomputers |
| C.P. Brooks E.L. Peghiny | 16 | Value Engineering applied to a large precision tracking mount |
| K.J. Martin | 22 | Using infrared signatures for PC-board failure analysis |
| J.J. O'Connor | 56 | Using pulse radar data to reconstruct missile reentry trajectories |
| C.W. Welch | 60 | Finding the best estimate of trajectory with the weighted least squares technique |
| D.L. Anderson | 63 | Identifying radar targets with automatic pattern recognition |
| M. Coomer R. Pepple | 66 | Digital filtering for radar antenna servo drives |

general interest articles

- | | | |
|--|----|--|
| A.W. Sheffler W.W. Metzger
G. Varadarajan | 26 | The finite-element method—a powerful tool for structural design |
| F. Sterzer | 34 | GaAs field effect transistors—versatile devices for microwave applications and gigabit logic |
| M.N. Slater | 40 | Conflict and cooperation: an environmental success story |
| L. Kaplan | 43 | The phantom double bridge—sixty watts of output in your auto or van |
| R.A. Geshner | 47 | The electron beam—a better way to make semiconductor masks |
| K. Karstad | 52 | A microprocessor-controlled am/fm automobile radio |

departments

- | | |
|----|---------------------|
| 72 | Dates and Deadlines |
| 73 | Pen and Podium |
| 74 | Patents |
| 76 | News and Highlights |



A launch from the Cape Canaveral Air Force Station of the Eastern Test Range.

RCA's Missile Test Project at the Eastern Test Range: an overview

T.E. Alman

Radars and electronic computer techniques at RCA's Missile Test Project keep pace with the increasing complexity of missile and rocket test requirements.

RCA's Missile Test Project (MTP) at the Air Force Eastern Test Range (ETR) has, since its inception in 1953, been involved in extensive engineering and data processing development. The professional staff consists of more than 250 engineers, physicists, and mathematicians. This staff plays a significant role in the increasing sophistication of range instrumentation and data processing techniques. In responding to ETR's changing requirements, unique capabilities have been emerging within the MTP staff, of a

type one would not expect to find in an operations and maintenance organization.

In supporting this first, major, long-range missile test facility, the RCA staff also has contributed to the development of standard techniques for operations and maintenance, as well as for management.

Tracking radars developed for military purposes in the 1940s were adapted to early missile flight testing, but were

relatively crude and barely able to satisfy accuracy and flexibility needs. This situation changed dramatically with RCA's development of high-precision instrumentation radars. These have become the standard systems at virtually all U.S. test ranges. The MTP participated in this evolution through the development of calibration techniques and the modernization of long-range trackers into computer-directed systems that resulted in the current accuracy capabilities of nearly 0.05 milliradians in angle and 10 ft in range. An ETR tracking station, built and operated by RCA, is shown in Fig. 1.

Electronic digital computers became available during the early stages of the ETR's existence. They have been an invaluable tool in processing the vast amount of data generated by missile tests and in the application of mathematical techniques otherwise too unwieldy for routine use.

The full capability of present day computers is utilized in trajectory regression and least-squares exercises; in complex real-time programs for range safety, tracking, and calibration purposes; and in numerous other large-scale programs employed at the ETR. For example, MTP people developed the complete mathematics and wrote the programs for the computation of "Best-Estimate-of-Trajectory", based on multi-tracker data input, from missile launch to impact. Almost all the other programs currently employed in real-time, near-real-time, and post-test

processing of data from land-based and shipborne sensors have resulted from the efforts of RCA personnel.

The research and development phases of today's sophisticated weapon systems are levying requirements on the test range that could not possibly have been met ten years ago. The tracking of multiple objects in space, determination of their spatial separation and independent trajectories, and detection of reentry phenomena by land or shipboard sensors demand that the tracking systems employed be controlled by computer, rather than human, command. As the testing phase continues, the accomplishment of various objectives requires that the associated software be constantly changed or updated.

The amount of data now collected and relayed during one missile flight is equivalent to that acquired during several launches in years past. The increased capability and productivity provide an attractive cost tradeoff for potential Range users. The technological "leap frogging" of requirements versus testing capabilities will undoubtedly continue as long as weapon system testing is conducted at the Eastern Test Range.

A more detailed discussion of the overall RCA mission at ETR may be found in the following article.

Reprint RE-24-3-16
Manuscript received August 7, 1978.



Fig. 1
The Grand Bahama Island tracking station of the Eastern Test Range, showing the radar and telemetry tracking antennas.



Tom Alman joined RCA's Missile Test Project in 1962 as a computer programmer. He then held several management positions including Manager, In-flight Analysis and Programming; Manager, Real-time Computer System; Manager, Data Processing; and Manager, Data Acquisition and Processing. In October, 1977, he was appointed Project Manager of the Missile Test Project.

Contact him at:
Missile Test Project
RCA Service Company
Patrick AFB, FL 32925
Phone: (305) 494-7624

RCA's role in missile testing at the USAF's Eastern Test Range

J. Simpson

What's involved in monitoring missiles and space-launch vehicles to within feet over thousands of miles of flight—planning, tracking, telemetry, communications, software, and support.

Since 1950, the Air Force Eastern Test Range (ETR) has been America's primary test facility for missile and space systems. The Range constitutes a vast laboratory for the Air Force Systems Command. Facilities in Florida include Patrick Air Force Base, where Headquarters is located, and Cape Canaveral Air Force Station, 15 miles to the north. The Range extends more than 10,000 miles across downrange stations in the Atlantic and into the Indian Ocean. A map of the ETR is shown in Fig. 1.

What is RCA's mission at MTP?

As the subcontractor for operation and maintenance of the ETR instrumentation systems, RCA monitors trajectories of ballistic missiles and space vehicles launched from the range.

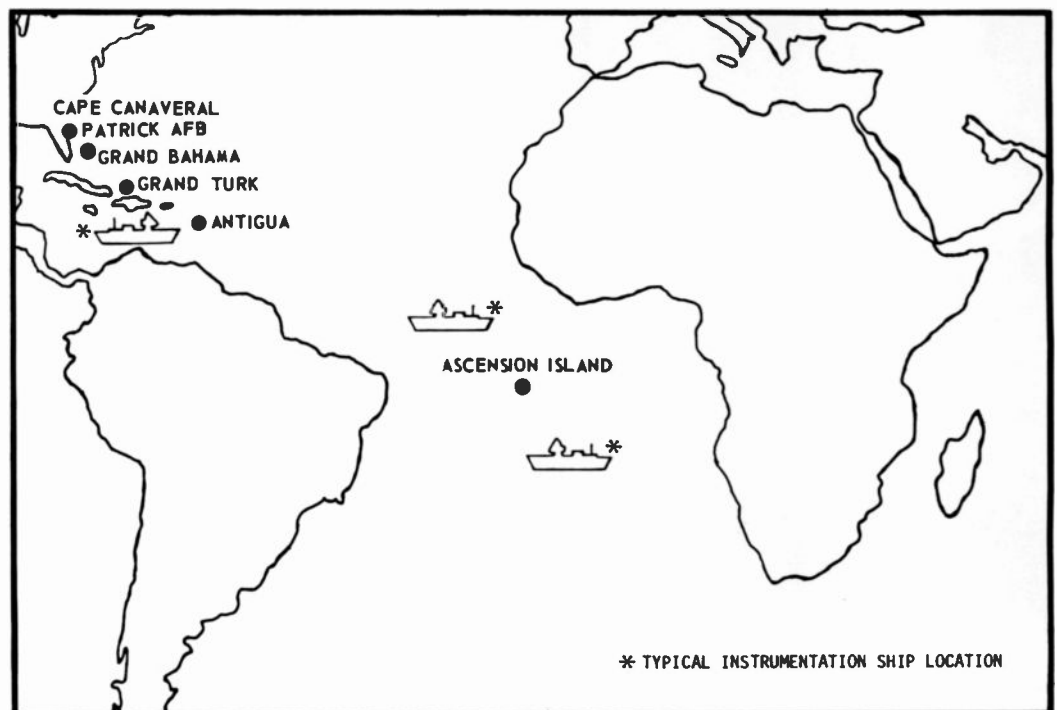
To accomplish its mission, ETR has a military-civilian workforce of over 7,000. A significant number of these are employees of the Range's prime contractor, Pan American World Airways, and its principal subcontractor, RCA Service Company. In 1953 the Air Force contracted the majority of the operative functions of Range facilities to Pan Am, who in turn, subcontracted the technical

functions of operating and maintaining the Range instrumentation systems to RCA. These include missile flight data processing, tracking instrumentation, and communications links between the islands and the mainland launch sites.

Tests in this immense laboratory are conducted under the most exacting conditions. Missile performance is monitored by a variety of instruments so located that the parameters of powered flight can be pinpointed and evaluated during the missile's entire flight. Radar, optical, and continuous-wave tracking devices follow the launch vehicle precisely as it streaks across the sky. Telemetry equipment receives and records vital information from the heart of the missile systems.

Data amassed during a test is reported to the Range user. Through skillful use of this complex of data gathering instrumentation, space and missile systems are perfected in a minimum number of flights. Engineers are able to analyze data to determine what happened, why, and when; they use these facts as a basis for further refinement of the testing procedures or for modifications to the vehicle systems.

Fig. 1
The Air Force Eastern Test Range extends from Florida to the Indian Ocean. Downrange tracking and data gathering sites are located at Grand Bahama, Grand Turk, Antigua, and Ascension Islands. Instrumentation ships and aircraft supplement the land stations.



In addition to the Air Force, the Army, Navy, NASA, foreign nations, and other government agencies use the Range, each relying on the support services of the ETR in their missile and space exploration projects.

Since the advent of the national space program in 1958, Cape Canaveral has been used by NASA as a launch site for space vehicles. Sixteen manned space missions were conducted during the Mercury and Gemini programs. Spacecraft have also been launched toward the moon and other planets from the Cape. Various communications, geophysical, and weather satellites have been orbited. Fifteen Saturn vehicles, some manned, were launched from Complexes 34 and 37: NASA's two Saturn sites at the Cape Canaveral Air Force Station (AFS).

NASA operations moved to the adjacent Kennedy Space Center for the launches of the Saturn V rocket, which was used in the Apollo 11 and subsequent lunar landing missions, and Saturns V and IB in the Skylab and Apollo-Soyuz programs.

Continuation of the manned space program awaits the Space Shuttle. In the meantime, NASA's unmanned launch operations boast an active schedule of launches from Cape Canaveral AFS for customers such as the European and Japanese Space Agencies, and communications/industry users including RCA, Western Union, and ComSat Corporation.

Cape Canaveral AFS covers a 25-square-mile area. It lies between the Atlantic Ocean to the east and the Banana River to the west; this provides a security and safety buffer on both sides of the launch area. Within its boundaries are located complete assembly and launch facilities for ballistic missiles and space launch vehicles, as well as storage and dispersing stations for fuels and oxidizers. It also has a landing strip, which permits the airlift of launch vehicles directly from the manufacturer to the Cape.

Along the southern edge of the Cape is a deep-water port and turning basin, where Range tracking ships and Navy ships and submarines used in the Polaris, Poseidon, and Trident programs are serviced.

The nerve center for this space-age installation and for the entire ETR is the Range Control Center located at Cape Canaveral AFS, from which all launches as well as the status of the Range are monitored. Another vital function performed in the Range Control Center is the Range Safety operation. A computer-driven display console is manned during all launch operations by an Air Force Range Safety Officer (RSO).

The range is changed from the early days of space.

In October 1977, RCA Service Company received a \$26 million subcontract from Pan American World Airways for continued technical services at the Eastern Test Range. Approximately 1100 RCA Service Company people in RCA's Missile Test Project organization now provide highly technical services at Patrick Air Force Base, Cape Canaveral, and all ETR downrange islands; and aboard three instrumented tracking ships, located in the Atlantic and Pacific Oceans. One of these vessels is shown in Fig. 2.

Considerably more people were involved in this effort during the early 1960s when the research and development phase of such vehicles as Thor, Atlas, Pershing, Minuteman, Polaris, Titan, and



Fig. 2
The U.S. Navy's General Hoyt S. Vandenberg, one of the three tracking ships assigned to the Eastern Test Range. RCA technicians operate and maintain its instrumentation and communication equipment.

early manned flights was in progress. The trend in recent years has resulted in fewer, but more complex, research and development operations plus a steady series of commercial and scientific unmanned satellite launches. The capabilities of the Range have also been used in non-launch operations involving drones, balloons, etc. The Aerospace Defense Command now routinely uses ETR tracking radars in its mission.

The ETR instrumentation and communications systems have been improved and modernized in the 1970s, leading to the acquisition, transmission, and processing of highly accurate, high-speed data. Since much of the Range equipment now employs solid-state devices, maintenance requirements have been significantly reduced.

Operations planning and documentation

Both U.S. and foreign agencies may use the ETR. A Universal Documentation System has been developed to specify the Range capabilities, the User requirements, and a relevant operations plan.

The many agencies which desire to use the facilities and services of the Eastern Test Range initially need some general information regarding the capabilities of the Range. The using agency must also express its requirements to the Range in a mutually understandable way. Thus, a documentation system allowing the exchange, in a standard format and terminology of technical information between the user and the Range, is necessary.

Several years ago, as the number and diversity of potential Range users increased, the Range Commanders Council's Documentation Group developed the Universal Documentation System, which is currently in use at the Eastern Test Range. The usual flow and sequence of the documentation exchange is as follows:

The Range user formally submits his general requirements, to which ETR responds with a statement of capabilities. The user

then submits a detailed listing of test requirements, to which ETR responds with a formal verification of feasibility and a plan for the test series. About two months before the first scheduled launch or test of the user's vehicle or system, the user documents in detail each test and his specific support and data requirements. The Range finally prepares an Operations Directive, which is a complete detailed operations plan to mobilize Range support through coordination of equipment, people, and services.

The ETR Range Safety Officer also generates his requirements for each launch or test, specifying the type of information which must be displayed to show the actual missile flight and performance against that planned. These requirements will vary depending on the missile characteristics, such as fuel type, expected flight path, velocities, and duration of powered flight.

RCA's Instrumentation Planning and Control section of the Missile Test Project analyzes the Range user's and Range Safety requirements; prepares the instrumentation, communications and data-processing sections of the program plan; the Operations Directive; and last-minute test teletype instructions. This group also provides the focal point of control for all systems throughout the Range operated by RCA during test countdown and data-gathering periods.

Tracking and measurement systems

A variety of sensors are coordinated to track, control, and measure the parameters of ballistic missile and space launch vehicle flight, as well as ship-position data for vessels engaged in related operations.

The flight of ballistic missiles or space vehicles launched at the ETR up to their subsequent impact or entry into orbit is tracked, controlled, and measured by technologies such as radar, telemetry, television, optics, command control systems, and missile impact-location systems (the last consisting of underwater sensors).

In addition, LORAC (long range accuracy) systems provide ship-position data for those vessels actually launching missiles (such as Poseidon- or Polaris-carrying submarines) or those engaged in the ocean recovery of spent or destroyed missile components.

Most of the radars in use at ETR are AN/FPS-16, AN/FPQ-13 and -14 types. These were designed and installed by the Missile and Surface Radar unit of RCA's Government Systems Division. Significant modifications have been made to ETR radars, so that the seven radars forming the primary tracking chain are now "on-axis" type, using computer drive techniques to provide smooth, highly accurate output data in a standard, earth-fixed geodetic format. An AN/FPQ-14 radar, located at Patrick AFB, is shown in Fig. 3.

In addition to their use for launch support at ETR, RCA operates two radar systems for the U.S. Air Force around the clock, seven days a week, tracking orbital objects for the North American Air Defense Command (NORAD).

Remote-control and high-power command transmitter systems are located at Cape Canaveral AFS, Grand Bahama Island, and Antigua Island, providing the Range Safety Officer with the



Fig. 3
The FPQ-14, C-band tracking radar at Patrick AFB was built by RCA. It is now operated by Service Company personnel.

capability of automatically or manually sending "arm" or "deconstruct" functions to the vehicle during its powered flight. These systems can also be used to control airborne drones.

Telemetry systems are located along the Range, on land and sea and in the air, from Florida to South Africa.

ETR's telemetry system is operated and maintained by RCA technicians. This is a large, multipurpose, data-acquisition network, specifically constructed and uniquely modified to provide missile and satellite performance data for Range users and ETR Range Safety. Telemetry systems are incorporated at six Range sites, extending from Florida to South Africa. During launch operations these systems are augmented by specially equipped aircraft and ships to provide data coverage beyond the view of the land-based sensors. A mobile telemetry van also provides coverage for special test applications. When interfaced with communications links, such as submarine cables, satellites, and HF radio circuits, the telemetry system provides an extensive means of reliably relaying flight-test data throughout the world in real time and near-real time. These flight test data are received, recorded, demultiplexed, and retransmitted for Range users and ETR functions.

Telemetry tracking antennas operate principally at S-band* frequencies; they incorporate parabolic dishes of various sizes (30, 33, 60, 80, and 85 ft in diameter). The telemetry antennas at Antigua Island are shown in Fig. 4. Processing and display functions are performed using data-formatter and data-corrector (computer) systems to produce computer-compatible tapes and various data products. Pen recorders, photo-oscillographs, and digital display units provide quick-look and post-flight data display capabilities. An oscillogram processor capable of processing recordings at 200 ft/min is also installed at Telemetry Central, located near Cape Canaveral, at the northern end of the ETR.

ETR has an extensive television, video transmission, and recording capability, with fixed TV cameras and monitors located

* S-band: 1.55-5.20 GHz



Fig. 4
Two telemetry tracking antennas, located on Antigua Island, on the Eastern Test Range. The reflector of the foreground antenna is 80 feet in diameter; that in the background is 30 feet.

in all launch areas, pads, and gantries. Mobile systems are available for Range Safety surveillance.

The ETR Missile Impact Location System (MILS) provides precise impact-location data for Range user missile programs. Three MILS Target Arrays are now in use: one in the Antigua Island area, one in the Grand Turk Island area, and one near Ascension Island. Each Target Array comprises six hydrophones located on the ocean floor. One hydrophone is positioned near the center of the array, and the other five form a pentagon around it. The hydrophones are connected to a ground station by submarine cable, over which data is transmitted to the Data Processing Facility at Patrick AFB.

Operation of the MILS System is shared by the U.S. Air Force and Navy. RCA, at the direction of the Air Force, operates the MILS Laboratory at Patrick AFB and the receiving/recording station at Ascension Island.

Two LORAC systems are installed, one in the Cape Canaveral area, the other in the Bahama Island complex. These provide position information for both ships and aircraft operating in support of ETR tests. Within the normal coverage area, position accuracy can be obtained to within 30 ft. The systems are generally operated remotely and unmanned. Periodic scheduled maintenance is performed by RCA technicians.

Data-processing systems

A wide-spread computer network manages the flow and processing of data.

The ETR computer hardware network is made up of 77 computers, consisting of 17 models from 10 manufacturers. These computers are located on the Florida mainland, at downrange instrumentation sites, and on-board Range Instrumentation Ships. There are two major computer facilities on the Florida mainland. One, at Patrick AFB, is operated primarily for post-test analysis of launch test data. The other, at Cape Canaveral

AFS, is designated the Central Computer System and is operated primarily to meet real-time requirements.

The Central Computer System provides a central point for data flow during test operations on the Range. The primary task of this system is to provide accurate trajectory-display data to the Range Safety Officer during the "powered flight" portion of missile or space-vehicle flight. A secondary task is to provide target-acquisition data to the Range tracking systems. Rapid target acquisition is vital in maintaining continuous and accurate data for the Range Safety Officer. Computers on the land-based tracking systems and range ships can communicate with the Central Computer System; their software allows them to operate as part of the Range network or in a stand-alone mode.

The best available tracking source for trajectory display or for target acquisition by other trackers is obtained by means of the source selection logic in the software of the Central Computer System. In addition, this system produces "quick-look" impact predictions, and refined computations for near-earth and deep-space orbital missions.

The computer facility at Patrick AFB is operated to process business and scientific data, including prelaunch processing of data such as theoretical trajectories, instrumentation "look angles", and range safety parameters. Meteorological data are also processed during test operations.

Post-launch processing involves editing, correcting and refining the raw data acquired by the various Range instrumentation systems, combining data from multiple sources to compute estimates of vehicle performance, the actual trajectory flown, and other related parameters—all information necessary in the production of a Flight Test Report.

RCA's Missile Test Project people operate all computers in use at the ETR and also develop, maintain, and modify the software required for these computers. A major modification and modernization program of the ETR Central Computer System now underway is scheduled for completion by the summer of 1979.

Communications network

The communications network, which accommodates both high-speed data and speech, is the largest of its type in the world. It is considered a major resource of the Department of Defense.

The ETR Communications Network System ranges in complexity from the relatively simple, single-line administrative telephone systems to systems that transmit high-speed, multiplexed, encrypted data signals over submarine cable; error-corrected, single-sideband HF radio; and satellite communications.

The communications network interconnects the ETR with external agencies, such as the Western Test Range, Satellite Control Facility, Goddard Space Flight Center, Kennedy Space Center, Aerospace Defense Command, COMSAT, British Cable and Wireless, the American Telephone and Telegraph Company, and the Bahamian Telephone Company.

The network also provides a versatile interconnecting medium among all the ETR instrumentation systems and sites, including

instrumented ships and aircraft. For example, 393 kb/s telemetry data is transmitted over land lines and submarine cable from the Telemetry Site at Grand Bahama Island to the Telemetry Central Building in Florida.

An extensive and switchable distribution system exists for 2400-b/s encrypted acquisition data to, from, and between all the radar and telemetry trackers at all ETR locations and the Central Computer System at Cape Canaveral. This distribution uses a variety of land lines, submarine cable, and satellite channels.

Many external agencies use the communications network to support activities not related to the ETR mission. Among these are the Federal Aviation Administration, the U.S. State Department, U.S. Navy and Air Force (for ships and aircraft operating in

the southern regions of the Atlantic and Indian Oceans and Africa), and various research and special-mission agencies.

Engineering and shop services

RCA provides engineering, drafting, and shop services for system design and modification, and for operational support beyond on-site capability.

RCA's engineering functions at ETR include the supporting elements of drafting and technical shops. In conjunction with Pan Am, they supply the Air Force with services to modify existing systems, acquire new systems, and integrate new or modified systems into the Range instrumentation complex. They also assist RCA's operating units by providing skills and shop support beyond on-site capability.

At RCA's MTP, we knew COSMOS 954 before it died

The recent reentry and earth impact of a Soviet nuclear-powered spacecraft in Canada may have been exciting, even frightening, news to many Americans, but several RCA employees concerned with "Spacetrack" operations expected the event. Spacetrack is the code word at RCA Service Company's Missile Test Project (MTP) at Patrick AFB, Florida, for the tracking of orbiting satellites and space objects. Although the MTP is primarily concerned with tracking missiles and space vehicles launched for various agencies from Cape Canaveral, some of the associated radars perform this valuable space tracking service for the North American Air Defense Command (NORAD). Radars located at Antigua and Ascension Islands are used for this service on a seven-day week, twenty-four hours a day basis.

As a result of many U.S. and foreign space launches since Sputnik I in 1957, there are thousands of objects circling the earth in different orbits, inclinations, and periods. It is the responsibility of NORAD to maintain current status and to "catalog" each of the objects, whether they are active operational satellites, spent propulsion vehicles, or "space junk" (various types of non-operational objects). NORAD must also determine if and when these objects will reenter the earth's atmosphere, and if they will present a danger to the North American continent. The RCA-operated radars on the Eastern Test Range form a part of a world-wide tracking system that transmits position, size, and shape data to NORAD's operation headquarters for each orbital object they request. High-priority tasks include the detection and tracking of new foreign launches in order to furnish NORAD with an early assessment of the mission of the newly launched satellite.

RCA analysts use advanced techniques to determine the object's size, shape, dynamics, and other valuable information by analysis of the radar signal return. Particular emphasis is given to those objects that exhibit signs of orbital decay. Computers predict the location of probable earth impact, if no "burn up" in the

atmosphere occurs (the most frequent circumstance), and continuously update these predictions based on more current tracking data.

When a satellite contains nuclear material, the controlling agency usually, upon mission completion, propels it into a much larger orbit, so that it may take hundreds of years to reenter the atmosphere. By that time, the payload radioactivity will have reached a safer level. Apparently the procedure was unsuccessful with Soviet Satellite COSMOS 954.

The launch of this satellite had been detected in September 1977. The RCA operators at the Antigua and Ascension Island radars continued to track the spacecraft, transmitting data to NORAD. By November the tracking data revealed an unusual behavior of the satellite that indicated a possible loss of control. NORAD requested more frequent tracks and an increased amount of data. In January 1978, RCA specialists at Antigua and Ascension, as well as other NORAD locations, observed a change in the satellite's orbital dynamics that threatened a dangerous situation upon reentry. NORAD then requested other Eastern Test Range radars operated by RCA, located in Florida and Grand Turk Islands, to track and provide data for computed reentry predictions.

As a result of this extraordinary effort, NORAD was able to accurately predict the time and location of the impact of COSMOS 954 in northern Canada. For their contribution, RCA's MTP radar operators and analysts shared in the receipt of a special message of congratulations transmitted by the Commander of NORAD's Space Detection and Tracking System.

In addition to the NORAD recognition, General George Brown, USAF Chairman Joint Chiefs of Staff, expressed his appreciation for a professional job well done.

To secure the benefits of increased reliability, maintainability, flexibility, and capability, every effort is made to employ and advance the state-of-the-art technology in addressing systems engineering tasks (for example, by the use of microprocessors, minicomputers, and integrated circuits).

RCA's Missile Test Project also provides the shop services required to support engineering tasks. Electronic and sheet-metal technicians, along with machinists, provide fabrication, modification, installation, repair, and field support of electronic systems, components, parts, and mechanical assemblies. RCA's drafting section develops design and modification packages, including machine and sheet-metal drafting, as well as printed-circuit design. Technical artists prepare the illustrations needed for technical reports and briefings required by ETR management.

Technical analysis

RCA defines and evaluates the accuracy of the Range instrumentation systems.

The Technical Analysis function also includes the responsibility to improve techniques, so that required accuracies can be achieved, and to ensure that the desired accuracy status is maintained. Inherent in these tasks (being a prerequisite for achieving tight instrumentation accuracy control) are system calibration, performance analysis, and system capability evaluation.

Calibration, an integral part of system accuracy and performance, serves two primary purposes. First, it is used to build a data base from which system accuracy can be evaluated. Second, performance analysis provides a quality-control function for determining operational performance for use by RCA, the Air Force, and Range users.

System performance and data quality analysis are accomplished on a "test-by-test" basis. As a result, these data provide a cumulative performance base for each instrumentation system and serve as an important source of information for other ETR activities. For example, this analytical effort provides statistical data on operational and accuracy capabilities for test-support planning and also data on system performance trends to be used by engineering and maintenance activities.

Maintenance

RCA's maintenance management function at the ETR assures that techniques and resources are made available as needed to support site maintenance personnel.

Maintenance is provided at three levels. The first level consists of preventive and corrective maintenance performed on-site by site technicians. The second level is that partially done on-site and partially in the shops (Repair and Return) at Patrick AFB. The third level is depot overhaul, again done partially on-site and partially in the shops, but using shop skills and tools.

First-level preventive maintenance is scheduled monthly from a computerized data base. Second- and third-level maintenance is provided by maintenance engineers and technicians scheduled for that purpose.

A major overhaul program, referred to as IRAN (inspect and repair as necessary), is conducted on a scheduled basis. RCA

maintenance engineers schedule system downtime and use shop and site technicians to inspect systems for major repair needs. Tools and parts permitting, the repairs are done at the time of inspection. Those equipments requiring added parts, time, tools, and skills are scheduled for later repair. The engineer then procures all parts and coordinates all supporting organizations and equipment for overhaul. The maintenance management organization also has a training function. This both trains RCA's operating people on new equipment and trains new employees on the complex hardware found on the ETR. Training on a new subject is initially done in the classroom, where it is simultaneously video taped. The video tapes are later edited and distributed to all stations and ships for local playback and training sessions. Instructors also conduct correspondence courses with RCA technicians and engineers located throughout the ETR.

A vast amount of test equipment is in use at the Eastern Test Range. The Air Force provides laboratory facilities for the repair, calibration, and certification of both physical and electronic test equipment using base reference standards. RCA's MTP organization manages and operates the Precision Measurement Equipment Laboratory (electronic) for the Air Force at Patrick AFB, and provides calibration teams who travel to downrange and shipboard locations. Since 1972, an average of 21,000 service operations annually are performed for users of test equipment at the ETR.

Reprint RE-24-3-2
Final manuscript received June 22, 1978.



Jack Simpson joined RCA Service Company Consumer Services in 1948 and transferred to the Missile Test Project in 1958. Since then he has held various operational management positions in that organization. He currently is Manager, Instrumentation Planning and Control, and is responsible for the analysis and documentation for Range User requirements as well as the planning and control of systems operated by RCA during launch countdown and tracking operations.

Contact him at:
Instrumentation Planning and Control
Missile Test Project
RCA Service Co.
Patrick AFB, FL 32925
Phone: (305) 853-3222

Directing tracking instrumentation with microcomputers

M. Miller|J. Burritt

Remote computer-controlled steering for cinetheodolites and other systems has always been desirable, but the microcomputer's small size and cost have made it practical.

Many instrumentation systems used on the Air Force's Eastern Test Range to gather data during past missile launches could have performed better if they had been computer controlled. Computer systems until recently have been too large physical-

ly and too expensive to be used for many such applications. A microcomputer's small size and cost now make it practical to provide computer control where it was previously impractical.

Microcomputers have changed the hardware-software tradeoff picture. Their small size and relatively small cost make them an ideal peripheral interface, with the additional flexibility of control by "firmware" (programs stored in read only memories).

Overview of applications

One basic microcomputer design can be applied to remote control of steerable systems, such as radar, telemetry, and optics.

A number of steerable systems that gather and transmit data pertaining to missile performance are currently being modified at the Air Force Eastern Test Range (ETR) so that they can be pointed at missiles by remote control. Included are radar, telemetry, and optics systems. The flexibility of the microprocessor, and the microcomputer designed around it, permits accommodation of these diverse systems with one basic design, requiring only minor hardware differences between systems. Much of the software is the same for different systems. One application is described here: the Contraves Cinetheodolite System, shown in Fig. 1.

The Contraves Cinetheodolite System is used to take pictures of a target. The film also records time of day, azimuth, and elevation of the mount. These data from several systems, when reduced and processed by a computer, provide the target's position in space and time throughout the target's trajectory.

Before the incorporation of microcomputers, steering was manually controlled using a joystick which, in turn, controlled motors that pointed the optics at the target. It often was difficult for the system operator to maintain track on a

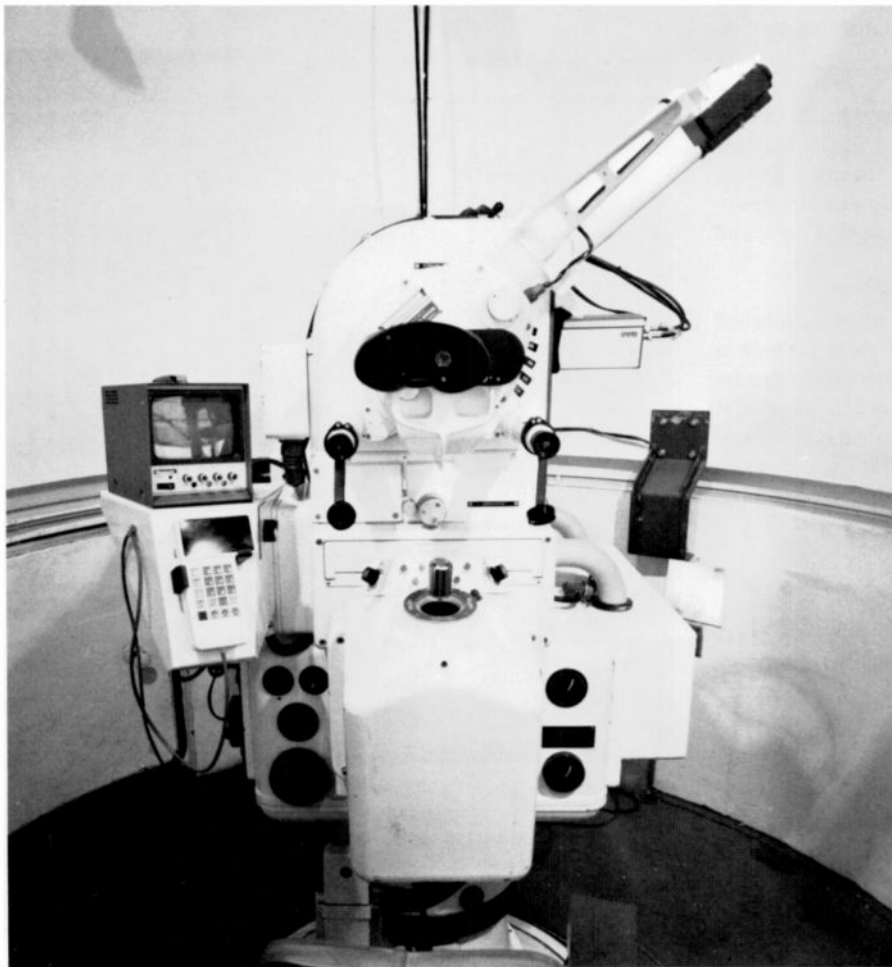


Fig. 1
A modified Contraves Cinetheodolite station. The hand-held terminal (hanging below the tv monitor) selects computer displays and controls. The tv monitor and a tv camera also have been added. The joystick (front center) formerly was the only control but now is used for backup and assist.

target, because he had to view the target in a low-power sighting telescope. When the target was far away, the image in the sighting scope was quite small. Cloudy or hazy skies also impeded the visual observation of targets and made target acquisition difficult. Targets, even when they could be seen well, were difficult to track at high angular rates.

The addition of microcomputers to the system allows it to be pointed at a target by digital electronic control. A remote radar or other instrumentation system which tracks the target can be used as the source. The Contraves system can also be pointed using stored theoretical data that defines the trajectory for which the target has been programmed. Anomalies of the Contraves system are stored in the microcomputer's memory, and the computer program provides correction for the mount's position, such that the target stays centered in the main objective telescope of the system.

A block diagram of the modified Contraves system, Fig. 2, shows the microprocessors, their inputs and outputs. The Digital Equipment Corporation's (DEC) LSI-11/03 Microcomputer, the RCA 6800

Intelligent Data System (IDS)—also a microcomputer—, and the Central Computer are discussed under separate topics in the following paragraphs.

The LSI-11/03 microcomputer

The microcomputer design provides computation, data handling, and system control capabilities.

The LSI-11/03 Microcomputer provides the system with a computational capability and the 6800 IDS provides data handling and system control. Inputs to the microcomputer system include:

- 1) An EFG vector message, which provides the time and the associated position and velocity components of the target in an earth-centered, earth-fixed system.
- 2) IRIG B timing, which provides the accurate time of day.
- 3) Azimuth and elevation encoder inputs, which provide the cinetheodolite mount position.

- 4) A hand-held terminal, mounted near the operator, which accepts operator control inputs and provides system performance displays.

Outputs from the microcomputer system go through digital-to-analog converters to drive azimuth-, elevation-, and focus-control motors.

The LSI-11/03 Microcomputer performs the math computations for the system. It has a computing power exceeding that of many minicomputers. It runs the DEC PDP11-35 software and includes a repertoire of over 400 instructions. It performs floating point math with 24-bit mantissa and 8-bit exponent. The program can be stored in read-only memory, which allows the system to come up running when power is applied. An operator with no computer experience can operate the system.

The LSI-11/03 Program computes a drive vector as follows:

The target vector is updated to the current time. The vector referenced to the center of the earth is converted to a rectangular topocentric vector in the plane of the instrument. Between times that the input vector is received, the vector is extrapolated (i.e., updated). The rectangular topocentric vector is then transformed to radar coordinates A, E, R; A, E, R; A, E, R (azimuth, elevation, range, and the corresponding velocities and accelerations). The A, E, R is interpolated between points and mount corrections are added. These corrections include: azimuth bias, elevation bias, skew, droop, mislevel, non-orthogonality, and refraction. The computed and corrected azimuth and elevation positions are differenced with the encoders to determine in which direction the mount should move. Servo K_v and K_a pushes are added, depending on the velocity and acceleration required of the mount. This azimuth and elevation drive is then output through digital-to-analog converters to drive azimuth, elevation, and focus in type-1 or type-2 servo systems as appropriate.

The RCA 6800 Intelligent Data System

The 6800 IDS, based on the Motorola 6800 microprocessor, provides the steerable system control.

A block diagram of the 6800 IDS is shown in Fig. 3. RCA participated in its design and fabrication at the Air Force's Eastern Test

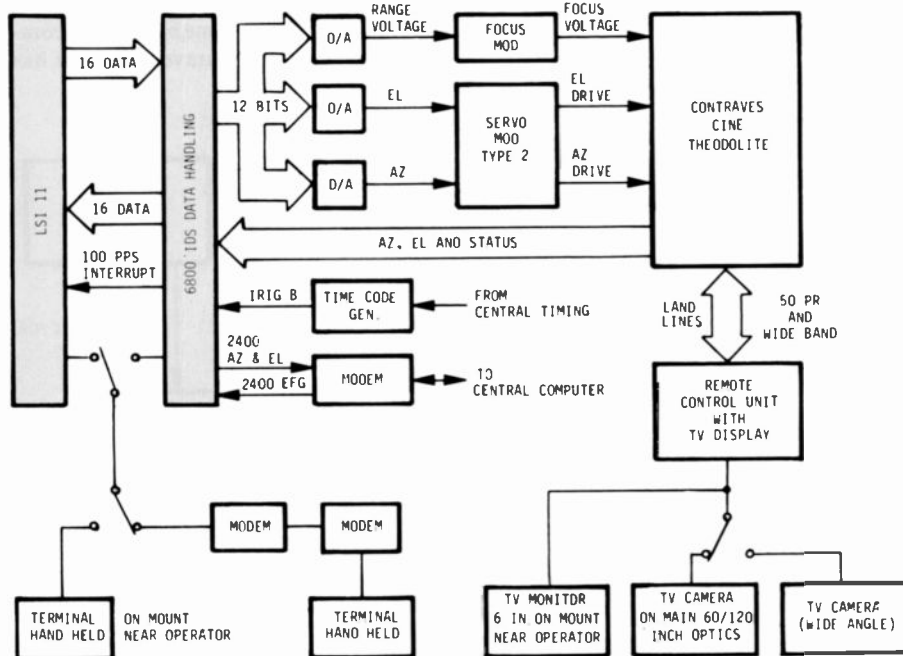


Fig. 2
The Contraves Cinetheodolite System's major components, showing provisions for Central Computer control as well as remote control and tv display.

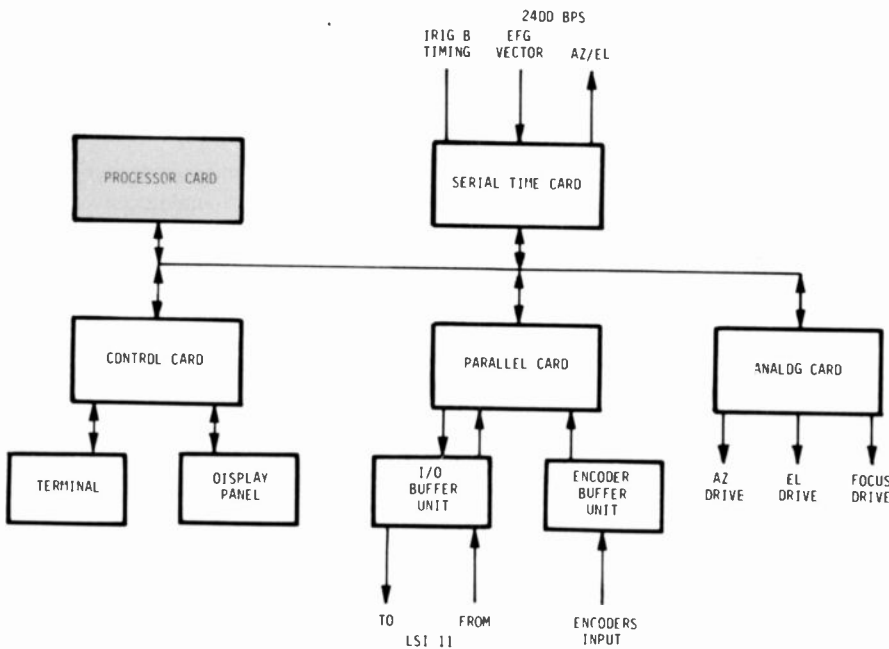


Fig. 3
The RCA 6800 Intelligent Data System is built around the Motorola 6800 microprocessor chip, which is contained on the Processor Card (upper left).

Range. The design, which incorporates the Motorola 6800 Microprocessor chip and its family of support chips, was oriented toward providing system control for a steerable system. However, because of its flexibility, the system has proven to be applicable to many diverse systems. Firmware (programs stored in read-only memories) is modified for these other applications and uses many subroutines developed previously. Hardware redesign for these applications is minimal.

The system is designed with a building-block approach both in hardware and firmware. The building-block approach allows an engineer with little or no previous experience with microcomputers to incorporate one in the design of his system.

Each of the major system components has been wire listed for automated wiring. The backplane connectors which the cards plug into require little or no wire wrapping to interconnect system cards. Connection between cards is accomplished using ribbon cables.

The system characteristics also include:

- *IRIG B time input.* This synchronizes internal clocks to an accurate time. However, the microcomputer free-runs under crystal control if IRIG B time input is lost.

- *Vectored priority interrupts.* These interrupts on the Processor Card allow for fast handling of interrupts.
- *A combination of power-up reset circuits and read-only memories.* These allow the system to come up running when power is applied. The operator does not have to have complex training to be able to operate the system.
- *Electrically Alterable Read-Only Memories.* These are on the Control Card and can be "written to" under program control. These memories hold their contents when power is turned off and on.
- *Serial interface designed for asynchronous or synchronous channels.* This allows for handling of wide variety of serial data interfaces.
- *Parallel interface.* This provides the necessary control functions for interface to many compatible devices.
- *A display panel with hexadecimal and discrete LED displays.* Each display has a unique address which allows displays to accommodate a variety of applications by a change of software/firmware and of the labeling on the front of the display panel.
- *A Sonalert audible alarm.* This alerts the operator when there are system malfunctions.

- *A hexadecimal key pad.* This provides for data entry.
- *An I/O buffer unit with first-in, first-out memories.* These allow for block data transfers between the 6800 IDS and the LSI-11/03 or other computer. The I/O buffer unit provides an interface to a Burroughs self-scan alpha-numeric display. Either processor may write to the display and they may share portions of the display.
- *An RS232 terminal interface.* This provides interface to a wide variety of alpha-numeric terminals, which are used for system control and display.

The Central Computer

A Central Computer, also utilizing microprocessors, provides two or more sites with functions beyond the capabilities of the local computers.

A Central Computer is used to provide functions beyond the capability of the microcomputer systems at the Contraves sites. This computer provides these functions to two or more sites and is configured as shown in Fig. 4. An EFG vector, defining target position and velocity, is transmitted to each site. Azimuth and elevation of target is transmitted from the site to the Central Computer.

A Central Computer is shown in Fig. 5. This system uses the same basic microcomputers used in the Contraves sites, but has

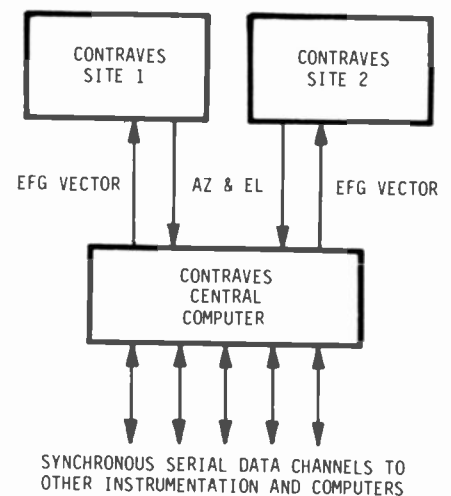


Fig. 4
The Central Computer supplies an EFG vector, giving target position and velocity to each Contraves site. Each site returns azimuth and elevation data to the Computer.

additional features which allow for more complex and diverse computing power. This system has 24K words of random access memory, dual floppy disks, a Burroughs self-scan, alpha-numeric display, and a Decwriter hard copy terminal.

Three functions performed by the Central Computer merit description here.

Star Calibration. The Contraves sites are calibrated using stars. The Central Computer has an ephemeris of many stars stored on floppy disk; it transmits a star vector to the Contraves sites. The sites then transmit data describing the pointing errors to the star. When this has been done on a number of stars, the central computer computes the system error coefficients (azimuth, elevation, range, etc.) for each site with an error regression program and transmits these coefficients to the sites. At the sites, these coefficients are stored on Electrically Alterable Read Only Memories. The coefficients then are used to correct system mechanical errors when the cinetheodolites are being driven by their own microcomputer system.

Target Vector Selection. The Central Computer has a number of synchronous data channels that can contain vectors to several different targets. It can be used to select the applicable vector to drive each of the cinetheodolite sites or to store, prior to a test, theoretical drive vectors, which can be used in lieu of real-time tracking data.

Two-Site Vector Solution. The Central Computer receives azimuth and elevation position information from each of two or more cinetheodolite sites. The Computer then computes the target position and velocity using a multiple-angle solution. For this solution, the sites are optimally located, with one cinetheodolite looking down the flight line and the other(s) looking crossflight.

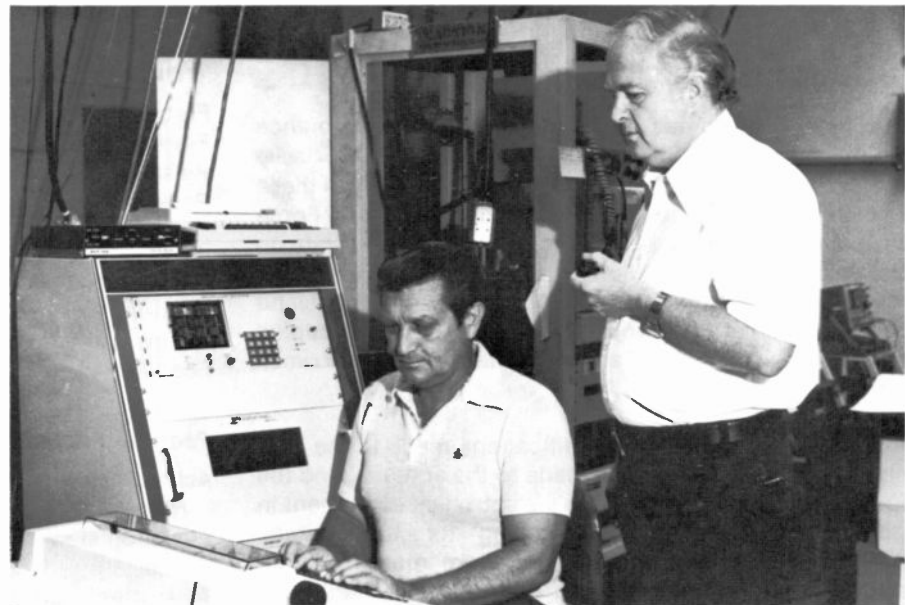
Conclusion

Microcomputers such as the Digital Equipment Corporation LSI-11/03 and RCA's 6800 IDS can provide system control and math computations which previously required larger computers and discrete-circuit or integrated-circuit logic design. The previous options took up considerably more space, were more expensive, and less flexible when modifications were required.

Reprint RE-24-3-5
Final manuscript received June 22, 1978.



Fig. 5
The three units comprising the Central Computer. Included in the equipment are the DEC LSI-11/03 Microcomputer and the RCA 6800 IDS.



Jack Burritt, seated, and Max Miller, right, at a remote computer terminal.

Jack Burritt joined the RCA Service Company in 1956 and became a programmer in 1968. He was part of the team that implemented ETR-developed on-axis tracking techniques in the Naval Ordnance Testing Radar at China Lake, CA, and is presently implementing similar programs in microcomputers for the ETR Contraves Cinetheodolite System.

Contact him at:
**Missile Test Project
RCA Service Company
Patrick AFB, FL 32925
Phone: (305) 494-4085**

Max Miller, with RCA's Missile Test Project since 1955, has been designing computer systems to drive a wide variety of steerable systems since 1968. His more recent assignments include updating steering systems for the optical components of the Nike Hercules radar at China Lake. He presently is the Project Engineer for the addition of microcomputer control to the Contraves Cinetheodolite Systems.

Contact him at:
**Missile Test Project
RCA Service Company
Patrick AFB, FL 32925
Phone: (305) 494-5372**

Value Engineering applied to a large precision tracking mount

C.P. Brooks|E.L. Peghiny

RCA built the Air Force a new tracking radar at the lowest possible cost by repairing, updating, and adapting already-owned equipment.

In the fall of 1976, RCA contracted with the U.S. Air Force to design and build a C-Band radar system—the AN/TPQ-18M—for installation at Ascension Island to support the Navy's Trident program. To produce this system at the lowest possible cost, some components already owned by the Air Force were to be used. These components were:

The Nike-Zeus Tracking Radar (TTR) formerly installed at the White Sands Proving Grounds.

A Missile Precision Instrumentation Radar (MIPIR) Antenna, which was damaged.

The AN/TPQ-18 electronics equipment and shelters formerly installed at the Merritt Island site of the Eastern Test Range.

Performance capabilities

The new system was to have the same performance capabilities as the MIPIR radar systems built by RCA Missile and Surface Radar in the early 1960s. (A summary of these is given in Table I.) The system was built at Patrick Air Force Base, and was interfaced and checked out at a test site on the Base. After completion of the subsystem tests, the equipment was dismantled and flown to Ascension Island for installation at a site which had been originally occupied by a MIPIR, AN/TPQ-18 Radar. The installation is shown in Fig. 1.

This article describes the modifications made to the TTR mount, the extensive repairs made to the antenna, and the up-dating of the pedestal drive's electronics equipment in order to provide reliable tracking for the system. Modifications, not described here, were made to other electronic subsystems, such as range, receiver, and data handling.

The pedestal

To adapt the TTR pedestal to the existing concrete foundation tower at the Ascension Island site, a new cylindrical base structure was designed and fabricated.

To eliminate the need to duplicate the high-precision machining on the top of the base (required to mount the drive gear boxes, azimuth bearings, etc.), the top portion of the original TTR base was flame-cut from the old base and rewelded to the top of the new base structure. The bottom of the new base consists of a two-inch-thick, mild steel ring, containing hold-down bolt holes to match those of the existing mounting ring cast in the top of the concrete tower.

An aluminum, honeycomb center sun shield was fabricated and installed around the outside of the base to minimize the effect of direct sun action on the pedestal level.

The turntable/yoke

The azimuth bearings from the original TTR pedestal—a 116-inch-diameter, ball-type thrust bearing and a vertical, roller-type, radial-centering bearing—were used to support the turntable/yoke.

Table I
Summary of the Radar System characteristics.

<i>Transmitter</i>	
Frequency range	5400-5900 MHz
Frequency stability	Less than 100 kHz/h drift
Pulse repetition rate	160,640 p/s
Peak power	2.8 MW
<i>Antenna</i>	
Diameter	29 ft
Mount	Elevation over azimuth
Feed	Cassegrainian
<i>Pedestal Angle Servos</i>	
Azimuth slew rate	530 mrad/s
Elevation slew rate	350 mrad/s
Azimuth/elevation track rate	350 mrad/s
<i>Range Tracking</i>	
Nonambiguous range	32,000 nmi
Slew rate	80,000 yd/s
Tracking rate	20,000 yd/s
<i>Precision</i>	
Range	23 bits (least significant bit (LSB) = 0.97 yd)
Angles	20 bit (LSB = 0.006 mrad)

Two 3-inch-diameter, 5-inch-stroke, adjustable hydraulic buffers, shown in Fig. 2, were installed on each side of the turntable structure to provide a cushioned stop for the elevation rotating assembly.

The elevation gimbal/bearing assembly

The pedestal was converted from a three-axis type to a two-axis type by the removal of the traverse housing, shafting, and bearings.

The modified pedestal is shown in Fig. 3. The space formerly occupied by the traverse housing was enclosed to form the rf compartment of the new two-axis configuration. There is ample space within this compartment to house all of the rf components, J-boxes, etc., as well as cooled parametric amplifiers and their cryogenic system, which were planned for later installation.

An 8¼-ft-diameter, aluminum antenna-mounting flange was installed on one end of the elevation gimbal structure, and was bolted in the cavity formerly occupied by one of the traverse shaft bearings, and was back-braced to the gimbal structure.

The primary counterweight leads were housed in the vacated traverse-shaft-bearing cavity on the opposite end of the gimbal structure. Supplementary lead weights were installed in the cavities formerly occupied by the TTR traverse hydraulic drive components, and on the exterior walls of the gimbal structure.

The antenna/feed assembly

Because of the severely damaged condition of the antenna, extensive repairs and rebuilding were required.

The antenna assembly, as received, is shown in Fig. 4. A new center bolt-ring section for the hub module was designed and fabricated. The damaged portions of the rib structure of the module, some of which may be seen in Fig. 5, were cut away; then the new bolt-ring section was welded into the structure. A heavy aluminum plate base was used to maintain correct alignment of the hub module during the repairs. This base was also used during the assembly and alignment of the entire antenna structure.

All of the damaged members of the twelve radial support modules were removed. New structural members, skin

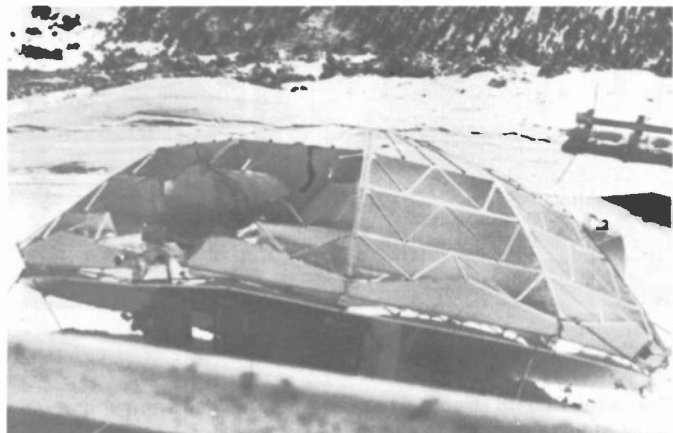


Fig. 1 (top left)
The rebuilt AN/TPQ-18M radar tracker as installed at Ascension Island, ETR. The antenna is in its operational position.

Fig. 2 (top right)
This view of the antenna being assembled to the pedestal, at Patrick AFB, gives a clear view of the pedestal modification to a two-axis configuration.

Fig. 3 (bottom left)
New elevation buffers and strikers were installed on the pedestal. Note, also, the service platforms that were added to both yoke arms.

Fig. 4 (bottom right)
Antenna reflector and support section damage are apparent in this view of the assembly as it was supplied by the customer.



plates, etc. were fabricated and installed by welding and riveting. Heavy aluminum jig plates were used to maintain correct alignment of the modules. The repaired center hub is shown in Fig. 6.

The reflector panels were rebuilt by cutting away the damaged portions and inserting new honeycomb material and new aluminum skin patches. The new skin patches were configured to overlap the old and new honeycomb to obtain maximum joint strength. A panel in the process of restoration appears in Fig. 7.

Fiberglass/plywood form molds were made of the front and back surfaces of the reflector panels, using the one undamaged panel as a pattern. The panels were clamped between the two halves of the mold while the adhesive was setting to assure the correct contour. Because of extensive damage to one of the original panels, one completely new

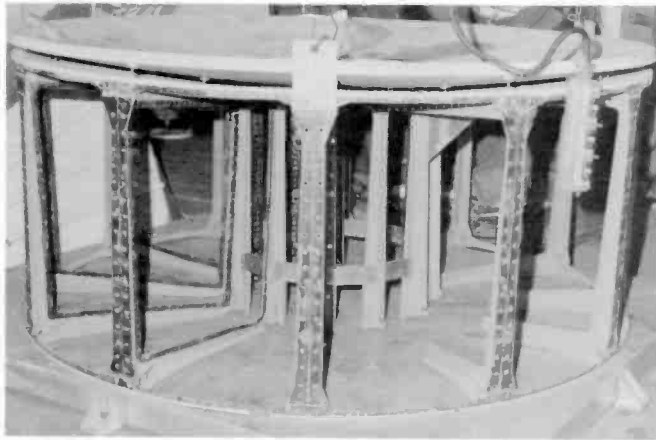


Fig. 5
The center hub structure is shown here mounted to a heavy baseplate to maintain its alignment during repairs. The intersection skin plates have been removed, permitting a view of the radial rib damage.

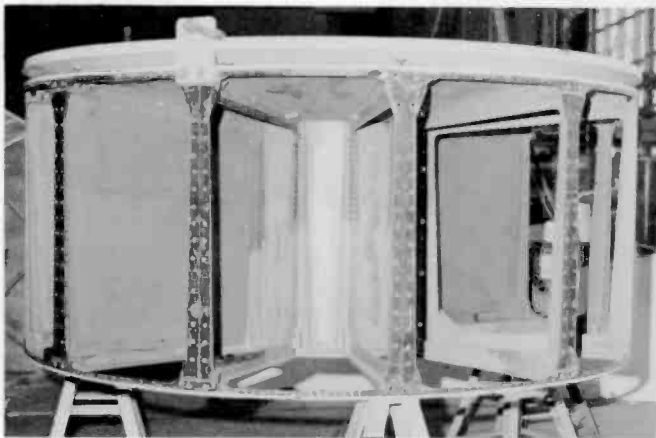


Fig. 6
The center hub rib structure has been repaired, and new aluminum skin has been partially installed.

reflector panel was fabricated. The edges of these panels were resealed by first applying micro-balloon epoxy material on the newly repaired sections and then applying a heavy coat of clear epoxy resin around all of the edges.

After the antenna structure was assembled, using the aluminum base as a foundation, a rotating parabolic-curve jig was installed and precision-aligned in the center of the antenna. By means of this rotating jig, the reflector panels were aligned to a true parabolic curve within 0.050 in. rms.

New support spars, an apex, and a subreflector assembly were obtained from existing stocks and installed. The subreflector was aligned using an auto-collimating telescope positioned in the center of the antenna by a specially fabricated alignment fixture.

A new MIPIR Feed Assembly (comparator) was obtained from existing stocks and installed. The reconstructed antenna assembly is shown in Fig. 8.

The pedestal drives

The original TTR hydraulic-drive components were replaced with equipment of more modern design, and new permanent-magnet type dc motors and solid-state (SCR) controllers were installed to provide pedestal drive power.

Retaining the original hydraulic-drive systems would have incurred the problems of high maintenance costs and the unavailability of replacement parts. Therefore, permanent-magnet type dc electric motors were used to provide pedestal drive power. Four motors were installed in the pedestal base for azimuth drive. These drive the turntable through the original TTR drive gear boxes. Two of these motors are shown in Fig. 9. Each gear box was modified by the addition of a bell housing around the input shaft. The

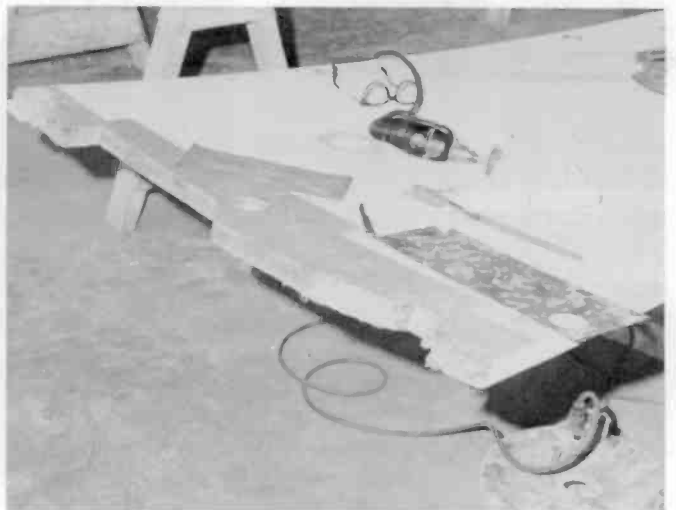


Fig. 7
An antenna reflector panel as it appeared during repairs. Damaged honeycomb core portions have been removed, and new skin sheets are being overlapped between old and new honeycomb material.

bell housing is precision-aligned to the input shaft and contains a precision mounting surface for the drive motor. The motor shaft is coupled to the gear-box input shaft by a Thomas-type flexible coupling. One end of the coupling is keyed to the motor shaft and the other end attaches to the gear-box shaft by splines. This mounting configuration provides precision alignment between the motor and gear box shafts at all times.

The motor can be replaced by removing four mounting screws from the motor flange, then lowering the motor and coupling to clear the splined gear-box shaft. The coupling is then removed and installed on the replacement motor at a fixed position on the motor shaft. The motor/coupling is then raised into position on the bell housing and the four holding bolts are installed. No alignment adjustments are required to assure correct positioning of the motor to the gear-box shaft.

The SCR controllers, transformers, etc., for the azimuth motors are installed on the inside wall of the pedestal base and are protected by expanded-metal cages.

Four elevation drive motors were provided; two are located in the right-hand and two in the left-hand elevation bearing housings. The elevation motors are also mounted on the original TTR drive gear boxes with precision bell housings. The elevation controllers are located in a cavity in the yoke arm below the bearing housings. The power transformers are contained in housings that are attached to the outside of the yoke arms.

These permanent-magnet type, dc motors are totally enclosed, providing protection against contamination. Each of the drive motors is equipped with a fail-safe type disc brake and a dc tachometer.

Servo electronics

Control of the pedestal drives is provided by a servo subsystem of modern design, located in the electronics shelters.

The design incorporates all-solid-state, integrated-circuit components. The azimuth and elevation card cases are standard Honeywell MT 32 units. Adequate test points are available on each card to allow servo loop balancing, set-up, and monitoring.

A built-in function generator and a two-channel recorder are provided to allow open- and closed-loop servo testing, measuring of transient response, and setting of the tachometer-loop dc gradient.

The Angle Servo Electronics. This circuitry accepts input position loop errors from: 1) the console handwheels, in Manual mode; 2) any of four preset synchros or the Mark 51 Optical Director, in Preset mode; 3) the LSI-11 Computer, in Computer Drive mode; or 4) the radar receivers, in Auto-Track mode. In addition, the position loop provides for an Angle Coast mode and angle offsets. The position loop is opened for slewing the antenna axes at two slew rates.

The azimuth and elevation position loops are similar, the main differences being the secant correction and plunge feature in azimuth, and the rate and servo limit controls used in elevation to protect the antenna from damage at the mechanical limits of elevation travel. A block diagram of the servo drive is shown in Fig. 10.

The position loop in Auto-Track and Computer Drive is a type -2 configuration, with the integrator on the Integrator Card switching in when the angle error is less than 8 mills. This provides a position loop with an acceleration constant, K_a , of $30/s^2$ and a velocity constant, K_v , of 4000/s.

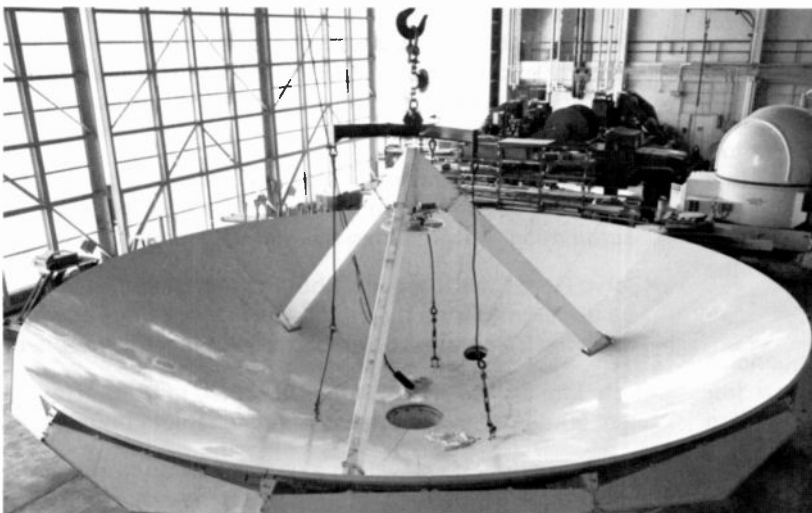


Fig. 8
The antenna here has had the reflector panels aligned, and new spars and subreflectors installed.

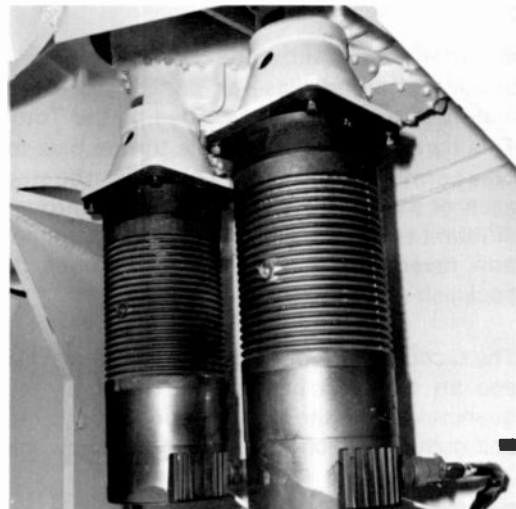


Fig. 9
Two azimuth drive motors are shown here, attached to the bell-housing adaptors that provide automatic alignment of the motors to the gear-box shafts.

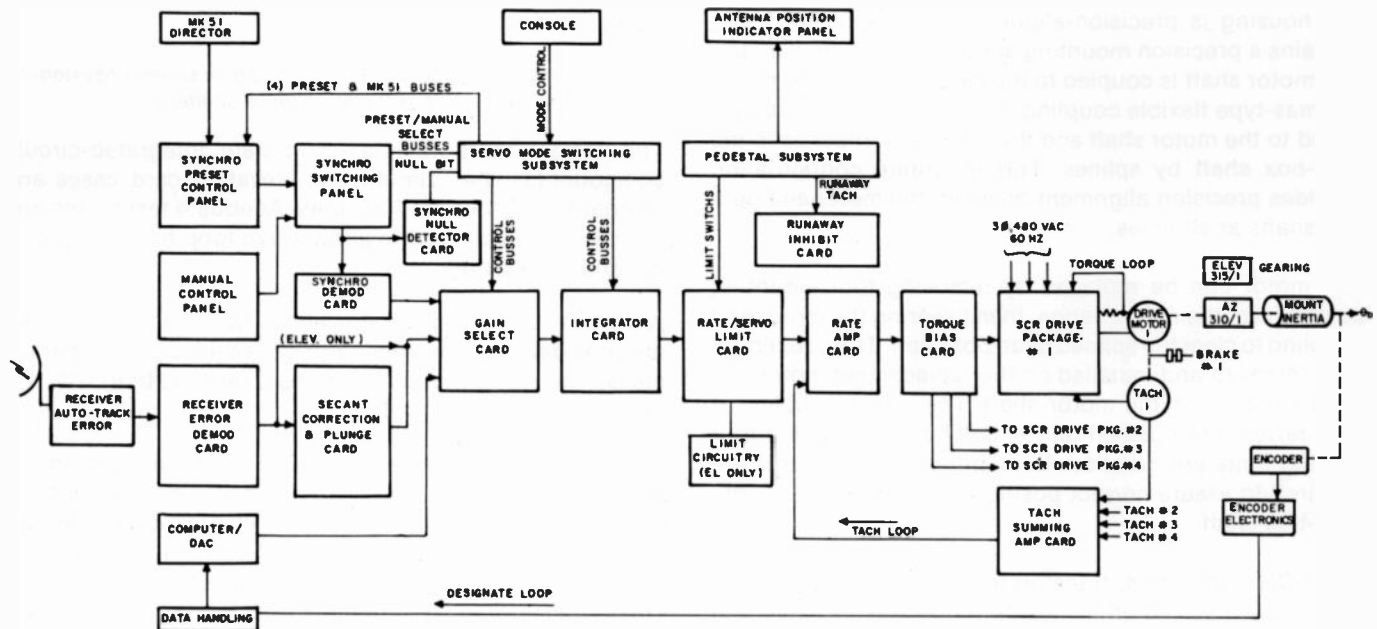


Fig. 10
The azimuth and elevation drive electronics were redesigned to incorporate modern, solid-state, integrated-circuit technology.

Two other loops—the torque loop and the tachometer loop—are enclosed within the position loop. The torque loop provides a means of controlling current to the drive motors. Since the dc motor is a current-to-torque converter and the SCR controller with current feedback is a command-voltage-to-current converter, the combination is a torque-command-voltage-to-torque converter. This means that the input voltage to the torque loop is a torque command that controls motor torque, independent of motor speed, over the linear speed-torque range of the dc motor. To insure long motor life, current-limiting circuitry at the input to the torque loop provides a means of limiting motor current to the continuous-current rating of the drive motors.

In order to minimize the adverse effects of drive-gear backlash, torque bias—or preloading—of the four drive motors in each axis is provided by the Torque Bias card. This card provides adjustable torque bias to each motor. This permits the torque bias settings to be staggered so that each of the four drive motors will go through backlash at different times, providing a smooth transition during direction reversal and a smooth continuous drive with the backlash wound out.

The tachometer loop features high gain at low frequencies and an optimum bandwidth. The high gain at low frequencies makes the loop "torque stiff" against wind loading and gusting, which occur at a frequency below 0.5 Hz.

Each axis has four tachometers—one mounted on each motor. Their output is summed in the Tach Summing Amplifier Card. Since there can be some output variations between different motors, caused by gear backlash and stress deformations in the gear trains, the summed output

of the Tach Summing Amplifier Card gives the best overall average of motor/axis velocity.

The input-rate command from the position loop is applied to the tachometer loop through the Rate/Servo Limit Card, which applies rate and servo limit protection only for the elevation axis, since the azimuth axis has slip rings.

Electronic Protective Features. A number of electronic means are provided to protect the antenna and pedestal structure from damage due to failure of hardware or software components.

- Runaway Inhibit. A separate dc tachometer in each axis of the pedestal monitors axis velocity. Should azimuth velocity exceed 40 deg/s or elevation exceed 15 deg/s, primary drive power is removed from the axis concerned and brakes are applied.
- Computer Inoperative. Should the computer fail while the pedestal is under computer drive, the pedestal is automatically switched to the Manual Handwheel mode.
- Servo Card Case Interlock. Should a tachometer loop card be unplugged from the card case, primary drive power is removed from the associated axis and brakes are applied.
- Rate Limits. The elevation axis is limited to 5 deg/s for the last 20 deg of travel toward the mechanical buffers.
- Servo Limits. The elevation axis is inhibited from driving toward the mechanical buffers when the axis is within 3 deg of the buffers.
- Electrical Limits. Should the elevation axis touch the mechanical buffers at the end of travel, primary drive power is removed from the axis and brakes are applied.

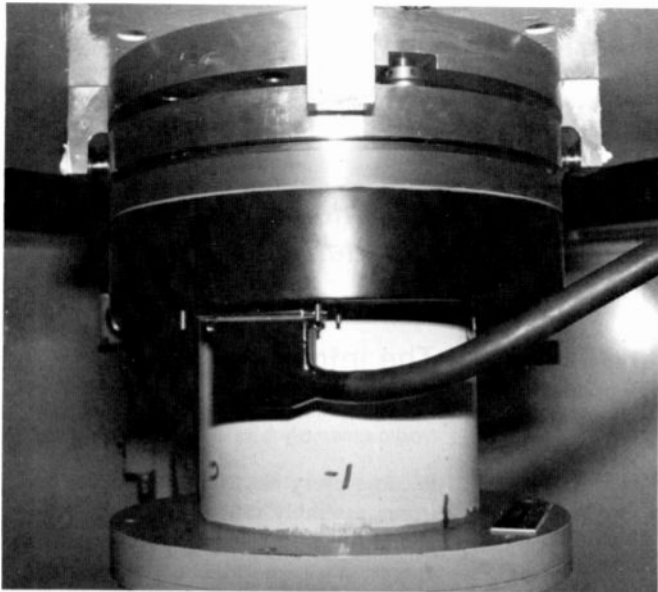


Fig. 11
A close-up view of an azimuth encoder shows the precision mounting-ring assembly.

The shaft-position encoders

Encoders are easily replaced, and realignment is simple.

To provide pedestal shaft-angle-position data in digital format, 20-bit optoelectronic type encoders (ITEC Model RA20/117S) were installed on the azimuth and elevation shafts. The encoder transducers are mounted on adjustable ring assemblies that provide the means of aligning the transducers to the shaft within 0.001 in. angular and parallel misalignment. One of the encoders is shown in Fig. 11.

The azimuth encoder transducer is mounted on a heavy steel plate, located below the slip-ring assembly inside the pedestal base. The steel plate is supported from the base wall by three I-beam brackets. The encoder electronics unit and the dc power supply are located in a housing attached to the base wall.

The elevation encoder transducer is located on the right-hand end of the elevation shaft and is mounted on a support bracket bolted to the elevation bearing housing. The associated electronics unit and power supply were located below the transducer in a housing that was added to the bearing housing.

Both of the encoder transducers can be removed and reinstalled by relatively inexperienced personnel; high precision realignment of the encoder mounting components is unnecessary.

Synchro data

The original 400-Hz synchros were replaced with 60-Hz units, which provide the required analog outputs for antenna position dials, manual hand-wheel controls, and antenna-position preset controls. A dc tachometer was installed on both axes to provide a velocity input to the servo runaway-protection circuitry.

Pedestal level measurement

For angle-data correction purposes, an Autonetics tiltmeter was installed on the pedestal turntable. The sensor unit and its electronics chassis were located in the center of the turntable structure. The tiltmeter has a resolution and noise of less than 0.1 arc second rms.

Conclusion

This modernization of existing components from older radar systems and the subsequent incorporation of them into a new radar has provided the Air Force with a system at a significantly lower cost than would have been incurred for an all-new radar having the same capabilities. This same engineering approach is being applied to several obsolete Nike-Hercules Target Tracking Radar Pedestals, which are being converted to mobile C-Band Radars and optical tracking systems.

Reprint RE-24-3-3
Final manuscript received June 22, 1978.



Ernie Peghiny, left, and Phil Brooks with tracking mount pedestal.

Phil Brooks is a Senior Engineer with the Metric Systems group of the Missile Test Project. He has been involved with the mechanical engineering of tracking mounts since joining RCA in 1962.

Contact him at:
Metric Systems, Missile Test Project
RCA Service Company, Patrick AFB, Florida
Phone: (305) 494-5172

Ernest Peghiny is a Senior Engineer with the Metric Systems group of the Missile Test Project. He is engaged in the design, fabrication, installation, and checkout of servo systems for ground radar and optical pedestals. He recently designed the pneumatic servos for two 48-inch telescopes used in laser and satellite systems. He is the inventor of a Precision Encoder Gyro—a device using gyros and digital encoders to provide a stable reference for pedestals mounted on ships and aircraft.

Contact him at:
Metric Systems, Missile Test Project
RCA Service Company, Patrick AFB, Florida
Phone: (305) 494-5173

Using infrared signatures for PC-board failure analysis

K.J. Martin

Comparing the infrared radiation pattern of a defective PC board with a normal "reference" pattern reveals failed and overloaded components.

During the early 1970s, RCA's Missile Test Project (MTP) began a Range modernization program at the Air Force's Eastern Test Range (ETR) that resulted in the world's most sophisticated and accurate tracking systems. The MTP's engineering program combined existing range hardware with modern computer and digital hardware containing approximately 6,000 printed-circuit (PC) boards. To match the increasing sophistication of this new technology, RCA saw the need to improve depot repair techniques and equipment.

A study of the available technology resulted in the combining of an existing capability with a relatively new "signature" concept, using infrared detection techniques. An infrared scanning machine was obtained from the Air Force and was combined with RCA's existing ME104 PC board tester.

A marked improvement in the quality of the repaired boards resulted from the use of this combination. Troubleshooting with the infrared system proved its ability to: a) detect "hidden" anomalies liable to cause a failure in the near, or not-so-near, future; b) disclose the consequences of a component failure on other "innocent" components located downstream; and c) pinpoint when it is time to replace a component on the basis of a verified need instead of a statistical calculation.

Infrared radiation

A new concept in noncontact testing of electronics hardware is embodied in the infrared approach.

Enough papers have been published during recent years on infrared fundamentals that extensive discussion of the subject here is not necessary. Infrared is a form of electromagnetic radiation, emitted by all physical matter at temperatures above absolute zero. The atomic and subatomic particles are acting as oscillators, with frequency and amplitude controlled by their mass and

energy content. The radiation band covers a wide frequency spectrum; infrared is only part of it.

The spectral emission band of the infrared radiation emitted by the surface of a physical body at any temperature above zero deg K is not linear, but shows a peak whose wave-length is determined by the temperature of the radiating surface and whose amplitude depends on the "emissivity"¹ of the surface. Fig. 1 shows the correlation between the wavelength of the radiation band's peak and the temperature of the emitting surface.

This correlation, and the correlation between the electrical power dissipated and heat generated by it, are the cornerstones of a noncontact approach to failure diagnosis. A measurement of the infrared radiation emitted by an electrically energized component can be converted into a measurement of its operating temperature. This, in turn, is a function of its electrical power dissipation, which consequently can be determined as a function of the infrared measurement.

The infrared signature

The infrared signature of an energized electronic assembly is as unique as a fingerprint.

Because every electrically energized electronic assembly radiates infrared energy, identification of normal or abnormal operation is possible. Energized electronic components in a circuit will exhibit their own radiation level² or infrared "signature." Several normally operating PC boards of the same type will exhibit nearly identical signatures under identical energized conditions. Such a signature is shown in Table 1.

Every electronic assembly has its own infrared signature, typical and repeatable (within the tolerance limits of its components) as long as the electrical energization remains the same; all the electronic assemblies of the same electrical and mechanical design will exhibit—within the allowed tolerance limits—the same infrared signature.

Reprint RE-24-3-4
Originally presented at the IEEE 28th Electronic Components Conference, Anaheim, CA, April 25, 1978.

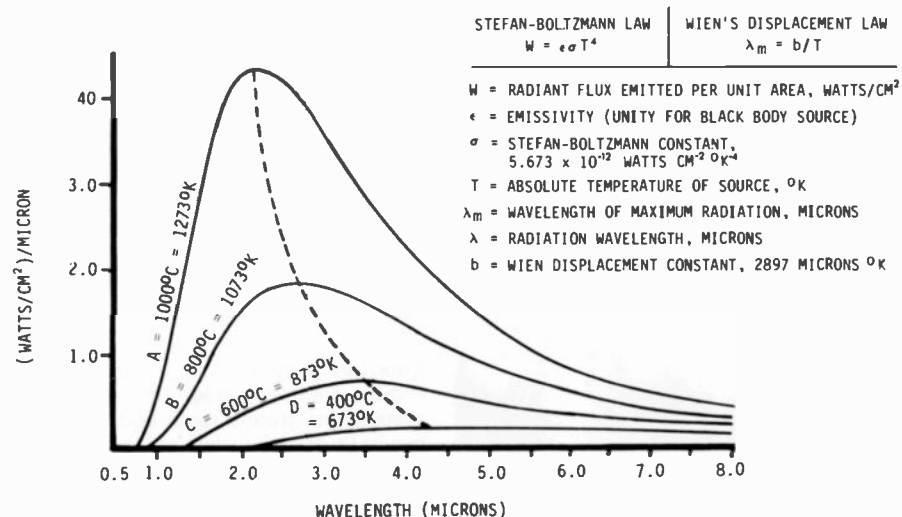


Fig. 1
Blackbody radiation curves show the infrared radiation "peaks" at various temperatures and wavelengths.

Both defective and repaired assemblies can be evaluated by comparing their signatures with a reference "standard".

Once defined, the infrared signature of a good electronic assembly can be used as a "reference" or "standard" against which the signatures of similar assemblies may be compared. Any deviation beyond tolerance limits indicates an anomaly that can be either an actual failure or the precursor of a future failure. The deviations from the standard are not limited only to the faulty components, they may also indicate the consequences of the failure upon "innocent" associated components. In this way dangerous overstresses can be detected and, only by replacing the overstressed components, can the original reliability be restored. Without infrared analysis, the conventional troubleshooting procedure generally involves only replacing the immediately noticeable defective component, which often does not remove the cause or remedy the consequences of the trouble.

In addition, with the infrared technique, early failures often can be predicted, since they often are the ultimate result of a previous overstress condition that is already apparent in the infrared signature. In this way, infrared testing lets you "look into the future."

Also, infrared analysis is useful in preventive maintenance. Generally the replacement of electronic components or assemblies to prevent failures has been based on statistical calculations of mean time before failure (MTBF). No one knows whether the replacement unit will last longer than the unit replaced. It could very well be the opposite. The infrared signature of an electronic assembly, compared with its signature taken the day the unit was initially tested, will reveal any deteriorating trend and, if it does, will pinpoint the component whose replacement is needed. The signature of the repaired unit will tell us whether the faulty trend was corrected, so that the unit will last as long as expected.

We can therefore conclude that use of infrared signatures from energized electronic assemblies can be of help in the following areas:

- engineering design evaluation
- component stress analysis
- realistic reliability calculation
- life expectancy projection
- inspection, test, fault-part isolation
- detection of "hidden failures"

The emergence of applied infrared technology

Within the last decade, infrared technology has found its way into such varied fields as space vehicles, forestry, farming, imaging, medicine, and electronics. For example, NASA has applied it to satellites for detecting pollution and disease-infested forests and crops. It is used in medicine for tumor detection, determining the menstrual cycle, sex of the unborn, etc. The Army has applied it to night photography, sniper scopes, and night vision. Its applications in electronics are so numerous, it is difficult to name them all. IR has been applied to missile tracking. Coupled with fiber optics, it is used to monitor parameters in otherwise inaccessible locations. Printed-circuit-board testing is just one, highly specialized application.

Table 1
Printout of the infrared signature of a printed-circuit board. The deviation from ambient temperature in infrared "points" is shown opposite the symbol for each component. Ten points are equivalent to one Celsius deg.

SS		UUT ID # HI/LO LOGIC #2	
	DEVIATION		
R1	44.9	R5	2.8
A1	17.5	R3	2.7
A2	14.6	D5	2.2
B1	12.6	C4	1.9
B2	12.2	C3	1.9
L1	11.6	D2	1.6
L2	11.5	UL1	0.6
R4	9.3	D3	0.3
R2	7.6	C6	0.3
C7	6.1	C2	0.3
R6	5.7	Q2	0.3
C5	4.1	R10	0.1
UL2	3.7	Q1	0.1
R7	3.0	C1	0.1
		TEST END	



Konklin Martin joined RCA in 1955 and has held various technical management positions at the Missile Test Project since that time. He presently is Manager, Communications Electronics Maintenance Support and is responsible for intermediate and depot maintenance of all MTP instrumentation equipment.

Contact him at:
Missile Test Project
Bldg. 423, Mail Unit 172
RCA Service Co.
Patrick AFB, FL 32925
Phone: (305) 494-7391

Konklin Martin, printed-circuit board, and INSPECT system.

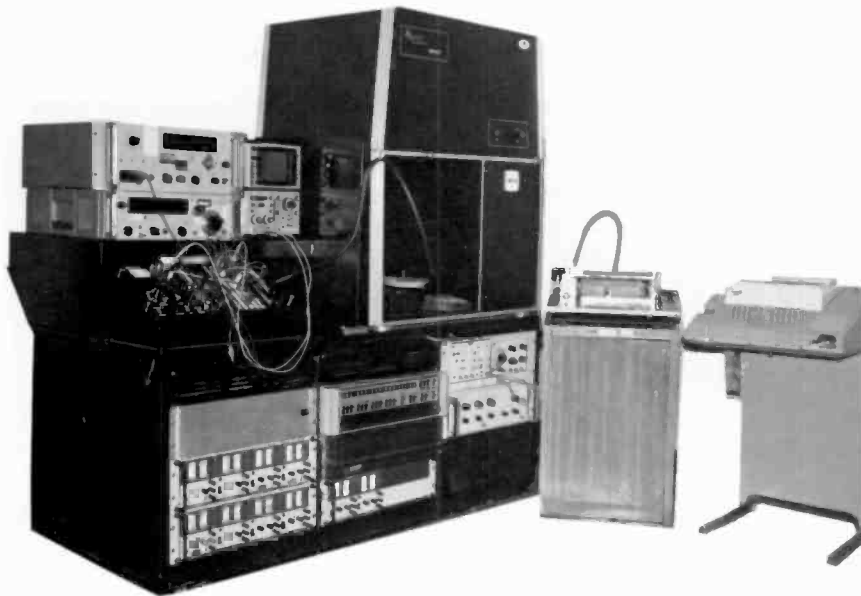


Fig. 2
The infrared test equipment consists of (upper left) the ME104 PC board tester, (center) the infrared scanner, (right center) the X-Y locator, (far right) the teletype printer, and (bottom left) the power supplies, signal and pulse generator, the computer, and its memory.

- detection of secondary overstresses
- component early-failure prediction
- rational maintenance policy, based on verified replacement needs.

The infrared test system

The test specimen is scanned, and temperatures or temperature deviations are printed out for each component.

The hybrid infrared test system developed by RCA at MTP is shown in Fig. 2. The new, basic components: the computer and its memory, in conjunction with the infrared scanner, are known as the IN-SPECT system. The X-Y locator allows quick programming of the designated component locations on the selected PC board. The teletype printer supplies, at the end of each scan, either the full infrared signature (i.e., actual temperatures) or the deviations from standard, according to the operator's instructions. In conjunction with the ME104 PC Board tester, this equipment constitutes the hybrid test set. The ME104 Tester was previously developed by RCA to energize boards under test with both

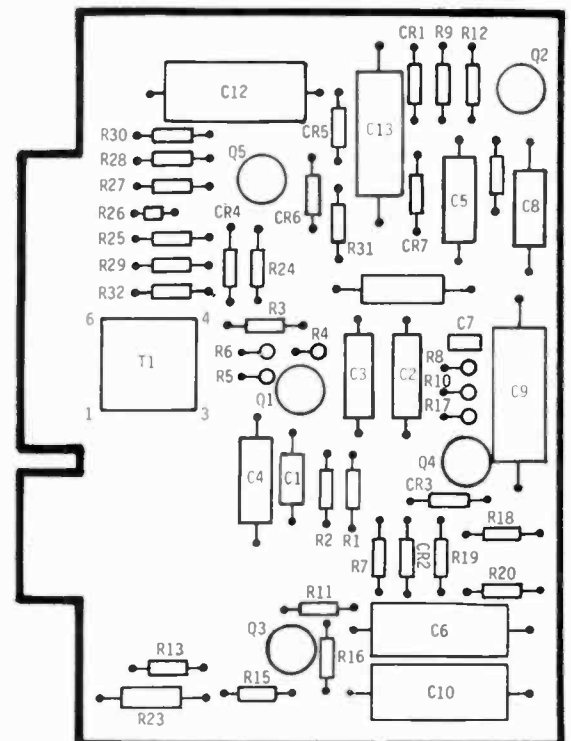
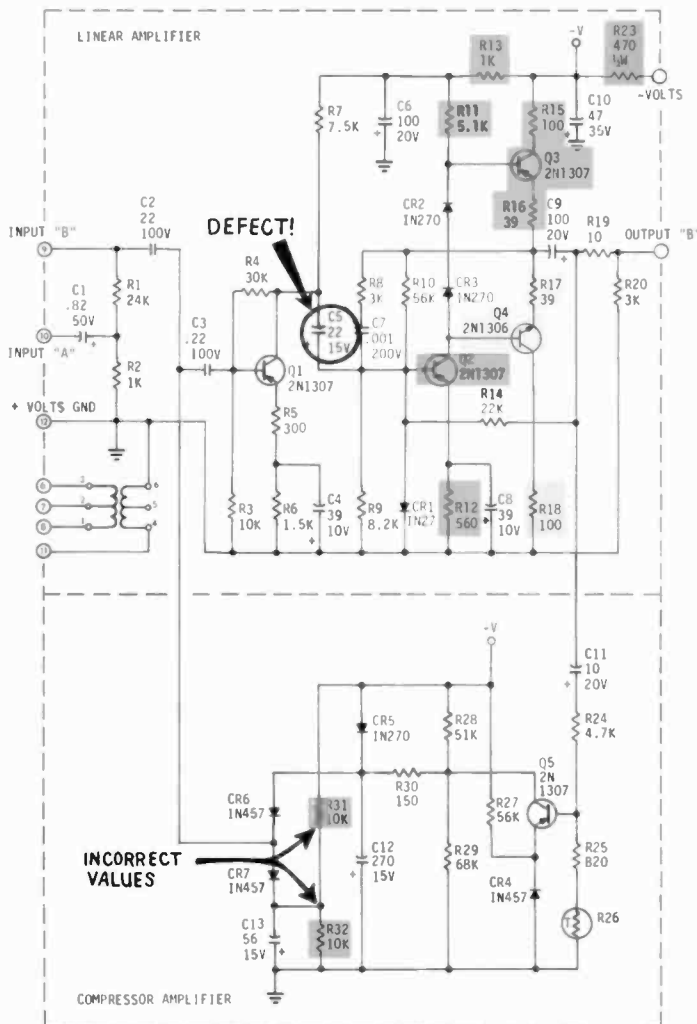


Fig. 3
Infrared test showed abnormally high temperatures (dark gray) and abnormally low temperatures (light gray) for components on upper half of schematic for AGC circuit board shown here. In one test, temperature deviations shown in Table II and knowledge of circuit showed a shorted capacitor C5. Another board (deviations shown in Table III) had incorrect components in place, producing deviations shown on lower half of schematic.

power and signal voltages to simulate their loading in actual operation.

Test system operation

Deviations from the design value of the component, due either to a defect or installation of the wrong value, can be identified.

The following two examples show the typical procedure used for isolation of faulty parts on PC boards.

Case 1: Fig. 3 shows the schematic and layout for a communications system AGC board that was run through the INSPECT System. Before this board was serviced, a normal signature had been established from known good boards. The normal signature plus a tolerance was loaded into the computer through the teletype machine.

After the board was placed in position to be scanned, it was energized until component temperatures stabilized and then was scanned. The resulting printout is shown in Table II. Reviewing the results revealed

Table II
Test set printout showing abnormally high (dark gray) and abnormally low (light gray) components in first example. Capacitor C5 was shorted, causing temperature deviations.

S2 PC# COMP	806317-215 DEVIATION
C09	-001* 033%
Q02	+001 025%
R20	-001 007%
Q04	-003 037%
R12	+001 025%
R18	-002 040%
R10	-003 033%
R17	-004 036%
R19	+002 022%
D02	+002 013%
R07	+011 039%
R01	+001 025%
R11	+044 112%+
R16	+029 145%+
Q03	+027 300%+
R15	+033 100%+
R05	-001 016%
R13	+034 075%
R23	+036 057%
TEST END	
* Minus values are below normal; plus values are above normal.	

R11, R12, R13, R15, R16, R23, Q02 and Q03 to be well above normal temperature. It was also noticed that R17, R18, and Q04 were running 36, 37, and 40 percent, respectively, cooler than normal running temperature.

Applying this knowledge and electronic theory to the schematic diagram, it was deduced that C5 was short-circuited. As it turned out, capacitor C5 was installed with its polarity reversed and, being a polarized capacitor, did act as a short circuit.

Case 2: Table III is a more comprehensive printout of the same type board, serviced at a later time. This card had two resistors of incorrect value installed. R31 and R32 were 300 ohms; they should have been 10k ohms. Note that they were running well above normal temperature by factors of 943 percent and 999 percent, respectively. Other components were also well above normal temperature, caused mainly by the amplifier gain being considerably above normal.

It will be noted that Table II contains less data than Table III, although the same type

Table III
Very high temperatures for two components, R31 and R32 (at bottom left of schematic), were because resistors were of incorrect value. Other components heated up abnormally because of this mistake.

S1 PC# COMP	806317-215 DEVIATION
C09	-001* 033%
Q02	-002 050%
R18	-005 038%
R20	-001 007%
Q04	-004 050%
R12	-002 050%
C05	+009 450%
C10	-001 033%
R10	-003 033%
R17	-006 054%
R19	-003 033%
D03	-008 057%
C06	-002 050%
C11	+007 233%
D01	+006 300%
D07	+022 550%
D02	-004 026%
R07	-006 021%
C13	+017 850%
R01	-001 025%
R31	+217 943%
R02	-001 033%
R11	-010 025%
D05	+038 760%
R04	+003 042%
D06	+078 780%
Q03	+004 044%
R15	+125 378%
R03	+030 300%
R24	+048 480%
C12	+002 200%
R05	+010 166%
R06	+029 414%
D04	+068 523%
R29	+130 866%
R13	+201 446%
R25	+040 444%
R32	+232 999%
R26	+011 091%
R23	+181 287%
T01	+004 400%
TEST END	
* Minus values are below normal; plus values are above normal.	

board was tested in each case. This demonstrates another feature of the test set; it may be programmed for selective readout in cases where only a subcircuit need be analyzed.

Conclusion

Integration of the RCA ME104 PC Board Tester with the INSPECT System has provided a flexibility to the resulting system that makes PC-board maintenance more cost effective. Additionally, a marked improvement in the final quality of the PC boards has been observed. This is mainly due to the fact that overstressed parts are now identified at the time of the scan and are immediately correctable, avoiding the possibility of future down-time periods.

References

- Green, D.; "Emissivity Independent Thermal Testing Method," *Materials Evaluation*, Vol XXIII, No. 2 (1965), p. 78.
- Herman, R.A.; "Aspects of Using Infrared for Electronic Circuit Diagnosis," *Materials Evaluation*, Vol. XXV, No. 9 (1967), p. 201.
- Jones, R.W. and L.M. White; "Infrared Evaluation of Multilayer Boards," *Materials Evaluation*, Vol. XXVII, No. 2, (1969), pp. 39-41.

The finite-element method— a powerful tool for structural design

A.W. Sheffler
W.W. Metzger
G. Varadarajan

In recent years, the finite-element method has developed into one of the most powerful analytical tools available to the research and design engineer. Its applications have grown in direct proportion to the growth of digital computer systems because the matrix equations used in the finite-element method take full advantage of the computer's ability to handle large numerical solutions with ease and low cost. The wide range of applications results from the basic simplicity and versatility of the method. In its basics, the finite-element method can be

The finite-element method solves problems that designers would not even attempt without it. "Building-block" analysis of large problems and low-cost, fast computers make this possible.

viewed as a set of building blocks, or elements. When assembled to model the actual structure, these elements can readily account for unusual geometry, loading, and boundary conditions. They can provide sufficient accuracy to verify designs and test predictions at low cost. As a result, the finite-element technique has become firmly established as an analytical tool to aid in the design process.

The finite-element method is presented here with the point of view of the structural

analyst. This is appropriate, since the method was primarily developed to aid structural design and analysis in the aerospace industry, such as complex aircraft wing structures and spacecraft launch vehicles. Since this development, the finite-element method has been applied to fluid-dynamics problems, pollution-control studies, and conductive heat transfer. For simplicity and clarity, however, these articles will be limited to applications in structural mechanics.

Structural analysis before computers

W.W. Metzger

To appreciate the value of the finite-element approach, it is important to look at the other possible methods of attacking a complex structural problem.

Before computers came of age, the only real choice for the engineer was to model a complex part as a small number of simple parts, then write and solve a set of linear equations. This procedure was quite time-consuming and even then was limited to relatively simple models—consider the time it takes to solve a 20 x 20 matrix by hand or mechanical calculator, or even a simple 6 x 6 matrix, for that matter.

Fig. 1 illustrates a "before computers" analysis that is no doubt familiar to structures engineers. The example shows a simple hydraulic actuator and how you would solve this problem without a computer. First, you would model the outside cylinder as a series of parts. Next, you would write six boundary conditions that matched slopes and deflections at all the

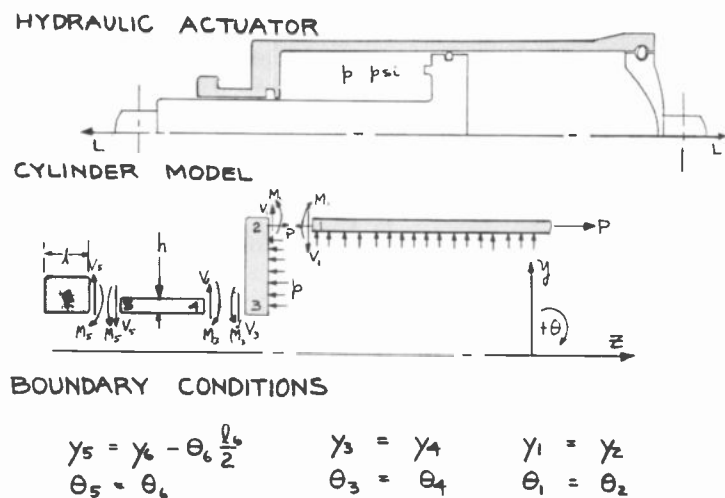


Fig. 1

"Before computers" structural analysis. This hydraulic actuator is modeled as a series of parts—a ring (6), short cylinder (5-4), plate (3-2), and long cylinder (1). Then, the engineer writes a set of boundary conditions, matching slopes and deflections where parts meet. With this information, equations of Fig. 2 can be written.

joints. Then, you would write a series of equations (Fig. 2) to give the deflection and slope at the free end of each element, taking the coefficients in these equations from standard references like Roarke's *Formulas for Stress and Strain*. Thus, Fig. 2 shows 12 equations in 18 unknowns (y_j ,

θ_j, V_k, M_l). If you took these 12 equations and substituted them back into the six boundary conditions of Fig. 1, you eliminated 12 of the unknowns and ended up with 6 linear equations in 6 unknowns—the internal loads, V_k and M_l at each of the three joints.

Reprint RE-24-3-13

These papers were originally presented at the RCA Finite Element Symposium, March 13-14, 1978, at RCA Laboratories, Princeton, N.J. They are presented here in considerably shortened form.

Solving six equations in six unknowns took about two hours by slide rule, or about an equal time for an engineering aide, clunk, clunk, clunk on the electro-mechanical calculator. Finally, you had a single answer, and after perhaps another 6 or 8 hours of solving for all the rest of the variables and sorting out all the mistakes, you were finished. There had to be a better way.

The computer did more than speed up calculations—it changed our whole way of attacking a problem.

During the late 1950s computers started to become available to many of us. We busied ourselves writing special little programs, and it's not surprising that the first one that most of us wrote solved a system of linear equations. Behold, the solution for six equations in six unknowns dropped right out. We rewrote the programs so we could do as many as 20 equations in 20 unknowns (nobody ever modeled anything with more than 20 pieces). But then some people started thinking, "Gee, why not?" and these programs were expanded so that they could handle hundreds of pieces. Eventually, in 1956, Turner wrote a very significant paper called "Stiffness and deflection analysis of complex structures," which is credited by many people as the beginning of the finite-element method.

Also in the 1950s, many engineers started writing computer programs that put cylinders and plates and beams and trusses together into complex structures and solved them. After solving the systems of linear equations, it was a straightforward step to program in all the coefficients so that all the engineer had to do was put in the dimensions of his special structure and obtain the answer. The program FRAN, written in the late 1950s by some people at

$$\begin{array}{l}
 \text{LONG CYLINDER} \\
 \left\{ \begin{array}{l} y_1 = -\alpha_{y_1}^{CV} V_1 + \alpha_{y_1}^{CM} M_1 + \alpha_{y_1}^{CP} p \\ \theta_1 = -\alpha_{\theta_1}^{CV} V_1 + \alpha_{\theta_1}^{CM} M_1 \end{array} \right. \\
 \\
 \text{PLATE} \\
 \left\{ \begin{array}{l} y_2 = +\alpha_{y_2}^{PV} V_1 - \alpha_{y_2}^{PV} V_3 \\ \theta_2 = -\alpha_{\theta_2}^{PM} M_1 - \alpha_{\theta_2}^{PM} M_3 + \alpha_{\theta_2}^{PP} p \\ y_3 = +\alpha_{y_3}^{PV} V_1 - \alpha_{y_3}^{PV} V_3 \\ \theta_3 = -\alpha_{\theta_3}^{PM} M_1 - \alpha_{\theta_3}^{PM} M_3 + \alpha_{\theta_3}^{PP} p \end{array} \right. \\
 \\
 \text{SHORT CYLINDER} \\
 \left\{ \begin{array}{l} y_4 = +\alpha_{y_4}^{SV} V_3 - \alpha_{y_4}^{SM} M_3 + \alpha_{y_4}^{SV} V_5 + \alpha_{y_4}^{SM} M_5 \\ \theta_4 = -\alpha_{\theta_4}^{SV} V_3 + \alpha_{\theta_4}^{SM} M_3 - \alpha_{\theta_4}^{SV} V_5 - \alpha_{\theta_4}^{SM} M_5 \\ y_5 = -\alpha_{y_5}^{SV} V_3 + \alpha_{y_5}^{SM} M_3 - \alpha_{y_5}^{SV} V_5 - \alpha_{y_5}^{SM} M_5 \\ \theta_5 = -\alpha_{\theta_5}^{SV} V_3 + \alpha_{\theta_5}^{SM} M_3 - \alpha_{\theta_5}^{SV} V_5 - \alpha_{\theta_5}^{SM} M_5 \end{array} \right. \\
 \\
 \text{RING} \\
 \left\{ \begin{array}{l} y_6 = \alpha_{y_6}^{RV} V_5 \\ \theta_6 = \alpha_{\theta_6}^{RM} (M_5 - V_5 \frac{l_6}{2}) \end{array} \right.
 \end{array}$$

Fig. 2 "Before computers" analysis produces twelve equations in 18 unknowns for the relatively simple example in Fig. 1. Substituting into the boundary equations gives six equations in six unknowns, which took hours to solve by hand or by mechanical calculator. Models consisting of much more than six elements were prohibitively time-consuming to solve and check.

MIT who had obtained industrial support, solved a series of beams, cylinders, and plates in much the same way as we had previously done it by hand. FRAN developed into a program called STRESS, which added some additional elements and some additional niceties. Eventually it developed into a program called

STRUDL, which became available in the public domain to whoever wanted to use it. Similar refinements and additions have taken place with other finite-element programs, so that now the engineer now has a wide choice of general and special-purpose programs available. We've come a long, long way.

An introduction to the finite-element technique

A.W. Sheffler

The finite-element method works by breaking complex structures into many readily-solvable "building blocks."

Now that we've seen the problems inherent in "before computers" analysis, a quick look at how the finite-element method works should show the method's advantages. In the finite-element method, the part being analyzed is divided into a mesh of standard shapes so that the computer can have a systematic way of handling the

analysis. This leads to a system of nodes, as in Fig. 3, with nodal numbering systems and a system of meshes to connect these nodes in specific ways. However, the existence of a numerical mesh alone does not imply a finite-element solution. The same mesh technique may be used for the direct numerical solution of the differential equations. For example, the finite-difference technique, with its nodes and meshes, is widely used in heat-transfer analysis to solve the system equilibrium

equations. On the other hand, a finite-element solution uses an element that is itself in total equilibrium. Thus, you have an element, or even a library of elements, that can be assembled to directly form a system that is in equilibrium.

When we refer to finite-element methods today, we are generally talking about the direct stiffness method.

The direct stiffness method is based on a simple equation—the load is equal to the

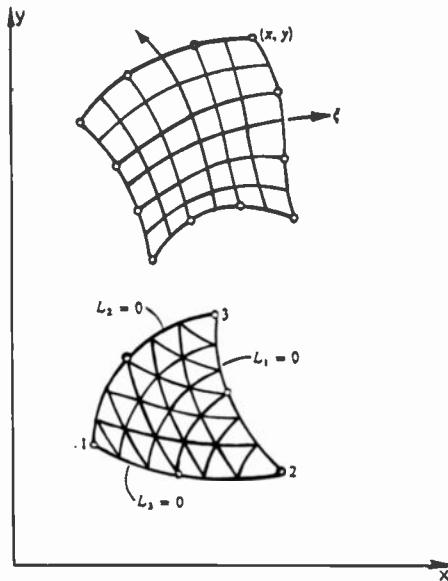


Fig. 3 System of nodes defining the part being analyzed is characteristic of the finite-element method. Meshes and numbering systems provide a systematic way for computer to do analysis.

spring rate times the deflection—expanded into matrix form. This way, you can produce an overall stiffness (spring-rate) matrix for an entire structure by using a “library” of standard shapes. You can generate the stiffness matrix of the entire system without regard to whether it is statically determinate or statically indeterminate. (This is not true with the earlier *force* and *displacement* methods, which required careful selection of determinate and indeterminate degrees of freedom. For example, a highly redundant structure such as an aircraft wing required an entire specialty group that defined the computer input for the force method.) With the direct stiffness method, you can program the entire structural system by following a regular pattern of assembling the element stiffness matrices. And finally, the real advantage of the method is its ability to accept any type of boundary condition.

In general, the direct stiffness method can be defined as a process of modeling a continuum with a finite number of unknowns.

This process includes generating an element or several elements (Fig. 4) and combining these elements to form a system. Numerically, this results in a system of linear equations in matrix form, shown at the bottom of Fig. 4. Because each element has a finite number of unknowns, the strain

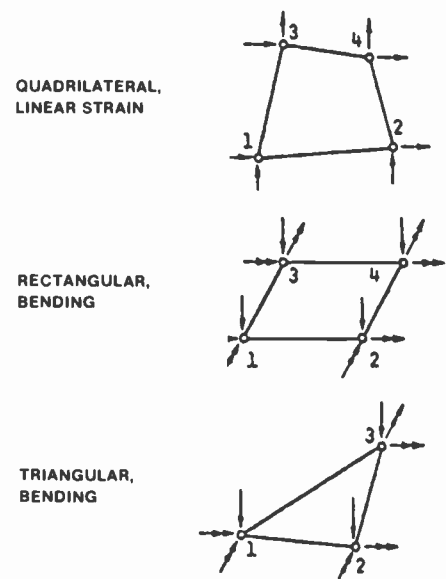
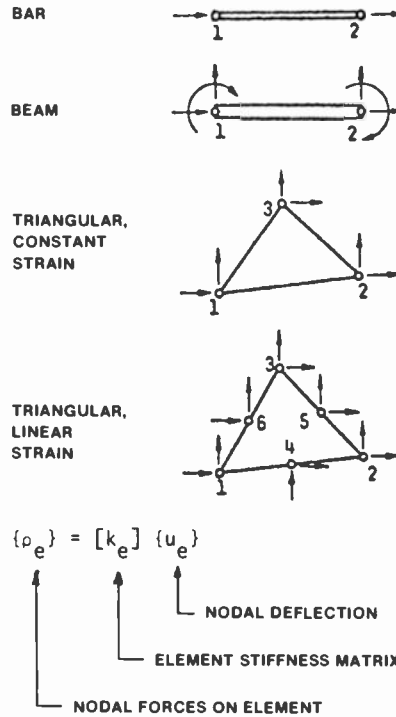


Fig. 4 “Library” of standard elements can be combined to form a nonstandard shape or part for analysis. If elements are chosen properly, the approximation of the actual part will be excellent. The important feature of the finite-element method is that each element is in equilibrium, so it follows a simple linear equation: force = spring rate times deflection. The overall system is analyzed by combining these element equations into one large matrix equation.

energy (or everything that is going on in that element) can be obtained by knowing the deflections at the node points. This sets the system apart as being a “finite element” system. As shown in Fig. 4, you can combine any type of compatible finite elements from the libraries available today. You can put together beam elements, triangular plates, and quad plates, and build up the system to represent the actual structure. No matter how complicated the system, each of these elements follows the simple equation at the bottom of Fig. 4. This simply reminds us that the load has to be equal to the spring rate times the deflection. It is as simple as that, a simple linear equation in matrix form.

What must the user do?

As an overview of the finite-element process, Fig. 5 summarizes the process in two parts. The left side of Fig. 5 shows the steps that we as engineers have to control—that’s where we have to show our engineering judgement. The right side of Fig. 5 shows the programmed operations, or what the computer does for us. So, our first step is selecting the nodes and the elements. The small sketches in Fig. 5 illustrate a typical system in three-dimensional coordinates. The material properties are chosen according to the type of material being used. Isotropic, orthotropic, or anisotropic materials all follow the same pattern, again illustrating the wide application of this method.

In the early stages of generating a model and before proceeding through the analysis, it is best to consider what the end product will be and compare it with what we need from this analysis. If we don’t show the proper judgement in defining a model, costly re-work may result. For example, if you know point loads exist, you will want to have a locally refined grid spacing and use the proper type of element. In this case, we have to invest a lot of judgement and iterations in this first loop. Certainly when you proceed through this process and end up saying, “Gee, I wish I had a finer grid,” it is too late. It is extremely costly and time-consuming to go back and do it again. Therefore, as a word of caution to new users, if there’s any place to invest your time, it is on this first step in generating a model. It is one that is easily overlooked in a desire to “get something running.”

The finite-element process begins by generating each of the elements, whether they are rectangular- or triangular-plate elements as shown in Fig. 5a or any of the other elements available today. A subtle point to keep in mind, however, is that each of these elements is generated in its own

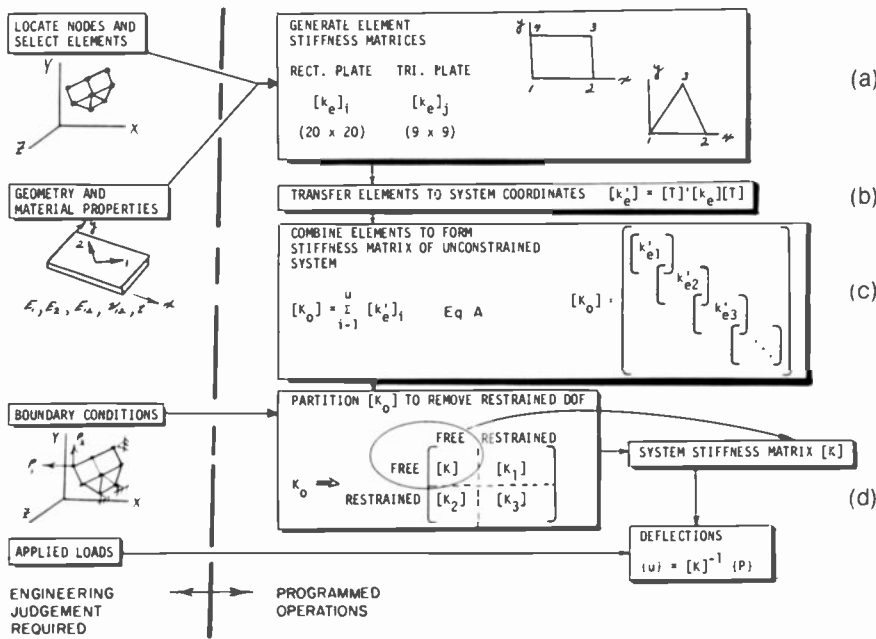


Fig. 5
The computer doesn't do all the work. This typical system analysis has been partitioned to show where the engineer uses judgement and where the computer follows its program. Much work must be done, for example, in selecting the proper grid—not too coarse, or the approximation will not hold, and not too fine, or the computer time will be too costly. Step-by-step explanation is in text.

local coordinate system. In order to be useful, the element stiffness matrix has to be transferred into the system coordinates (Fig. 5b). This requires a coordinate transformation and a nodal renumbering operation on the element. This is a straightforward operation, but it must not be overlooked when interpreting the results.

After the element stiffness matrix is transformed into system-coordinate format, these elements are summed to form a system. Equation A in Fig. 5c oversimplifies the problem, but at least it illustrates the operation. It is a matter of summing the stiffness matrices for each element according to the degrees of freedom of that element. This is not an easy task, because you need to keep track of all the degrees of freedom of that element in the system coordinates. But, for illustration purposes, it is just a summation, and the summation occurs where the stiffness matrices of each element overlap. Fig. 5c shows how these terms are added to form a stiffness matrix for the (unrestrained) system.

Thus far, we have not discussed boundary conditions on the structure. The boundary conditions would be applied if certain points cannot have any displacement or

rotation. In the direct stiffness method, statically determinate and statically indeterminate structures produce no difference in the analysis—the system stiffness matrix is simply partitioned according to the restrained degrees of freedom and the free degrees of freedom. These free degrees of freedom then form the stiffness matrix for the constrained system. Once this system stiffness matrix has been generated, it is inverted, as shown in Fig. 5d, and combined with the given set of loads to produce the nodal deflections in the system model.

Several commercial analysis programs, NASTRAN, STARDYNE, and STRUDL, to name a few, follow a standard sequence.

This sequence involves going from the element stiffness matrices to a system stiffness matrix and finally to the application of boundary conditions. Typically, these operations are done in the active core of the computer. Other commercial programs, such as ANSYS, however, use a different approach. Called a wavefront solution, it is similar to the sequence shown in Fig. 5, except that it uses the specified boundary conditions and a Gaussian elimination technique to eliminate the

restrained degrees of freedom on a one-for-one basis. As the program generates the stiffness matrix for each element, the boundary conditions are applied, and the reduced element is stored in external storage.

These two program types have a difference in their formulation. In NASTRAN or STARDYNE, for example, the user wants to have a nodal numbering system that produces a minimum bandwidth for the stiffness matrix, as in Fig. 5c. These types of programs take advantage of the small bandwidth during matrix inversion. With ANSYS, on the other hand, the user must be careful of the elemental numbering system (rather than the nodal numbering system) so that the Gaussian elimination or "wavefront solution" is minimized. The end product from any of these programs is a single stiffness matrix for the entire system. With this stiffness matrix, the analyst can determine the structural deflections, load distributions, stresses, and even natural frequencies and mode shapes.

How do you produce the stiffness matrix for each of your building blocks?

The heart of the finite-element method is the generation of the stiffness matrix for a single element. In general we, as users, are not in the business of generating elements, but we need to know how they work and their limitations. As discussed above, there are many ways of generating these element stiffness matrices; the examples presented in Fig. 6 show the basics. The unit-displacement method in Fig. 6a is based on the loads necessary to produce a single unit degree of freedom. The forces required to produce this unit deflection produce the stiffness matrix directly (note that the loads are pounds per inch of deflection). By proceeding through all the degrees of freedom on the element, the entire element stiffness matrix is generated. Similarly, the second method in Fig. 6b involves solving the equilibrium equations and leads to the same direct stiffness approach.

Castagliano's theorem (Fig. 6c) is a strain-energy method that has broad application to the development of an element stiffness matrix. An even more general and widely used approach is the "minimum of the total potential." As illustrated in Fig. 6d, the total potential is a function of the strain energy, the work of the external loads, and the kinematic energy. The primary drawback of the minimum-total-potential

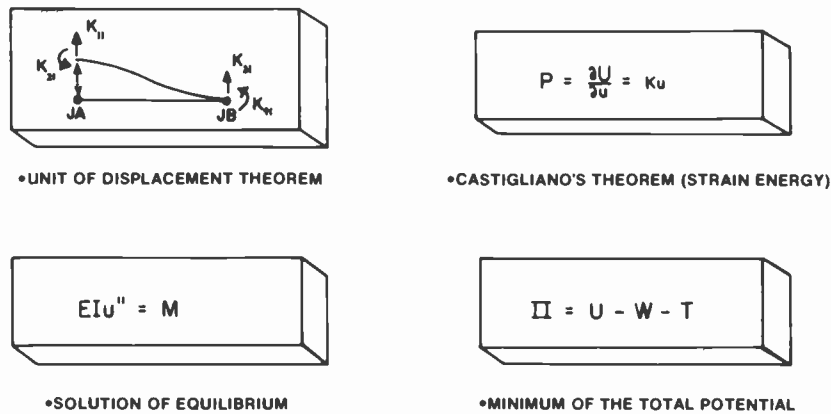


Fig. 6
Generating the element stiffness matrix can be done in a number of ways. Of the four shown here (and explained in text), the "minimum of total potential" is the most general and most widely used. Users do not normally generate elements, but must be aware of limitations in the process.

method is in accurately determining the strain energy. Just as in the commonly used Rayleigh-Ritz method, a deformed shape function (typically a polynomial series) must be assumed in order to obtain an expression for the strain energy. This is an approximation, however, just as in all strain-energy work. The finite-element techniques based on these methods, therefore, are only as good as the shape functions that are used.

As we learned in basic mechanics, if the shape function matches the actual system perfectly, then the calculated strain energy will be accurate. If there is any mismatch on either side of the true deflection patterns, then some higher strain energy exists in the math model. This higher strain energy implies that you have a stiffer system, which results in smaller deflections for given loads. Finite-element techniques,

therefore, will always lead to stiffer-than-actual results if they are based on a strain-energy approach. Since the finite-element solution approaches the true solution from the stiff side, it is important to know how good these shape functions are. Fortunately, over the years, these techniques have been developed to a highly reliable method—any of the commercially available programs can be selected as being accurate and dependable.

What are the outputs?

Remember that the finite-element method calculates the deflections as its basic output for a static analysis. If stresses are required, the method has to go back to the element stiffness matrix. It depends, once again, on those element shape functions. For example, if the engineer wants to know the stresses from the applied loads for a

particular element in the model, the deflections of the system must be calculated first. Then, using the distortions of the element, the stresses are calculated from the element stiffness matrix. So, the stress analysis depends highly on the accuracy of the element shape function. Guidelines suggest that it is important to be conservative with this point. If you have rapidly changing stress patterns, put a large number of elements in that area and gradually increase the element size as the stress gradient decreases. This is where experience and judgement pay off.

The finite-element method produces a powerful tool for the dynamic analysis of a system.

Finite-element analysis can produce the frequencies, mode shapes, modal forces, and the generalized mass of a dynamic system. The main part of this eigenvalue process lies in determining the frequencies and mode shapes derived from the stiffness and mass matrices. Knowing these modal characteristics, the harmonic, random, acoustic, and transient response analyses can be carried out by a number of normal-mode methods. These normal-mode methods are built into the commercially available programs or the modal characteristics can be used in other special-purpose dynamic-analysis programs. In either case, the finite-element model is the primary tool for generating the modal properties—it produces both the stiffness and mass matrices and must be able to produce accurate mode shapes over a wide frequency range. This is especially true when calculating loads and stresses, where a significant number of modes must be superimposed for accurate results. So, once again, in setting up a dynamic model, the user must exercise good judgement and planning to get accurate results.

Using the finite-element method at Astro Electronics

G. Varadarajan

Now that we've seen the advantages of using the finite-element method, let's see some examples of structural analysis. Although the method has very wide application (see the box on the opposite page), we will only go into detail about how Astro Electronics has used it.

Finite-element analysis plays an important role in present-day spacecraft structural

analysis because spacecraft are being designed for increased performance and lower weight. Designers attempting to meet these requirements need to be able to predict the characteristics of these advanced designs accurately, and the finite-element method does so quite well.

Also, the spacecraft and many of its individual substructures and subsystems

must pass qualification and acceptance tests that simulate launch and orbit loads to verify their structural integrity. Accurate and cost-effective finite-element models of these structures are created to perform a set of analyses that will predict the response of the structures for the given test loads. This allows the designer to make changes on paper rather than in metal so that, for example, the structural tests can be passed

Where we've used the finite-element method at RCA

Spacecraft design, as described in the accompanying article, has been one of the major applications of the finite-element method (FEM) at RCA. There, FEM calculations are used to understand the responses to mechanical forces so that stresses, displacements, and frequencies of vibration can be predicted before construction of the spacecraft begins.¹⁻² Such structural applications are typical of the finite-element work being done throughout RCA, although the method has been extended to solve problems involving heat flow and electrostatic fields.³ The following synopsis of non-spacecraft applications at RCA indicates how the FEM may simplify a broad range of applications and reduce the time spent on them.

Color picture tubes. The FEM has been used to analyze existing and new tube designs. This work⁴ examined the stresses caused by: atmospheric pressure acting on the evacuated bulb, as a function of bulb geometry; manufacturing tolerances that allow for less than perfect alignment of mating parts; implosion-protection band placement and tension levels; and thermal processing history. The shadow mask can also be modeled to determine vibrational characteristics and the effects of heating by the impinging electron beam. These FEM calculations provide hard numbers in places that are often difficult to probe experimentally. Further, they provide understanding of the nature of a problem (for example, whether glass breakage is related to basic design and material incompatibilities or to poor thermal processing schedules). The accuracy of these calculations is impressive: when the proper boundary conditions are applied, the calculated stresses and frequencies are virtually identical with those determined experimentally after the structure is fabricated and tested.

High-energy tubes for fusion power. The design of a 25-megawatt switching tube and a 24-megawatt (thermal) neutral beam absorber for the Princeton Plasma Physics Laboratory fusion research program was performed utilizing the FEM.⁵ Because the FEM could handle nonlinear material properties and heat-convection coefficients, it was indispensable in the solution of the transient and steady-state heat transfer and the thermally-induced stresses in the water-cooled power tube anode sections. Based on these calculations, the tube was built and has been successfully tested. Also, the FEM optimized the fin design for the transfer of heat from the impact area of the incident, non-neutralized beam to an internal cooling water channel and minimized the thermally-induced stresses and the accompanying distortion. Both would have been difficult otherwise.

Broadcast towers. The natural frequencies of vibration of guyed or free-standing broadcast towers subject to wind loading, thermal expansion, and nonlinear guy-wire characteristics are treated by a finite-element program (TVTWR) developed by Dr. R. Pschunder in Moorestown. This program is on the RCA computer system in Cherry Hill and is available for general use within RCA. A typical analysis requires about 2 to 4 hours of preparation and about 10 dollars of computer time. This is a considerable saving over a 3- to 4-week effort to produce the solution by hand analysis. Dr. Pschunder has also developed DYNA-3, a large, general-purpose finite-element program used initially to analyze **ships structures** for the AEGIS program. The program has both static (point, line, and area loads, spin, sway, and g-loads) and dynamic (steady state, 3-D shock, and random-frequency driving inputs) as well as thermal capabilities. The output is both tabular and graphic. DYNA-3 is also on the Cherry Hill computers.

Other analyses have been directed toward predicting the strength and deformation of **silicon wafers** supported on a ring and subjected to a point load as a means of understanding wafer breakage.⁶ Since currently available textbook-type formulas are not available to analyze both the membrane and the bending properties for large deflections, a FEM analysis is the only practical solution. Dr. R. Stepleman at the Laboratories has developed the POT3-D program, a finite-element-type method useful for the design of **non-circular electron lenses**.⁷ Stresses and deformation of the **Videodisc** resulting from the force of the pickup stylus have been analyzed by Dr. A. Bell to provide insight into the response of the polyvinyl-chloride base material; the accuracy obtained would have been difficult without FEM. The FEM approach has also proven valuable in the thermal analysis of new types of **electronic circuit boards** by J. McCusker.

The above are but a few of the problems at RCA that have been successfully addressed by the FEM using commercial (ANSYS, STARDYNE, NASTRAN, STRUDL) and RCA proprietary (DYNA-3, TVTWR, POT3D) programs. Outside of RCA, others have used FEM to solve problems⁸ in crack and fracture analysis,⁹ fluid flow and transport (such as dispersion of pollutants in Massachusetts Bay), nonlinear plasticity and creep, impact, vehicle crashworthiness, soil-structure interaction, buckling, and magnetism. In these applications, the FEM predictions generally differ less than 10% and in many cases less than 1% from the experimentally-observed values.

A number of people within the Corporation, as follows, have used these FEM programs and would be willing to serve as consultants in their use:

- ANSYS (2D, 3D, structural thermal, fluid flow, dynamic): R. Bauder and A. Bowalick, Lancaster, or R.E. Enstrom, Princeton.
- DYNA-3 and TVTWR (structural, vibration): R. Pschunder, Moorestown.
- NASTRAN, STARDYNE, STRUDL (structural, dynamic): W. Metzger, G. Niederoest, and A. Sheffler, Astro-Princeton or D.A. Graves, Moorestown.
- POT3D (electronic lens design): R.S. Stepleman, Princeton.

References

1. A. Sheffler; "An overview of finite element methods and their applications to engineering problems," to be published, *RCA Review*.
2. G. Niederoest; "Finite element methods in spacecraft dynamic analysis," to be published, *RCA Review*.
3. The presentations at the RCA Finite Element Symposium held at RCA Laboratories in Princeton in March, 1978, are on videotape and are available from R. Enstrom, the Symposium Chairman.
4. R.E. Enstrom; R.S. Stepleman, and J.R. Appert; "Application of finite element methods to the analysis of stresses in television picture tubes," to be published, *RCA Review*.
5. R.C. Bauder; "Finite element analysis of a twenty-five megawatt power tube and a high energy water cooled heat sink for fusion research," to be published, *RCA Review*.
6. R.E. Enstrom and D.A. Doane; "A finite element solution for stress and deflection of a centrally loaded silicon wafer," *Extended Abstracts*, Vol 78-1, p. 666, Electrochemical Society Spring Meeting, May 1978.
7. S.A. Keneman, R.S. Stepleman, and J.B. Harrison, Jr.; "Design of non-circular electron lenses using POT3D—a finite element type method," presented at RCA Finite Element Symposium, Mar 1978.
8. R.E. Enstrom; "Recent developments in finite element methods," *Company private technical report*.
9. T.H.H. Pian; "Variational and finite element methods in structural mechanics," presented at the RCA Finite Element Symposium and to be published in the *RCA Review*.

—R.E. Enstrom, RCA Laboratories, Princeton

at minimum weight. The type of model and its level of detail are determined by the performance requirements of the structure, the nature of the loads experienced by it, the type of analyses to be performed, and the degree of accuracy required.

What do spacecraft designers have to know about the spacecraft structure?

The spacecraft designer must do much more than make it light and strong. Adequate frequency separation is required between the primary structure and the various substructures and subsystems to avoid cascading responses for vibratory loads. Deflections produced by launch loads should not overcome available clearances between the spacecraft and the shroud/heatshield.

Structure strength is important for launch and orbit loads input to avoid yielding, instabilities, fracture, or failures. Fatigue life is considered in some orbit loads analyses because of the repetitive nature of the loading during the mission life of the spacecraft.

Instrument alignment and spacecraft stability are important in the orbit-load

analysis. Results from the dynamic analysis of the spacecraft in orbit configuration are often used as inputs for further advanced attitude-control analyses.

The loads on spacecraft are many and complex, and are different during launch and in orbit.

Launch loads consist of static acceleration, vibration, and acoustic inputs from the launch vehicle. Heat soakback into the structure from the engine and radiation heat transfer from engine plume are some examples of thermal loads occurring during launch.

The principal orbit loads in the spacecraft are caused by thermal gradients and fluctuations in the structure and subsystems. These loads come from two sources—systems and instruments in the spacecraft, and radiation between the spacecraft and sun, earth, and cold space. Centrifugal forces in spin-stabilized spacecraft and on-orbit maneuvering and deployment of solar arrays, antennas, etc. are some of the other orbit loads.

Typical loads input to the computer model are given in terms of uniform acceleration

levels in spacecraft thrust and lateral directions for static analysis, and shaped acceleration level over a frequency range for sinusoidal vibration input. Acoustic and random vibration levels are specified in terms of sound pressure levels in decibels and power spectral density in g^2/Hz over a given frequency range. Thermal loads are in the form of temperature distributions over the spacecraft structure and subsystems.

Specifically, these loads are used as inputs to the following types of analysis:

- modal analysis for the extraction of the natural frequencies of the spacecraft primary structure, substructures, and subsystems;
- harmonic analysis to simulate the vibratory loads experienced during launch;
- acoustic and random vibration analyses to simulate the noise levels during launch;
- static analysis to simulate the thrust exerted by the launch vehicle; and
- thermal distortion analysis to consider the temperature gradients caused by heat input and output in the spacecraft during launch and orbit.

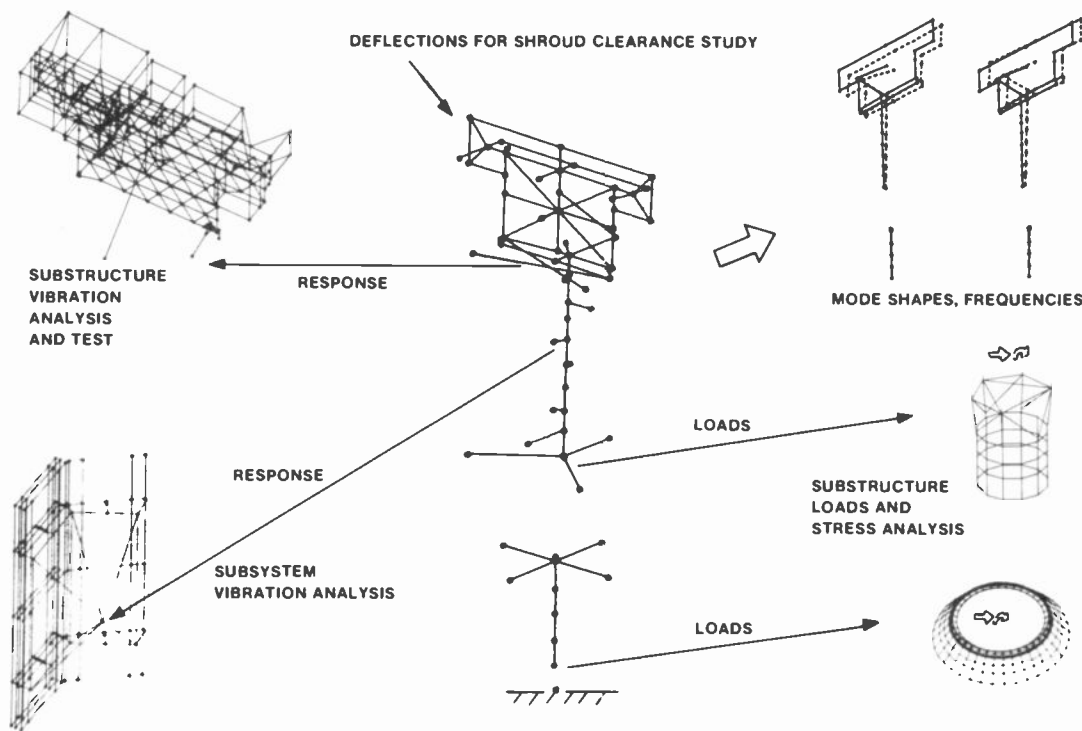


Fig. 7
Finite-element dynamic model of spacecraft was used to determine clearances between shroud and spacecraft while the liftoff forces and vibrations were present. Most of the structure is represented by simple equivalent beams and springs (center), determined by subsystem finite-element analysis (shown in gray). Vibration-mode shapes and frequencies (upper right) are outputs.

These analyses are done for the overall spacecraft and for subsystems and substructures. In each case, complex portions of the spacecraft are reduced to simple spring, beam, and plate elements (by adding stiffness matrices) of appropriate degrees of freedom.

The spacecraft dynamic model is a good example of the finite-element method at work.

The principal objectives behind the construction of the spacecraft dynamic model are to extract the various natural frequencies and mode shapes of the primary structure and obtain the loads and deflections in the spacecraft for vibratory loads.

The dynamic model, in most cases, does not represent the actual geometry of the structure. The major load paths in the structure, the primary structure stiffness, and mass and inertia distribution of the spacecraft are, however, adequately represented to simulate the actual dynamic behavior of the spacecraft. Proper construction of the model ensures the extraction of responses at convenient locations in the spacecraft structure for input to substructural analysis and test.

Simple and modular representation of the spacecraft using simple elements like beams and springs in the dynamic model makes modifications in the finite-element model relatively easy, a feature that is extremely useful in the proposal stages and early design stages of a spacecraft program.

Fig. 7 shows a spacecraft dynamic model. While most of the structure is represented by simple equivalent beams, the most complex structures are condensed to spring elements in the form of stiffness matrix additions developed from separate detailed substructure models. Asymmetrical stiffnesses are modeled by an offset of the neutral axis of each component from the spacecraft thrust axis.

After the model is complete, the designers input the appropriate loads, and the finite-element program calculates the model's responses. Acceleration responses and loads are used for further detailed substructure and subsystem loads and stress analysis, and also as inputs for their qualification and acceptance vibration tests. The deflection data are used for shroud clearance studies. All these data are

later verified during qualification and acceptance tests.

Astro Electronics uses the finite-element method throughout all the stages of spacecraft design.

Even though a detailed set of analyses using the different finite-element models of a structure is carried out mainly under a spacecraft contract program, the finite-element method is also used extensively in the proposal stages of a prospective contract program. The simple and cost-

effective dynamic model is an invaluable tool for structural design in the proposal stages and in the early design stages. More complex models of the spacecraft structures and substructures are usually used for detailed loads and stress analysis. The analytical predictions of the structural responses and loads are also verified by qualification and acceptance tests before the actual launch. The finite-element method thus plays a valuable role in spacecraft design, analysis, and test at the RCA Space Center.

Bill Metzger has over twenty years experience in the engineering of mechanical systems for aerospace vehicles. Since 1972, he has worked at Astro Electronics where he is currently Manager, Mechanical Engineering. In this position, he has initiated new methods in finite-element analysis of structures, advanced composite materials applications to spacecraft structures, normal-mode vibration testing of structures, thermal analysis of spacecraft components, and compact electronic packaging.

Contact him at:
Mechanical Engineering, Astro Electronics, Princeton, N.J., Ext. 2912

Raja Varadarajan has been with Astro Electronics since 1975, working on computer-aided analysis of spacecraft structures and subsystems using the finite-element method. He has also done qualification vibration testing of spacecraft subsystems and worked on the mechanical design and analysis of space shuttle tv camera subsystems.

Contact him at:
Mechanical Engineering, Astro Electronics, Princeton, N.J., Ext. 2443

Al Sheffler joined the mechanical engineering staff at Astro Electronics in 1973 and has developed numerous finite-element modeling techniques for the static and dynamic analysis of lightweight spacecraft structures. Currently, he is Manager, Structural Analysis, and is responsible for the analysis, design, and testing of many of the current communications and meteorological spacecraft. Prior to joining RCA, he was on the Aerospace Engineering teaching staff at West Virginia University, where his research work included the development of a finite-element method for the analysis of laminated composite materials.

Contact him at:
Mechanical Engineering, Astro Electronics, Princeton, N.J., Ext. 3241

Bill Metzger, left, and **Raja Varadarajan** at a video terminal used to input finite-element grids. **Al Sheffler**, standing behind the terminal, is holding hard-copy output.



GaAs field effect transistors—versatile devices for microwave applications and gigabit logic

F. Sterzer

They're very, very fast.

The importance of field effect transistors (FETs) in electronic technology has increased dramatically during the past two decades. Digital integrated circuits using Si MOSFETs have grown into an industry that produces hundreds of millions of dollars worth of products ranging from simple flip-flops to LSI circuits such as microprocessors. In analog applications, Si MOSFETs are widely used today at frequencies below the microwave range, particularly in applications where linearity, high input impedance, or freedom from second breakdown are important. FETs made from gallium arsenide (GaAs) have established a strong position at microwave frequencies, and are generally considered to be the most important new solid-state microwave devices of the past decade and a half. GaAs FETs also show promise for digital applications at gigabit rates.

RCA scientists and engineers have made major contributions to the development of GaAs FETs. The first GaAs FETs reported in the literature were built in 1965 by Hans Becke at the RCA Solid State Division in Somerville, N.J.¹ The industry's first

microwave power GaAs FETs were described in 1973 by Louis Napoli, John Hughes, Walter Reichert and Stewart Jolly of the RCA Laboratories in Princeton, N.J.² Record efficiencies for GaAs microwave FET amplifiers were demonstrated by Ho Huang, Ira Drukier, Raymond Camisa, Yegna Narayan, and Stewart Jolly, also of the RCA Laboratories.³ Today, members of the Microwave Technology Center (MTC) of the RCA Laboratories are developing GaAs FETs for a variety of specific applications relating to communications, radar, electronic warfare, and even to the transmission of power from space to Earth. Sample quantities of power GaAs FETs can be obtained from the Center.

How do GaAs FETs work?

In field effect transistors the flow of charge carriers from a source electrode to a drain electrode is controlled by one or more gate electrodes. These gate electrodes can be metallic Schottky barriers (MESFETs), p-n junctions (JFETs), heterojunctions (HJFETs), metals on insulating layers

other than oxides (MISFETs or IGFETs), or metals on semi-insulating semiconductor layers (SIGFETs).

The high-frequency performance of FETs fabricated from GaAs is, in general, substantially better than the high-frequency performance of similar FETs built from silicon. GaAs has a higher electron bulk mobility and greater maximum electron drift velocity than silicon. Furthermore, the electron mobility in submicron films of n-type GaAs grown on semi-insulating GaAs approaches the bulk value. In contrast, the electron mobility of thin films of silicon are grown on insulators such as sapphire is significantly poorer than the bulk value. As a result, GaAs FETs, in general, exhibit lower parasitic series resistances and higher transconductances than similar silicon FETs.

At the present time the most popular GaAs FETs for microwave applications are Schottky-barrier FETs. Fig. 1 is a schematic diagram of a single-gate GaAs Schottky-barrier FET. In this transistor,

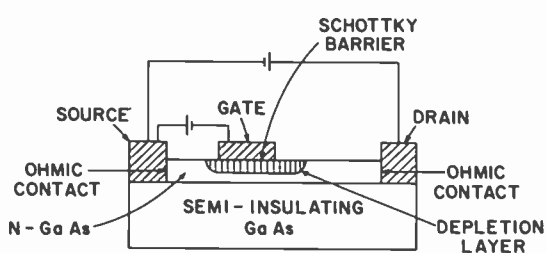


Fig. 1

Schottky-barrier GaAs FET works by using a gate to control the flow of electrons from source to drain as they move through a thin layer of n-type GaAs. The negative voltage on the gate produces a depletion layer that blocks the flow of electrons moving through the n layer. The higher the negative potential on the gate, the deeper the depletion layer penetrates into the n-layer, and the higher the resistance between source and drain. Cutoff occurs when the depletion layer reaches the semi-insulating substrate.

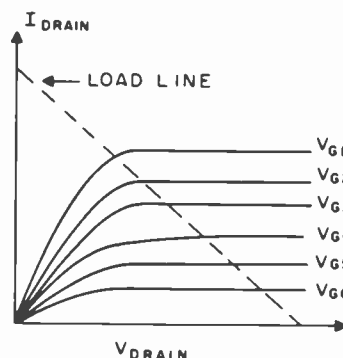
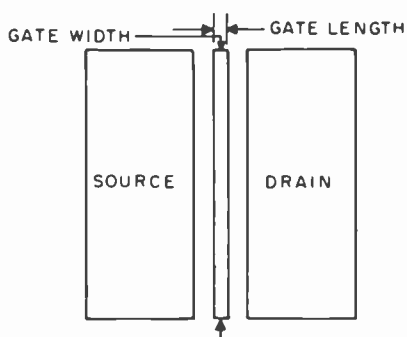


Fig. 2

Characteristic curves—drain current versus drain voltage for a Schottky-barrier-gate GaAs FET as a function of gate voltage. Moving from V_{G1} to V_{G6} , the gate voltages are increasingly negative.

electrons flow from the source to the drain through a thin layer of n-type GaAs. The flow of these electrons is controlled by the depth of the depletion layer formed underneath the Schottky barrier gate: the higher the negative potential on the gate, the deeper the depletion layer penetrates into the n-layer, and the higher the resistance between source and drain. (Electrons cannot travel through the depletion layer.) When the depletion layer reaches the semi-insulating substrate, current flow between source and drain is cut off. The I-V characteristics resulting from this type of gate action are shown in Fig. 2.

The structure of FETs with p-n junction gates is similar to that of the MESFET of Fig. 1. Instead of a Schottky-barrier gate there is a back-biased p-n junction. The resistance of the channel between source and drain is a function of the depth of penetration into the n-layer of the depletion layer of the p-n junction.

Fig. 3 is a schematic diagram of a majority-carrier GaAs MISFET. MISFETs can be operated as enhancement-mode transistors (drain current increases with increasing positive gate voltage), or as depletion-mode transistors (drain current decreases with increasing negative gate voltage). In enhancement-mode MISFETs, a negative bias on the gate depletes the number of electrons in the channel, increasing the channel resistance.

In many applications it is useful to have a transistor with two gates in series. Such tetrode configurations are usually referred to as dual-gate transistors. Fig. 4 is a

schematic diagram of a dual-gate Schottky barrier GaAs FET.

Microwave applications

GaAs FETs can do a superior job in many different types of microwave functions. They are excellent for amplifying, generating, switching, limiting, detecting, frequency multiplication, frequency discrimination, etc. In fact, the microwave portion of a number of systems can be built entirely around GaAs FET circuits.

GaAs FETs are particularly attractive devices for small-signal and medium-power microwave amplifiers.

Since GaAs FETs are multi-port devices, amplifiers using GaAs FETs do not require circulators or hybrid circuits to separate input and output signals, as is the case with Impatt or conventional transferred electron amplifiers. The small-signal behavior of GaAs FETs can be accurately characterized by means of S-parameters, so that small-signal GaAs amplifiers can be designed using well-established computer-assisted techniques. The noise figures of GaAs FET amplifiers up to frequencies of about 30 GHz are lower than that of any other microwave amplifier except for parametric amplifiers and masers, both of which are, in general, substantially more expensive than low-noise GaAs FET amplifiers. Up to approximately 20 GHz, the efficiency, bandwidth, and linearity of medium-power cw GaAs FET amplifiers tend to be superior to that of amplifiers using competing solid-state devices. Finally, GaAs FET amplifiers can be pulsed on



Fred Sterzer and GaAs device.

Fred Sterzer is Director of the RCA Laboratories Microwave Technology Center, and has over twenty years of experience in the microwave field.

Contact him at:
Microwave Technology Center
RCA Laboratories
Princeton, N.J.
Ext. 2633

Reprint RE-24-3-9
 Final manuscript received August 22, 1978. A similar version of this article appeared in *Microwave Journal*, Nov 1978.

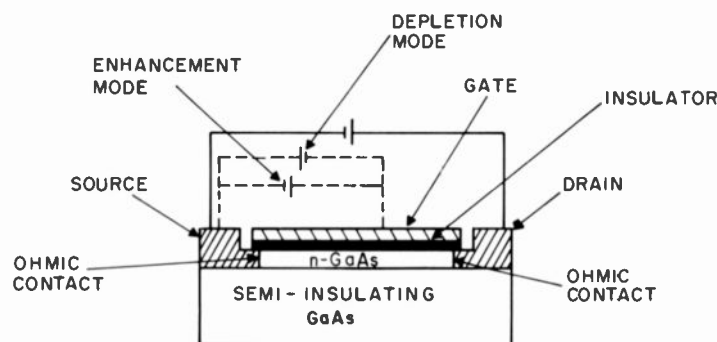


Fig. 3 Insulated-gate FET (IGFET or MISFET) can operate in depletion or enhancement mode, depending on the voltage applied to the gate.

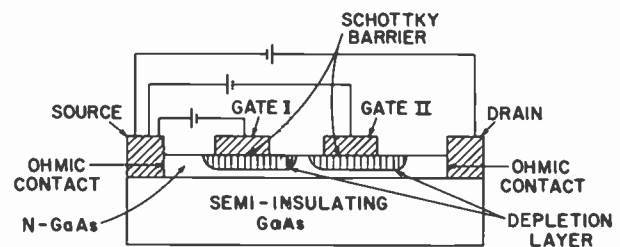


Fig. 4 Dual-gate configuration is often useful, with each gate accepting a separate input.

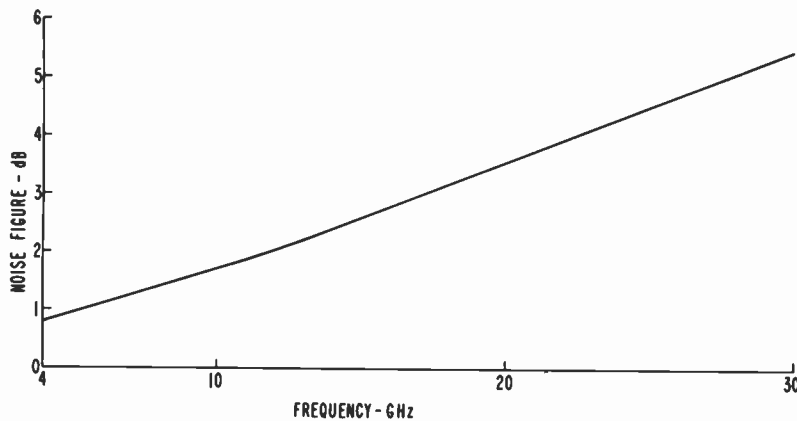


Fig. 5
Best noise figures obtained to date for room-temperature operation of GaAs FETs. Values for commercially available transistors are significantly higher than those shown here; lower noise figures are possible by cooling devices to below room temperature.

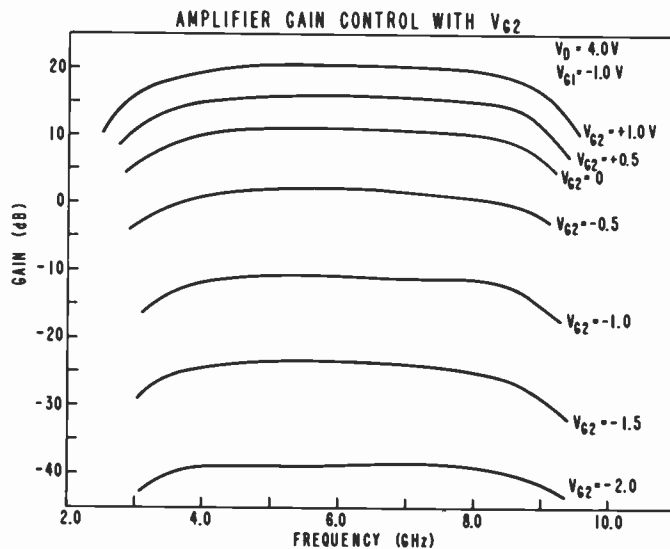


Fig. 6
Variable gain is possible in dual-gate FET operation by applying rf input signal to the first gate and dc control voltage to the second gate. Note the large change in gain possible (+20 dB to -40 dB) with a small change in dc voltage (+1 V to -2 V).

or off in tens of picoseconds, and AGC is simple to implement, particularly in amplifiers using dual-gate transistors.

At present, the most widespread use of GaAs FETs is in low-noise amplifiers.

GaAs FETs designed for low-noise applications have Schottky-barrier gates with typical gate length of the order of 0.5 to 1.0 μm . Fig. 5 is a graph of the best spot-noise figures obtained to date at room temperature as a function of frequency. These experimental noise figures are somewhat higher than the theoretically predicted values for GaAs MESFETs with 0.5- μm gate length. The noise figures of commercially available amplifiers, or amplifiers designed for wide bandwidth, a.e., of course, significantly higher. The best

noise figures of commercially available transistors range from about 1.5 dB at 4 GHz to a little over 3 dB at 12 GHz.

Lower noise figures than those shown in Fig. 5 can be obtained by cooling the FETs below room temperature. For example, workers at Bell Laboratories have reported a noise figure of 0.4 dB at 4 GHz from an FET cooled to 77° K.

Many microwave applications require variable-gain amplifiers.

Amplifiers using dual-gate FETs are particularly useful in such applications because their gain can be controlled with dc voltages. The rf input signals are applied to the first gate of the transistors, and the dc

control voltages to the second gate. Fig. 6 shows gain versus frequency as a function of dc bias voltage on the second gate of a two-stage dual gate GaAs FET amplifier (graph courtesy of J. Goel, RCA Laboratories, Princeton, N.J.). Note that the gain of this amplifier can be continuously varied from +20 dB to -40 dB by varying the voltages on the second gate from +1 V to -2 V.

Power amplifiers using GaAs FETs can be highly efficient.

The highest cw power outputs obtained to date from single GaAs FETs range from close to 20 W at 4 GHz to several watts at 10 GHz, to between 1 to 2 W at 15 GHz and several hundred milliwatts in the 20-25 GHz range. The best reported efficiencies range from close to 70% at 4 GHz to 30-40% at 5-10 GHz, 10-20% at 16 GHz, and 5-10% at 33 GHz. The highest commercially available cw power outputs range from about 5 W at 6 GHz to 1 W at 12 GHz.

The maximum power output that can be obtained from power FETs is limited by several factors. First, there is a limit to the size of the transistor. In order to have reasonably uniform distribution of voltages and currents, the maximum dimensions of the transistor pellet must be kept to a fraction of the operating wavelength. Furthermore, the gate width cannot be made too long because of impedance considerations. The longer the gate width, the lower the impedance of the transistor, and the more difficult it becomes to match to the high-power transistor over wide bandwidth. Designers of power FETs are now attempting to minimize this impedance problem by incorporating impedance transformation networks as close to the transistors as possible.

Another factor that can limit the power output of FETs is the maximum allowable temperature rise in the transistor. The MTBF of GaAs FETs generally decreases exponentially with increasing temperature. It is therefore highly important to minimize the thermal resistance of power transistors, since some high-power transistors must dissipate tens of watts of dc power. One method of achieving low thermal resistance is to plate metal posts on the source, gates, and drain of the transistor, and then flip-chip mount the transistor on a beryllia carrier (see Fig. 7, courtesy of Dr. E.F. Belohoubek, RCA Laboratories, Princeton, N.J.).



Fig. 7
Flip-chip mounting helps increase power output by minimizing thermal resistance of the power transistors and so keeping down the operating temperature. Transistor shown here had metal posts plated on its source, gate, and drain before it was flip-chip mounted on its beryllia carrier.

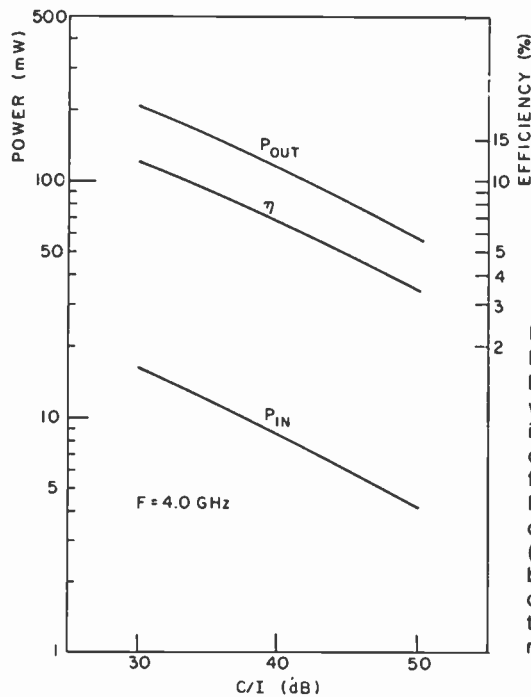


Fig. 8
MESFETS can have high linearity designed in over wide dynamic ranges. This is an advantage in satellite communications systems, for one example. Good linearity produces low carrier-to-intermodulation (C/I) ratios, or interference between carriers. Many carriers can then operate in the same satellite communications channel.

The performance of power MESFETs is also limited by the maximum permissible gate currents. If the rf voltage on the gate of a power MESFET swings to a positive value greater than the barrier potential, the Schottky-barrier gates will start to draw significant forward gate currents. These currents, if they become too large, will destroy the transistor. In FETs with insulated gates there is no gate conduction current irrespective of whether the gates are driven positive or negative, provided, of course, the gate voltages are not large

enough to break down the gate insulators. This is one of the reasons there is interest in MISFETs for microwave power generation. Encouraging microwave performance of GaAs MOSFETs in both enhancement- and depletion-mode operations has recently been reported by Mimura *et al.*⁴

GaAs FETs have qualities useful in many other high-frequency analog circuits.

Linear amplifiers. GaAs MESFET amplifiers can be designed to exhibit ex-

cellent linearity over large dynamic ranges. This is because uniformly doped MESFETs have a square-law transfer characteristic. Fig. 8 shows the relationships between input and output power, efficiency, and carrier-to-intermodulation ratio for a 4-GHz MESFET amplifier designed for a combination of good linearity and high efficiency. Note that an efficiency of about 12% was achieved for C/I ratio of 30 dB (courtesy of Dr. F. Sechi, RCA Laboratories, Princeton, N.J.).

Why use GaAs FETs? and where?

Nearly all transistors in use today are made from silicon. Why do we need transistors made from GaAs?

The answer is that transistors fabricated from GaAs have lower noise figures, higher gain-bandwidth products, are more efficient, can operate at higher frequencies, and can be switched faster than similar transistors fabricated from silicon. These advantages of GaAs transistors over silicon transistors are due to the superior electronic properties of GaAs crystals: the mobility of electrons is several times as great in GaAs than in silicon, and the maximum electron velocity is about twice as great in GaAs than in silicon.

The major disadvantage of GaAs FETs is that they are currently a lot more expensive than silicon transistors. As a result, GaAs FETs are used today mostly in microwave applications such as satellite ground stations, point-to-point communication links, radars, electronic warfare systems, etc. where it is usually cost-effective to pay a premium for performance. However, laboratories around the world are trying to reduce the cost of GaAs FETs. It is therefore likely that GaAs FETs will eventually become cost-effective in applications involving frequencies below the microwave range, such as, for example, in low-noise preamplifiers in UHF-TV tuners.

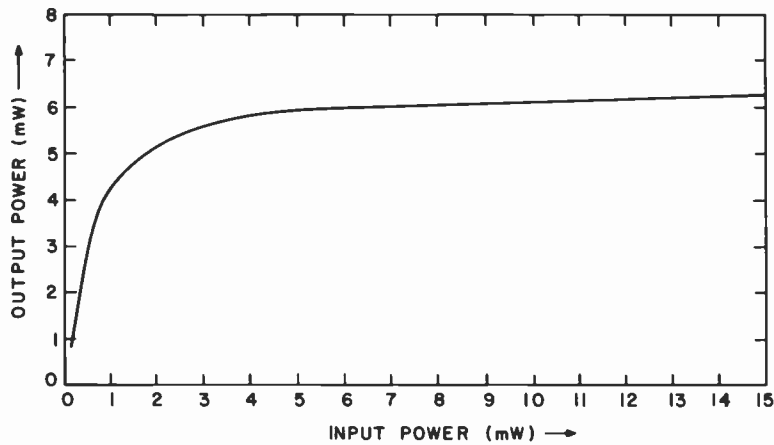


Fig. 9 Limiting action of dual-gate MESFET, a result of "hard" saturation, is important in many applications.

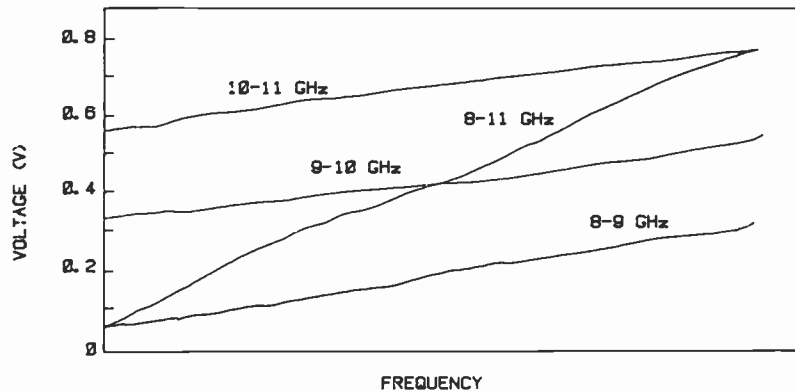


Fig. 10 Wideband frequency discrimination is possible with GaAs FETs and simple filter networks.

Limiters. GaAs FET amplifiers saturate "hard" and are therefore useful in applications requiring limiters. The limiting action of a dual-gate MESFET amplifier is shown in Fig. 9 (courtesy of J. Goel, RCA Laboratories, Princeton, N.J.).

Frequency discriminators. GaAs FETs can be combined with simple filter-type networks to fabricate wide-band frequency discriminators. Fig. 10 illustrates the performance of such a discriminator covering the 8- to 11-GHz frequency range (courtesy of D.D. Mawhinney and A. Rosen, RCA Laboratories, Princeton, N.J.).

Frequency multipliers. GaAs FETs, particularly transistors with dual gates, can be used to construct frequency multipliers with conversion gain. In a dual-gate FET

multiplier, the input signal is fed into the first gate, and the second gate and the drain are tuned to maximize the desired harmonic output. At milliwatt power levels, conversion gains of several dB have been obtained with doublers and triplers at 16-GHz output frequencies.⁵

Frequency mixers. GaAs FET mixers, unlike conventional diode mixers, can be designed to have conversion gain,⁶ or be self-oscillating mixers.⁷ The noise figures of GaAs FET mixers reported so far are, however, somewhat higher than the best reported noise figures for low-noise GaAs FET amplifiers on Schottky-barrier diode mixers.

Dual-gate FETs are particularly simple to use as mixers. The input signal is applied to

the first gate, the local oscillator to the second gate, and the IF frequency is taken from the drain via a low-pass filter.

Oscillators. GaAs FETs produce approximately the same power output and efficiency in oscillators as in large signal amplifiers. Thus, for example, efficiencies of 25-30% with a power output of 1 watt can be readily achieved at 10 GHz.⁸

The noise output of GaAs MESFET oscillators is usually significantly higher than that of transferred electron oscillators (TEOs). However, Dr. Sechi of MTC has recently shown that if care is taken to minimize rf-induced voltage breakdown in the Schottky-barrier gate of the transistor, then noise performance similar to that of TEOs can be achieved.⁹ The voltage breakdown in the gate can usually be reduced to very low values with only a small reduction in power output and efficiency.

Digital microwave circuits

In the past, microwave circuits were exclusively analog.

Recent advances in silicon and GaAs device technology have made it possible, however, to design digital circuits that can change states in small fractions of a nanosecond, thus making it possible for the first time to process digital signals at microwave (i.e., gigabit) rates. This breakthrough of digital technology to the microwave range is likely to have a major impact on many types of microwave applications, including radars, electronic warfare, communications, etc.

Several approaches to building integrated gigabit digital circuits using GaAs FETs are now being investigated in laboratories around the world. Candidate devices include MESFETs, JFETs, and MOSFETs.

Three major types of integrated digital circuits use GaAs depletion MESFETs: TTL, DTL, and circuits using both MESFETs and transferred electron devices.

GaAs TTL and DTL logic circuits can operate at multigigabit rates. Figs. 11 and 12 illustrate how a typical simple logic function (2-input NOR gate) is realized in GaAs TTL and GaAs DTL. Propagation delays of only 80-90 ps have been demonstrated in NOR gates of the type shown in Figs. 11 and 12.^{10, 11} With TTL, a

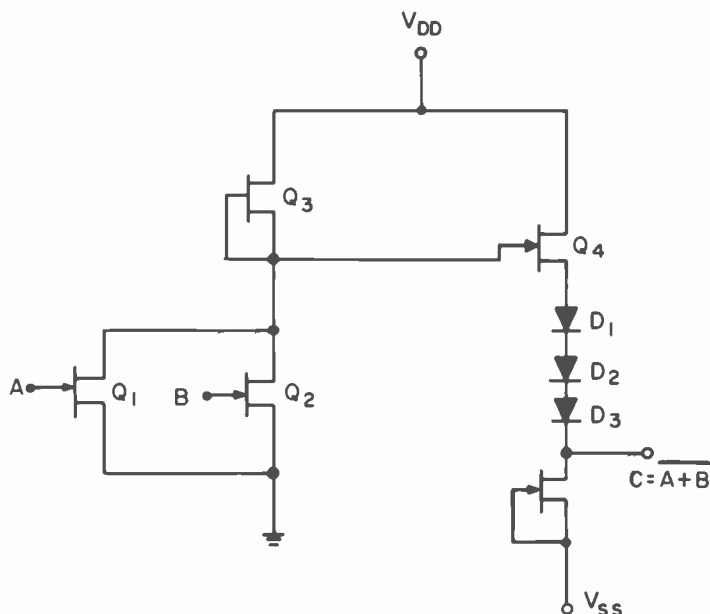


Fig. 11
TTL gigabit logic. In this two-input GaAs NOR circuit, gating is performed by two FETs (Q1 and Q2) that share a common load transistor (Q3). Transistors Q4 and Q5 and Schottky diodes D1, D2, and D3 operate as load drivers and provide the voltage-level shifting required in this circuit for consistent input and output logic levels.

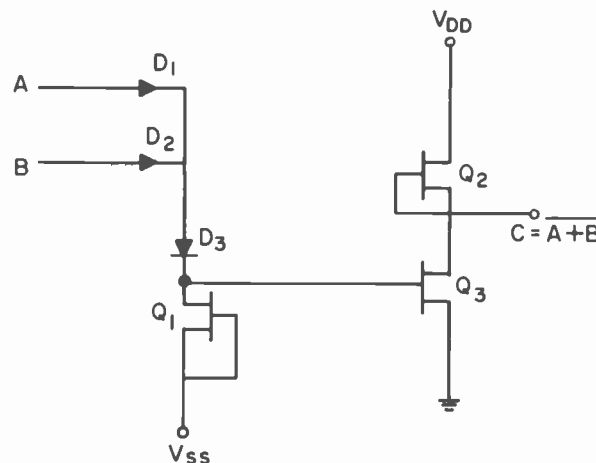


Fig. 12
DTL gigabit logic. In this two-input GaAs NOR gate, diodes D1 and D2 are the logic gates. Diode D3 is for level-shifting, and FET Q1 is a constant-current source biasing the diode network. FETs Q2 and Q3 form an inverter that provides both gain and output current.

3-stage divide-by-eight 4.5-GHz prescaler has been built in MSI form.¹⁰ Of the two technologies, DTL offers lower power dissipation, easier interconnection, and higher packing density. TTL, on the other hand, appears to be less sensitive to variations in device parameters. Both approaches are relatively complex because level shifting is required, and race conditions are likely to be difficult to avoid in large MSI circuits.

A variety of logic systems using transferred electron device depletion MESFET combinations are now under development. With these TED-FET circuits, logic gates can be realized with fewer elements than in TTL and DTL, and gate delays as low as 20 ps/gate have been achieved.¹²

With enhancement-mode FETs, the basic logic circuit is a simple inverter, either with a resistive load or a depletion FET load.

Such inverters can be directly interconnected without level shifting. As a result, enhancement FET logic circuits use the GaAs wafer area more efficiently and dissipate less power than similar circuits using depletion FETs. On the other hand, enhancement logic circuits are generally slower than depletion logic circuits. The best propagation delays reported so far for enhancement JFET inverters in ring counters are about 1 ns (power dissipation

100 μ W), but 200-ps delays are projected for improved JFET geometries.¹³

Recent advances in growing native oxides on GaAs have made n-channel enhancement GaAs MOSFET technology an important contender in the gigabit logic field.¹⁴ Perfection of this technology could lead to LSI gigabit logic circuits.

The future

The future for GaAs FETs in analog microwave applications looks bright. One can confidently predict that in the next few years, GaAs FETs that can operate at low millimeter-wave frequencies will become available, that power output will continue to increase, with several watts at 15 GHz likely, and that noise figures at all frequencies will be further reduced. As the use of GaAs FETs in microwave equipments increases, prices for FETs will come down and most of the device manufacturing will become concentrated in a few companies.

The crystal ball becomes more cloudy when looking into the future of digital GaAs FET devices. A narrow role for gigabit GaAs FET logic in specialized applications such as microwave counters seems assured. The big question, however, is whether cost-effective, broad-based GaAs FET logic families can be developed

to compete with silicon-based logic. GaAs MOSFETs appear to hold the biggest promise to eventually accomplish this.

References

1. Becke, H.: "GaAs MOS transistors," *Solid State Electronics*, Vol. 8, (1965) p. 813.
2. Napoli, L.S., et al.: "GaAs FET for high-power amplifiers at microwave frequencies," *RCA Review*, Vol. 34 (Dec 1973) pp. 608-615.
3. Huang, H.C., et al.: "High-efficiency GaAs MESFET amplifiers," *Electronic Letters*, Vol. 11 (Oct 16, 1975) pp. 508-509.
4. Mimura, I., et al.: "GaAs microwave MOSFETs," *IEEE Trans. Electron Devices*, Vol. ED-25, (Jun 1978) pp. 573-579.
5. Chen, P.L., et al.: "Dual gate GaAs FET as a frequency multiplier at K_a-band," *Digest, 1978 IEEE MTT-S International Microwave Symp.*, pp. 309-311.
6. Gipps, S.C., et al.: "An X-band dual gate MESFET image rejection mixer," *Digest, 1978 IEEE MTT-S International Microwave Symp.*, pp. 300-302.
7. Iajima, Y.: "GaAs FET applications for injection-locked oscillating mixers," *Digest, 1978 IEEE MTT-S International Microwave Symp.*, pp. 303-305.
8. Rector, R.M., and Vendelin, G.D.: "A 1.0-watt GaAs MESFET oscillator at X-band," *Digest, 1978 IEEE MTT-S International Microwave Symp.*, pp. 145-146.
9. Sechi, F., et al.: "Waveforms and saturation in GaAs power MESFETs," 8th European Microwave Conference, (Sep 4-8, 1978) Paris, France.
10. Van Tuyl, R., et al.: "4-GHz frequency division with GaAs MESFET ICs," *Digest, 1977 IEEE International Solid-State Circuits Conf.*, pp. 198-199.
11. Eden, R.C.: "Low power GaAs digital ICs using Schottky diode-FET logic," *Digest, 1978 IEEE International Solid-State Circuits Conf.*, p. 68-69.
12. Hashigume, N., et al.: "20 ps gate Gunn-effect high-speed carry finding device," *Electronics Lett.*, Vol. 14 (16 Feb 1978).
13. Zuleeg, R., et al.: "Femtojoule high-speed planar GaAs E-JFET logic," *IEEE Trans. Electron Devices*, Vol. ED-25, (Jun 1978), pp. 628-639.
14. Colquhoun, A., et al.: "Prospects for GaAs MOSFET Integration," *Radio and Electronic Engineer*, Vol. 48, (Jan Feb 1978) pp. 47-52.

Conflict and cooperation: an environmental success story

M.N. Slater

This is the story of accomplishment... of conflict, cooperation, and a three-year dedicated effort by two teams: one from state government and one from industry. Their joint efforts over that period, sometimes in tandem and sometimes in heated opposition, upgraded Bow Creek from what was, at times, a nearly dead stream to a thriving, biologically hospitable environment, with a healthy diversity of benthic organisms and substantial numbers of native trout, from fingerlings to well over legal size.

The fish kill of 1973

For most of the eighteen years that the RCA Solid State Division has been located at Mountaintop, the Pennsylvania Department of Environmental Resources (DER) and its predecessors have commended RCA for having a model waste treatment system, for its ecological awareness, and for its efforts to achieve clean air and clean water.

An exception occurred in the spring of 1973 when about 50 of the 1200 trout that had been stocked in Big Wapwallopen Creek were reported killed. DER biologists and engineers investigated and concluded that toxic materials contained in the industrial

wastewater discharge were the most probable cause of the kill. (RCA discharges its wastewater into Bow Creek, the nearest upstream tributary into Big Wapwallopen.)

RCA, lacking biological expertise of its own, called in the Academy of Natural Sciences of Philadelphia, which has some of the finest aquatic biologists in the country. The Academy, under the guidance of Dr. Ruth Patrick, Chairman of their Board and Chief Curator of Limnology, determined that the fish were probably killed by a large excess of residual chlorine in cooling water. It was further determined that this chlorine came from the local water company and could not be attributed to RCA. (The water passed untreated through RCA's cooling system). Nevertheless, RCA pursued the problem and was instrumental in arranging for the water company to lower and control its chlorine levels. Since then, the measurement of free chlorine in RCA effluent has remained below the level of detection and there have been no more fish kills.

A new designation and tighter restrictions

The Academy study had suggested some additional changes in the RCA

system to further improve effluent water quality. RCA immediately moved to strengthen its technical staff and began making the suggested changes.

Then, in September 1973, as part of a state-wide effort to upgrade water quality in Pennsylvania waterways, DER issued an order drastically tightening RCA's effluent requirements, and imposing several new and stringent limits. The most severe of these resulted from the classification of Bow Creek, which had not previously been classified, as a "cold-water trout stream."

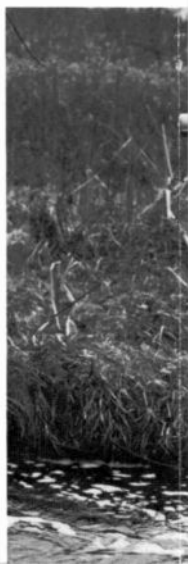
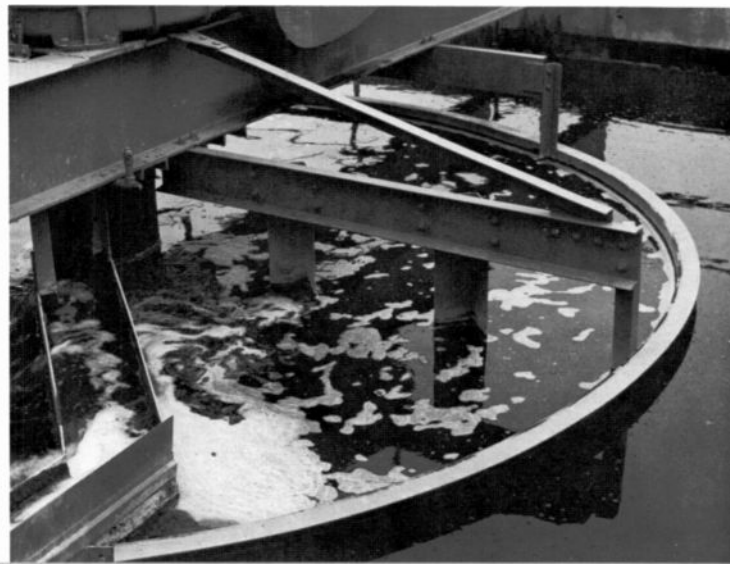
It took RCA some time to obtain the relevant effluent measurements (some never before measured), to investigate and comprehend the effect of the order and, with the advice of RCA Corporate Staff and of several expert consultants, to respond.

Some points of contention

RCA pointed out:

- Earlier Fish Commission reports, issued before the plant was built, had listed Bow Creek as unsuitable for trout, and recommended against stocking;
- It was not possible to reduce effluent fluoride and ammonia (from

Photo captions, left to right. The plastic-ring filters of the Trickling Filter System are black when new, but appear lighter because of layers of bacteria which break down organics in the waste stream. The Primary Clarifier System's wastewater intake is through the trough at lower left of picture. Water outside the ring is clear except for bubbles rising from sludge layer below. This sensor probe provides continuous monitoring of pH in aerated lagoon to help assure proper operation of the effluent control system



story

the plant) or copper (from incoming water, like the chlorine) to the ordered levels by any economically practical techniques; and

- Lower Bow Creek (below RCA's effluent entry) was beginning to flourish with fish and other aquatic life after elimination of the chlorine. This observation was based on stream surveys by DER and the Academy (jointly in the spring of 1974 and several times thereafter).

RCA did not, however, take exception to all parts of the DER order. In fact, the Company surprised DER by urging *tightening* of one parameter, pH, from the DER-ordered 6 to 9 range to 6 to 7.5. This recommendation was based on published information that indicated the lower pH limit would detoxify the ammonia present, and was made in spite of the substantial cost that would result from adding pH monitoring and controls.

Even tighter restrictions

DER accepted RCA's efforts as evidence of its good faith, but insisted on the tighter limits...and added more. It gave as its justification its charter to protect and upgrade the waterways, and the generally accepted literature (California Water Quality

Criteria, and others) which specified these more stringent limits as requirements for a cold-water trout stream.

The major points of contention over the California regulation were the fluoride and ammonia levels which were considered to be acceptable in the effluent. In response to the California data, RCA countered with other literature (Colorado School of Mines, etc.) that showed trout thriving at 32 ppm F vs. approx. 10 ppm in the RCA effluent, and 1 ppm in the DER order; and with data and calculations that proved toxic un-ionized NH_3 would be kept at orders of magnitude below harmful levels if the pH were maintained below 7.5.

An "interview the fish" approach

Lengthy and sometimes heated discussion led to no resolution, until the two sides decided to test reality and "interview the fish" about their own environment.

DER made the suggestion and RCA agreed that a controlled bioassay with actual stream water would be more persuasive than any amount of theory or reference to work performed elsewhere. Accordingly, an eight-day bioassay was planned and conducted by Academy personnel, using 2½" fingerling trout, Upper and Lower Bow Creek water, high and low temperatures, varying pH's, and some cells dosed with double the expected maximum levels of F and NH_3 . All fish

The Story in Brief

Five short years ago, Bow Creek in Luzerne County, Pa., was polluted. Nearly dead. There was little aquatic life and parts of its bottom were coated with a heavy growth of the sewage bacteria *Sphaerotilus*.

Today the stream is a showplace. A "cold-water trout stream," with a healthy population of fish, and an abundance of the mayflies and stoneflies on which trout thrive.

This is the story of the transformation. Of the accusations and conflicts that led to cooperation and accomplishment.

survived all tests except those with both pH above 7.5 and high toxin concentrations.

This "interview" resolved all major issues between DER and RCA. After thousands of hours of hard work and dozens of hours of discussion, some very intense, RCA and DER achieved a much better understanding of the biological system in the stream; substantial agreement on effluent impurity limits and their effect on the biota; and an effective working relationship... as well as a greatly improved stream.

A summary of the actions

In the course of this successful effort to clean-up Bow Creek, RCA has:

- Arranged to reduce chlorine levels;

and the correct stream pH. **The results of effluent control** are obvious: fish (all legal size and mostly trout) were brought to the surface by a "shocker" test conducted a few hundred yards below where the effluent from the RCA Mountaintop facility enters the stream. **Equally convincing** is the clarity and purity of the beaker of water held by L. Pawlusch of the Pennsylvania Department of Environmental Resources.



- Installed aeration equipment to increase dissolved oxygen;
- Installed a novel trickling filter medium (now being copied throughout the country) to reduce organic wastes; and
- Hired additional skilled personnel and instituted tests to monitor and control effluent quality.

Also, the Corporation planned and has nearly completed construction on a major upgrading of its waste treatment system, including:

- A large equalization tank to reduce chemical surges;
- An advanced lime-addition system and high pH at liming to improve clarification and heavy metal precipitation;
- Heavy-duty sludge pumping to improve clarification;
- A flocculation system to remove suspended solids;
- A pH adjustment system for incoming water to prevent corroding copper piping and thereby to reduce copper in the effluent;
- A multi-stage pH control system for the effluent system to assure proper

operation and correct stream pH; and

- Improved sludge handling treatment and disposal.

The Pennsylvania Department of Economic Resources continues its high level of interest in Bow Creek. In addition to their normal monitoring and testing, they have set up periodic intensive stream surveys, including electrical shocking for fish census and diversity index for benthos. DER accompanies these surveys, as needed, with in-stream fish bioassays at several critical points, upstream and downstream.

The results and the recognition

In one of the recent surveys, DER was accompanied by representatives of an alerted community, including local sportsmen, a state legislator, boy scouts, and news media. DER reported more fish and bottom organisms than had ever been seen before in the Bow Creek environment.

But perhaps the most dramatic change has been in the attitude of two groups of people involved. This attitude has changed from suspicion (tinged with

some hostility) of each other's motives to a mutual respect and sympathy that is based on a comprehension of each other's objectives and problems.

RCA's efforts in this project have not gone unnoticed. As a result of this achievement, the Corporation has received:

- A national commendation from the U.S. Environmental Protection Agency (1977);
- The Conservation Service Award of the Pennsylvania Fish Commission (1977);
- A feature story in the Pennsylvania Angler magazine (1977); and
- The Izaak Walton League Award (1978)—for which it was nominated by the Pennsylvania DER! (RCA Mountaintop is the only industrial plant in Pennsylvania to be nominated by DER.)

And, finally, Mr. L. Pawlush, the Regional Administrator for the DER Bureau of Water Quality and once RCA's most severe critic, is now one of its strongest supporters. He brings ecology classes to view an "excellent waste treatment system," and refers to the recovery of Bow Creek as "a near miracle...the most complete stream comeback" he has seen in his career.

In conclusion

In the Bow Creek project, the efforts of both DER and RCA teams represent a mixture of idealism and practicality and constructive combination of opposition and cooperation. The project stands as an example of a realistic and workable approach to solving other problems of industrial pollution.



Author Slater, right, and L. Pawlush hold samples of Upper Bow Creek water and RCA effluent.

Morris Slater is Manager of Quality Control Engineering and the Chemical and Physical Laboratory in Solid State Power at Mountaintop. He has worked in glass-to-metal sealing, filming and aluminizing, adhesives, radiotracers, rectifier design, high-purity water, laminar-flow clean rooms, night-viewing devices, and optical interference filters for single-tube color cameras. In 1973 he was brought to Mountaintop to assist in a major waste-treatment crisis.

Contact him at:
Solid State Division
Mountaintop, Pa.
Ext. 441

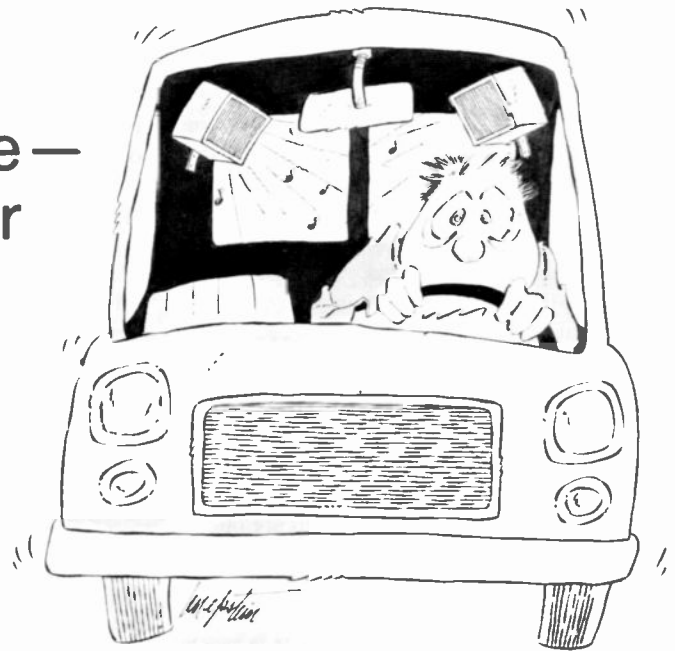
Reprint RE-24-3-18
 Final manuscript received Nov. 2, 1978.

Acknowledgments: The RCA team consisted of a small and changing army, but some names in leadership positions stand out: H.C. Waltke, the team manager; F.G. Block and J.E. Mainzer, as plant managers who led and supported the effort; S.A. Benczkowski, B.A. Jacoby, T.E. Nash, E.M. Troy, C.R. Turner, P.T. Valentine and B.V. Vonderschmitt; K.D. Lawson and R.J. Mannella of Corporate Staff; and Don Crane, the system operator.

build it yourself

The phantom double bridge— sixty watts of output in your auto or van

Want to triple the audio output available from a 12-V supply? Try this circuit.



L. Kaplan

Why would anyone want to introduce yet another audio amplifier? The literature is full of audio amplifiers of all sizes and descriptions, leaving the constructor with a seemingly unending choice of designs having power outputs from zero to infinity and distortion figures from 50% to zero. Yet if you wish to build a high-quality system for an auto, truck, or van with a 12-volt power supply, you would find no published designs with a power output greater than fifteen watts. Most automobile radios are limited to only five or six watts of output,

the amount arrived at most conveniently when a 3.2- to 4-ohm load is applied to the traditional "totem pole" output circuit (Fig. 1) supplied with the 13.2 to 14.4 V available with engine running and charging system in good order. Changing the output configuration to that of a full-wave bridge, Fig. 2, multiplies the theoretical power output by a factor of four, but practical considerations tend to reduce that number. Even so, full-wave bridge units supplying up to 20 watts of output are starting to appear on the market.

The way to higher power

The way to higher power in a vehicular amplifier is through increasing the supply voltage and/or decreasing load impedance.

Let's consider the consequences of these alternatives. Raising the supply voltage requires a dc-to-dc converter. Although not an impossible solution, the converter certainly is as complex as the amplifier

Reprint RE-24-3-10

Final manuscript received June 26, 1978.

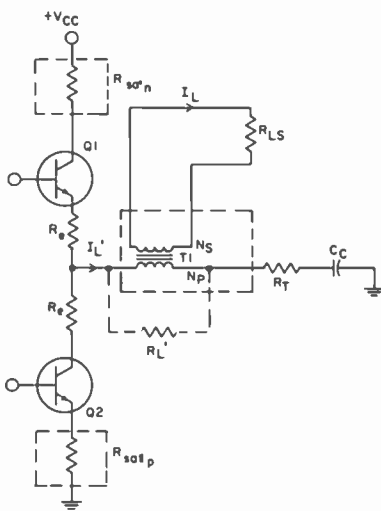


Fig. 1 Traditional "totem pole" output circuit is limited to about 5 or 6 W audio output in a 12-V system. Voltage drop in primary circuit (R_{sat} , R_e and R_T) subtracts from available voltage across load R_L .

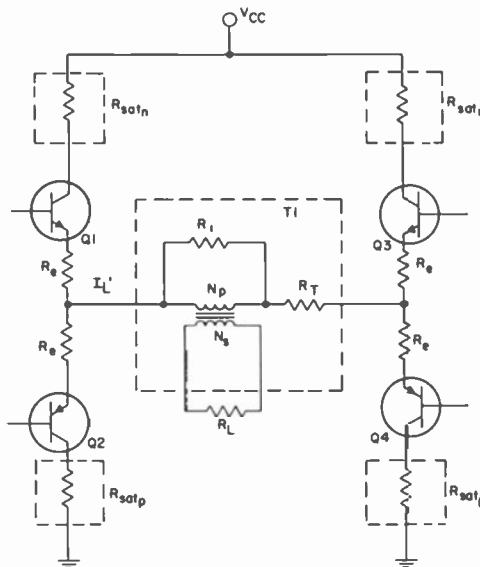


Fig. 2 Full-wave bridge output circuit multiplies theoretical output power by four; such units supplying up to 20 W are now appearing on the market. Load voltage is theoretically doubled, so voltage drops are less severe.

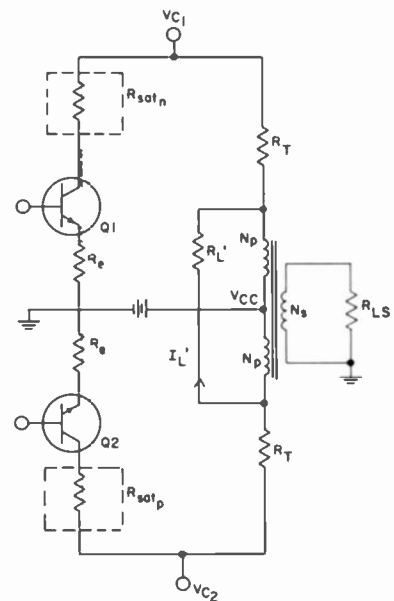


Fig. 3 Conventional push-pull circuit effectively doubles supply voltage. Circuit has been called the "phantom double bridge" because it resembles conventional full-wave bridge with twice the voltage.

alone, and also generates noise that is difficult to suppress.

Lowering the load impedance involves one of the following: 1) non-standard speaker impedance, 2) multiple parallel speakers, or 3) an output transformer. The first two methods can be eliminated for rather obvious reasons, but the use of a transformer should be considered in more detail.

The transformer solution

Totem-pole, full-wave bridge, or phantom double bridge?

There are many ways to configure output transformers, depending on the type of output stage used. For the familiar "totem-pole" connection, the transformer would be a straight step-up type, with the secondary loaded by a standard impedance. The disadvantage of this connection (and it is not an obvious one) is that the required peak currents are raised by the same ratio to which the load impedance is lowered. The result is that all the cumulative IR

drops in the primary circuit (transformer, emitter, and ballast, plus the $V_{CE(sat)}$ of the output transistors) gang up on you and lower the available V_{CC} . Since power output is proportional to the square of the voltage across the load, the resulting system can be very inefficient.

The same comments apply to the full-wave bridge connection, except that the drops are somewhat less severe, since the load voltage is theoretically doubled.

What about "conventional" * push-pull? Conventional push-pull, besides allowing the load to be coupled in several ways, Fig. 3, is advantageous because it effectively doubles V_{CC} . In this circuit it is possible to connect the load directly across the plates (oops!) collectors of the output transistors Q1 and Q2. This connection reduces the secondary load current to zero, leaving as loss elements the same impedances as before ($R_T + R_{(sat)} + R_e$), but, since the effective V_{CC} has been doubled, the im-

* That word "conventional" dates back to tube amplifier days when no other connection was practical.

pedances are less significant. This arrangement has been dubbed the "phantom double bridge" because it resembles a conventional full-wave bridge with twice the supply voltage.

If the load is moved from the secondary and connected across the two collectors, the transformer becomes effectively a center-tapped choke. The secondary can then be used exclusively as a feedback winding, carrying no load current, and can be wound with thin wire. This arrangement provides a more efficient transformer by effectively eliminating the secondary IR losses, but has the disadvantage of requiring an ungrounded load.

The amplifier itself

Fig. 4 is a schematic diagram of the complete amplifier showing the output stage in the phantom double bridge setup with the load across the primary. The PC board layout and component location are shown in Fig. 5, and performance parameters are given in Table I.

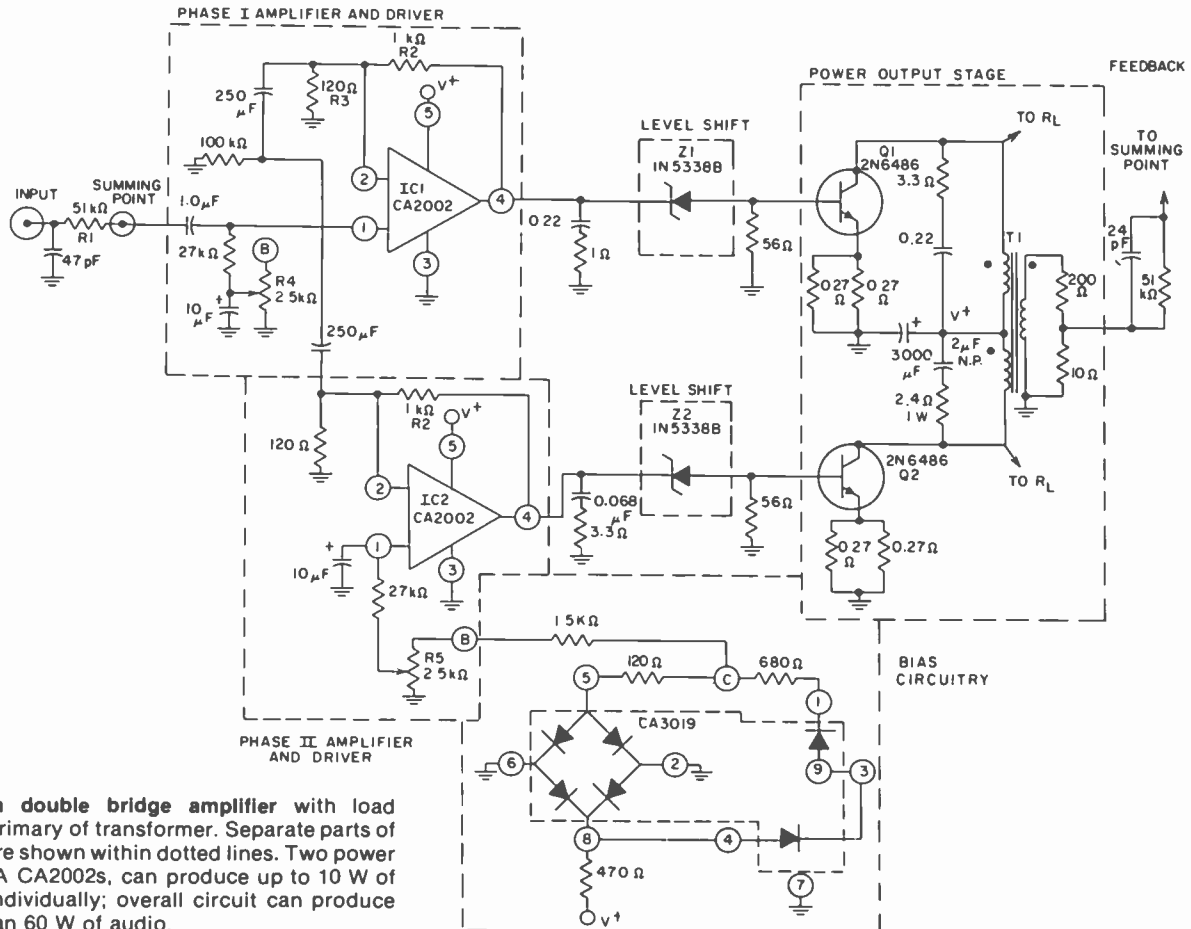


Fig. 4
Phantom double bridge amplifier with load across primary of transformer. Separate parts of circuit are shown within dotted lines. Two power ICs, RCA CA2002s, can produce up to 10 W of power individually; overall circuit can produce more than 60 W of audio.

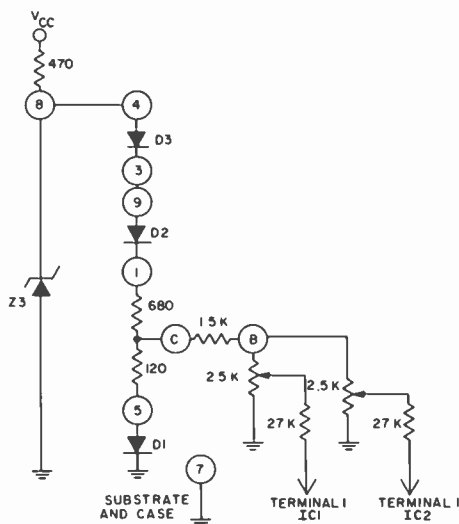


Fig. 6 Temperature compensation is done by this CA3019 diode array. (Redrawn from Fig. 4.)

biased well to the positive to avoid any possibility of saturation. Zener diodes Z1 and Z2 level-shift the signal back down to the bases of Q1 and Q2, where it is actually used.

Temperature compensation is continuously adjustable from negative to positive.

The base-to-emitter voltages of Q1 and Q2 have negative temperature coefficients that are supplemented by the slightly negative

coefficients of Z1 and Z2. Since any negative temperature compensation placed at the inputs of IC1 and IC2 is multiplied by the dc gain of the devices, it is necessary to provide a negative coefficient which is less than that of a silicon diode. This is accomplished with the CA3019 diode array shown in Fig. 6. The CA3019 (also see Fig. 4) consists of a diode "quad" and two isolated diodes.

Zener diode Z3 (actually two parallel diodes from the quad section) is connected in the reverse direction; this connection provides a stable reference source independent of the supply voltage. The anode of D1 (actually the two remaining diodes from the quad connected in parallel) presents a voltage with a negative coefficient of about 2.5 mV/°C, while the cathode of D2 presents a voltage with a positive coefficient of about 5 mV/°C. By placing a tap at the appropriate point on the resistor string between these two voltages, a continuous range of temperature coefficients may be obtained, ranging from negative through zero to positive.

Overall feedback around the amplifier is taken from a resistive tap on the secondary winding and fed back only to a "summing point" at the input of the phase-I amplifier. The addition of input and feedback currents results in a low signal level at the summing point and a constant input impedance to the amplifier (R1).

running a socket up to the base of the CA3019 from the PC board by means of flexible wires.

Main heat sink: The main heat sink was made to mount over the PC board. A flat-bottom model (Thermalloy No. 6181) with brackets to hold it was used on the test model. The CA2002s are mounted on the board and are individually heat-sinked with bolt-on-type finned sinks made for RCA Versawatt (TO-220) devices.

Bias adjust: First set both R2 and R3 so that the wiper arms on each are at ground. With a V_{CC} of 14.4 V, the current indication should be less than 150 mA (use a meter scale of about one ampere). Advance R2 until the meter indicates approximately one-half ampere. Then advance R3 until there is a total of 800 to 900 mA of current. Be sure to ground the input during this procedure so that there is no signal to the amplifier. Allow the circuit to stabilize for fifteen minutes or so, and then go back and make any touchups necessary to bring the current back to the prescribed value.

Acknowledgment

The author thanks George Checkowski for his board layout and for his patience in coping with many changes as they were given.

Construction hints

Transformer T1: On a one-inch bobbin, simultaneously wind two strands of No. 18 AWG and one of No. 26 AWG wire until the bobbin is filled. Connect the start of one of the two No. 18 wires to the finish of the other. This connection becomes the center tap of the primary. The dots on the schematic diagram in Fig. 4 represent the starts of each winding and show the connections in the circuit. The laminations should be fully interleaved and secured with a "U" frame or brackets. The test model was made with a 6-mil audio-grade lamination, but even a very cheap grade will work, with only minor compromises in performance.

CA3019: The thermal stability of the amplifier depends on equal temperatures for the CA3019 and the output transistors. In the test model this was done by mounting a TO-5 heat sink (Wakefield No. 260-10SH5) to the main heat sink and

Cautions

The leads to the battery should be of heavy wire. Any resistance in the power-supply leads will increase distortion because of the high currents drawn.

If there is any possibility that the amplifier may ever be operating while the vehicle is being jump-started or while the battery cable is disconnected with the motor running, the following changes should be included: In place of the jumper wire from the incoming V_{CC} line to the terminal No. 5 connections on both CA2002s, connect an inductor of 5 mH minimum, 15-Ω dc resistance maximum, 150-mA rating. From terminal No. 5 of either CA2002 to ground, connect a 250 μF, 16-V capacitor. There are extra holes in the PC board for this purpose.



Len Kaplan has been with RCA in Somerville since 1966. He has been engaged in the applications and design of integrated circuits and MOS devices for tv, multiplex, audio and radio circuits.

Contact him at:
Solid State Division
Somerville, N.J.
Ext. 6261

The electron beam— a better way to make semiconductor masks

RCA has invested nearly \$2 million in a system that makes it possible to increase the number of circuits on a semiconductor chip.

R.A. Geshner

The complexity of integrated circuits has been growing exponentially. Manufacturing design requirements have progressed from discrete devices in 1948 through small-, medium-, and large-scale integrated circuits to very-large-scale integrated circuits (VLSI's) with as many as 100,000 transistors in 1978. This increase in complexity has made it possible for single semiconductor chips to handle all the electronic functions for such designs as pocket calculators, electronic watches, and even microprocessors and large memory devices. This push toward more complex and smaller devices will continue. If in the future we can make devices with more functions per device, at the same cost as today's devices, the cost per function will be reduced. However, this increase in design complexity brings manufacturing problems that must be solved. One of the major problems is in the field of microlithography, developing methods for reliably delineating the dense circuit designs with their tiny circuit elements on the device substrate or wafer. A new electron-beam microlithography machine, just installed in the Solid State Technology Center (SSTC), Somerville, solves many of the problems. It can make VLSI masks with smaller lines, with less distortion, and with a quicker turnaround than is possible by older conventional graphic techniques.

Conventional optical mask manufacturing

Before discussing what's new in microlithography, it's important to understand the conventional process. Conventional approaches of manufacturing LSI circuits involve the use of tools called

"masks," which are normally thin sheets of glass with an even thinner coating of chromium. This chromium layer defines the desired circuit configuration to be produced by a particular process step in the manufacture of a multiple-chip silicon wafer. (For example, the mask may define an area that is to be etched out of the wafer.) After all process steps are completed, each one with its own mask, the wafers are sliced apart and the individual chips are packaged. The glass masks used to define these steps must be manufactured quite precisely—the manufactured semiconductor devices can be no better than the tools (masks) used to make them.

With the push to increase the number of functions on a semiconductor chip, the size of the lines ("design rules") drawn on the mask must be made smaller.

However, the conventional optical approach to mask making (Fig. 1) has reached its limit—it cannot draw lines smaller than about $2\ \mu\text{m}$.^{*} This limit is principally a result of wavelength of light used ($\approx 0.4\ \mu\text{m}$) and optical distortion produced in the wide-field lenses. The diffraction-fringe problems at this wavelength limit practical resolution to something larger than $2\ \mu\text{m}$. Distortion in wide flat-field high-resolution lenses is also a problem. In addition, the depth of focus of these high-resolution lenses is less than $\pm 1\ \mu\text{m}$. This could cause variations in line width or resolution across the uneven glass mask substrate.

Besides these optical-mechanical problems that can cause misregistration from mask to mask in the wafer process steps, there are other optical problems. Lenses and images

must be illuminated evenly by some light source so that line sizes can be controlled uniformly across the projection field. But, as images become larger, uniform lighting becomes difficult.

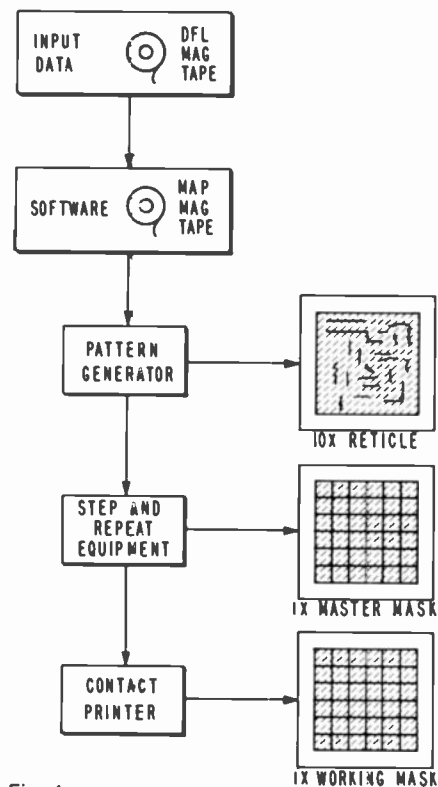


Fig. 1
Conventional optical procedure for mask fabrication. First, a designer prepares pattern design data input information using RCA computer-aided design techniques (the "DFL" tape). The MAP tape that drives an optical pattern generator then makes a glass "reticle" of a single pattern of the desired circuit configuration at a 10X scale factor. This reticle is mounted in an optical multiple-image step-and-repeat reduction (S&R) camera to produce the desired multiple-image 1X master mask, which in turn is used to produce "working masks" for the process facility that prints the wafers.

Reprint RE-24-3-B
Final manuscript received September 22, 1978.

^{*} One μm , or micron, equals 10^{-6} meter (0.000039 inch)

Four main factors determine the limit of minimum geometry (chip size and line size) in devices.

The first factor is alignment accuracy. All masks in a mask set must register accurately to each other so that pattern detail printed on a wafer can register precisely.

Misregistration between mask levels can locate devices improperly, form parasitic devices, or produce metal conductors that miss contacts.

The second factor is pattern diffraction. All pattern details on the mask must be uni-

formly clear and crisp. If the mask has random fuzzy edges, light diffraction during wafer printing will be amplified and the printed lines will vary in size. Size variations can change the electrical parameters of the devices being made, produce undesirable short circuits between devices, and create unwanted parasitic transistors.

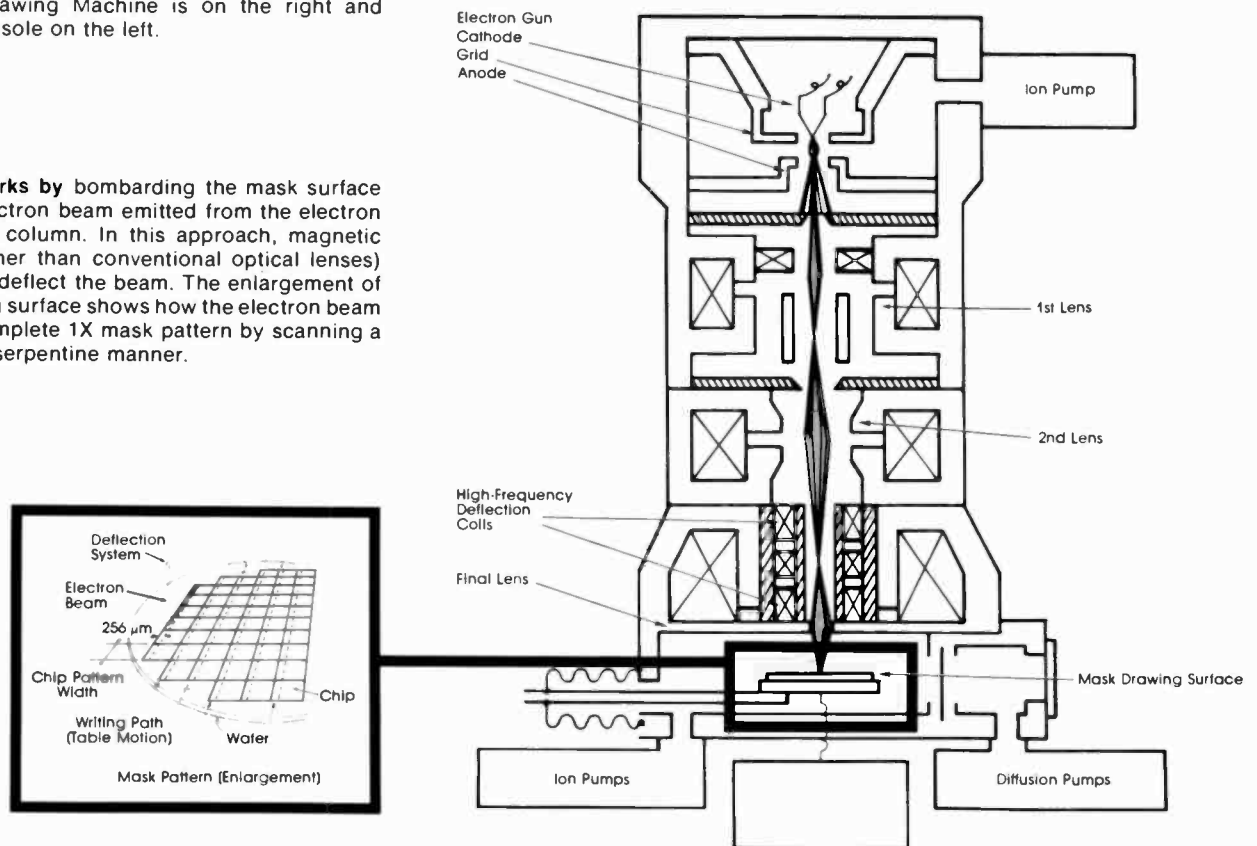
The third factor is lateral diffusion. In processing semiconductors, impurities such as boron are diffused into the silicon to produce the desired semiconductor properties. In smaller lines this is a problem. Recent advances have allowed the impurities to be interjected by a new process called ion implantation, which allows the use of smaller lines. Sharp line edge masks are needed to make the smaller lines.

The fourth factor is called punch-through voltage limitation. As the distance between source and drain on an MOS device gets smaller, the leakage current increases. Recently process engineers have developed new compensation-doping techniques that maintain the voltage breakdown so smaller line sizes or design rules can be used. This allows higher circuit density and better



Fig. 2
New MEBES facility installed in special clean room at Solid State Technology Center, Somerville. MEBES Drawing Machine is on the right and control console on the left.

Fig. 3
MEBES works by bombarding the mask surface with an electron beam emitted from the electron gun in the column. In this approach, magnetic lenses (rather than conventional optical lenses) shape and deflect the beam. The enlargement of the drawing surface shows how the electron beam forms a complete 1X mask pattern by scanning a raster in a serpentine manner.



circuit performance. Higher-quality lithographic techniques are required to use these new process techniques to advantage and improve circuit density.

Innovations in mask manufacturing

In order to maintain a competitive posture in the semiconductor field, RCA has looked to alternative mask-fabrication techniques to reduce defects and allow smaller design rules. One of the new methods investigated involves the use of electron-beam mask drawing. This method has been around for many years, but only recently has the proper marriage of several innovative technologies made "E-beam" drawing more attractive. These new technologies include:

- scanning electron microscopes,
- interferometric control,
- ion vacuum pumps,
- precision air bearings,
- new computer controls and computer machine interfaces,
- higher-speed electron-beam-sensitive resists,

modern magnetic lenses and deflection and blanking techniques, and innovations in computer software.

Recently all of these technologies have been incorporated in one system—MEBES (Manufacturing Electron-Beam Exposure System). This system is more accurate, faster, and has a higher resolution capability than previously-developed equipment—it draws a final 1X chrome master directly with line sizes as small as $0.5\ \mu\text{m}$, over a 4.1-inch by 4.1-inch area with an absolute accuracy of $\pm 0.125\ \mu\text{m}$. Because of these improvements over existing optical techniques, RCA has made a capital investment of nearly \$2,000,000 to specify, test, purchase, and install a complete MEBES system. Figs. 2-4 show the system and how it works.

Advantages of MEBES masks

Masks made by the E-beam approach have higher quality, less distortion, more uniform line size, and, probably most important, lower cost with a quicker turnaround in the delivery cycle.

The following paragraphs discuss these advantages in detail.

Effective elimination of distortion. Fig. 5 illustrates the types of distortion that occur using the conventional optical approach. The absolute accuracy of MEBES is $\pm 0.125\ \mu\text{m}$ anywhere in the drawing field. Therefore, all the conventional optical aberrations are eliminated. This includes any lens-barrel distortion, pin-cushion distortion, keystone, reduction anomalies caused by optical reduction and mechanical variation caused by 10X reticle misalignment or misplacement, and step-and-repeat placement errors. A MEBES mask set has true mask-to-mask registration of $\pm 0.125\ \mu\text{m}$. This is a very important advantage because the yield-improvement potential of this one crucial specification alone is very high. An internal RCA study¹ on the causes for yield loss in LSI circuits indicates that losses caused by misalignment often run as high as 50 percent. These yield losses are not caused solely by the inability of the operator or machines to produce accurate alignments, but involve problems in the level-to-level registration of masks.

¹ W.E. Ham and C.S. Kim; *Company Private Technical Report.*

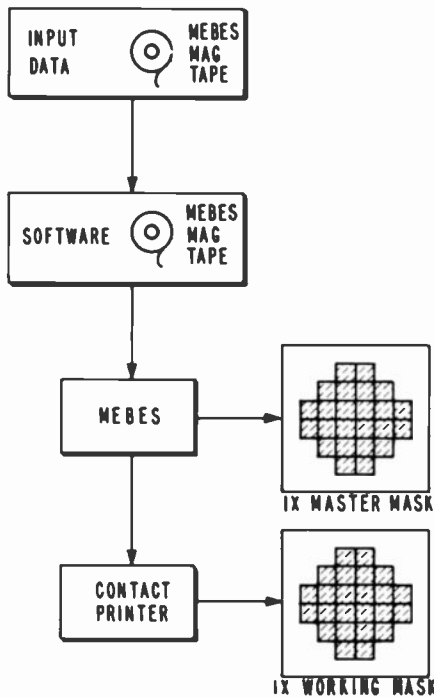


Fig. 4
Simplified electron-beam process needs fewer steps to make a master mask; compare this procedure with the conventional one shown in Fig. 1.

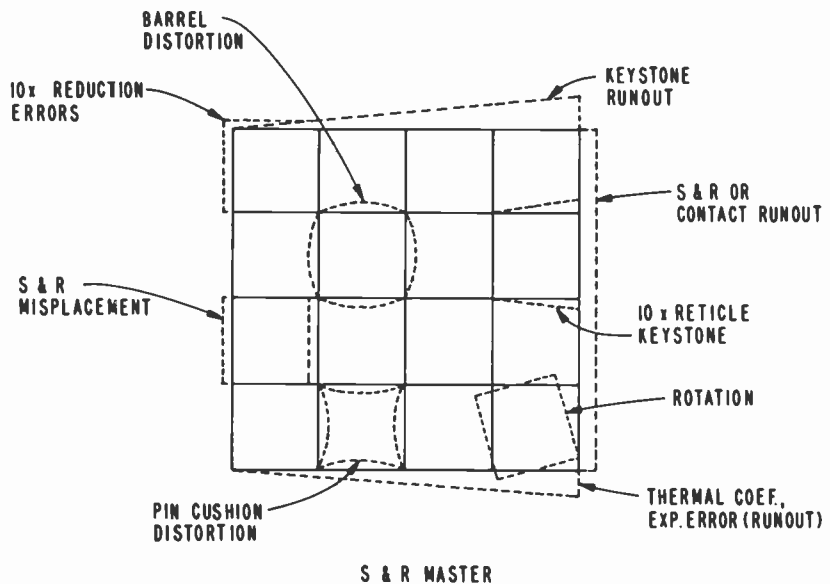


Fig. 5
Optical method produces errors and distortions. This diagram shows the typical step-and-repeat optical-mechanical distortions that could be present in an optically generated mask and so cause misregistration between layers in a mask set. MEBES masters do not have these distortions.

Quick turnaround. Since the 10X reticle is not required, the lead time to make and inspect it, which can be anywhere from one day to two weeks, is not required. (With MEBES, the IX mask is made directly from a numerically controlled magnetic tape input.) This is a direct saving in production lead time.

Uniformity of line size. Since there are no conventional lenses, the exposure over the electron beam drawing area will not suffer the possible $\pm 5\%$ variation in intensity that can be expected from optical lenses, condensers, or light sources. Therefore, exposure is uniform and line size is held constant. This feature also increases device yield and device response uniformity.

Defect reduction. The quality of final masks that are produced depends, in reality, on a number of interrelated factors. One of these considerations in defect-density reduction relates to the electron resists being used. The MEBES machine, of course, requires the use of an electron-sensitive resist. A net reduction in the number of defects to be found in the final, developed pattern is directly related to the quality of this resist. Although uv-sensitive resist materials are more widely used in

photolithographic techniques today, RCA has had many years of experience in synthesizing electron-sensitive resists for its VideoDisc program. We are confident that any resist problems that might evolve will be solved and that the defect density on MEBES-generated masks will be as good, or better, than those made with conventional uv-sensitive materials.

Line-size resolution. RCA's MEBES has two drawing modes, 0.5- μm or 0.25- μm electron-beam spot size. Using the larger spot size, lines as small as 1 μm on 2- μm centers have been drawn over the entire drawing surface. This is not possible with conventional optical techniques. Moreover, with the smaller spot size (and an accompanying increase in the time to produce a mask) it is possible to draw lines much smaller than 1 μm .

The MEBES system

The system is essentially an electron column with a host of controls.

MEBES consists of an electron column with blanking and deflection controls, a servo-controlled stage-positioning system with laser interferometer position readout,

an airlock for loading work while maintaining a vacuum in the main chamber, and a computerized control system for the raster scan of the electron beam. The close-tolerance capabilities of this machine, outlined in Table I, lets us prepare better than state-of-the-art masks for LSI applications. These specifications indicate that ultra-precision, low-defect masks can be made on 5-in. glass over a 4-in. field with line sizes smaller than 0.5 μm . This accuracy can be achieved with both negative- and positive-resist processing.

The MEBES is installed in a special 1200-ft² laminar-air-flow clean room to optimize the potential accuracy of MEBES. This 100-class clean room is maintained at $70 \pm 0.5^\circ\text{F}$ and $40 \pm 2.5\%$ rh. To obtain the best MEBES lithography process result, the clean room also has special chrome process equipment, including spray developers for processing E-beam resists and dry plasma and wet etchers for etching circuit configurations.

With MEBES, the circuit designer becomes more of a maskmaker.

Using MEBES technology involves user-oriented problems that should be addressed. Previously the design engineer used CAD (Computer-Aided Design) software to generate magnetic tapes containing control data for a pattern generator that created a single-pattern 10X reticle of that artwork. The mask maker worked with this reticle to produce a step-and-repeat master mask with the right tone and orientation at the proper step distance. However, using MEBES and new CAD programs, the designer not only designs the pattern, but now also designs the arrangement and tone of the final IX master mask complete with "drop-outs," test inserts, and identification information. Therefore, the designer must become familiar with the following facts:

- 1) A special Design Automation program is used to convert the computerized representation of the mask artwork to a format capable of controlling the MEBES machine.
- 2) A second program generates the exact locations for each chip (step-and-repeat data) for the drop-outs, test inserts, etc.
- 3) A third program can be used to automate the above steps, generate the appropriate paperwork, and encode all standard information into a file.

Table I
Typical E-beam machine specifications.

Drawing area	4.1 in. x 4.1 in. (5-in. x 5-in. plates)
Table speed	4 cm/s (≈ 94 in./min)
Interferometer correction resolution	1/32 μm (≈ 1.2 $\mu\text{in.}$)
Raster scan	256 μm (≈ 10 mils)
Solid E-beam pattern coverage speed	2 cm ² /min (≈ 29 min over 3-in. x 3-in. area)
Maximum chip size	16 mm (≈ 0.63 in.) x 32 mm (≈ 1.3 in.) without special partitioning
Pattern input type	Trapezoids
Raster butting error	$\pm 1/8$ μm (≈ 5 $\mu\text{in.}$)
Writing address modes	2 (0.5- μm and 0.25- μm address)
Pattern resolution in 6000- \AA positive resist	1 μm consistently, 0.25 μm with thinner resist using smallest address
Line-size control	± 0.01 μm
Line definition	$\pm 1/8$ μm (0.5- μm address)

4) Since two E-beam resists are available, the design engineers must understand how to use them to obtain proper end-product tone and line-edge definition.

5) MEBES operates in metric units. Special techniques allow English units to be used if the original information was digitized on an 0.020-mil or 0.040-mil grid. Half-micron errors may be created if information is originally generated from an 0.050-mil grid.

6) Since MEBES masks are more expensive than reticles, all designs submitted to MEBES must first be "deformatted" so that a checkplot can be produced. This can minimize costly errors and provide the equivalent of a "blowback" (not possible from a 1X mask).

Contact the author for more information on any of these points.

Conclusion and future plans

Although RCA has a limited production background in electron-beam mask manufacturing, we have a viable system that provides definite advantages over conventional optical approaches.

We have produced masks with close design-rule requirements and used these

masks to produce significant yields on many types of semiconductors. As an example, our group received a CAD magnetic tape for a specialized automotive-type chip one day and delivered a 1X chrome print of the final mask set in less than 4 hours. The design engineer that learns to use this system will be years ahead of older technologies.

In addition, RCA can use MEBES as a tool to investigate other state-of-the-art wafer-production techniques.

Process outlines of several of these future approaches are shown in Fig. 6; one or several of them can or will be used in the next 2 to 8 years. One obvious method is to use the MEBES to write directly on the wafer, (see Fig. 6a) eliminating the need to use a mask. The present equipment can write directly on the wafer for experimental purposes. During 1978 experiments are planned to determine the effect of direct writing on final circuit performance.

Another approach, Fig. 6b, could be to produce reticles on the MEBES and to step and repeat (S&R) on the wafer using special optical S&R cameras. The MEBES can print 2X, 5X, or 10X reticles as well as 1X masters. RCA Lancaster is contemplating this approach for large CCDs. It may seem paradoxical that MEBES

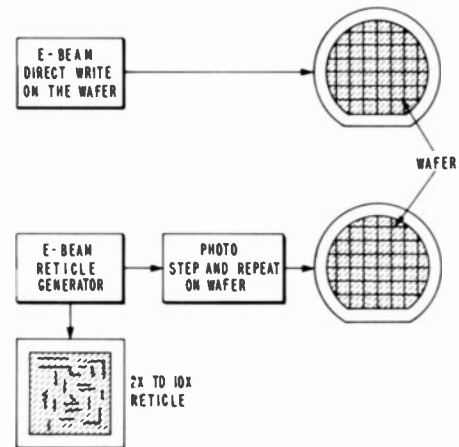


Fig. 6
Future ways of using MEBES. Directly writing on the wafer (left) will eliminate the need for masks; preparing a reticle on MEBES (right) and using it to step-and-repeat on the wafer will eliminate 1X masks.

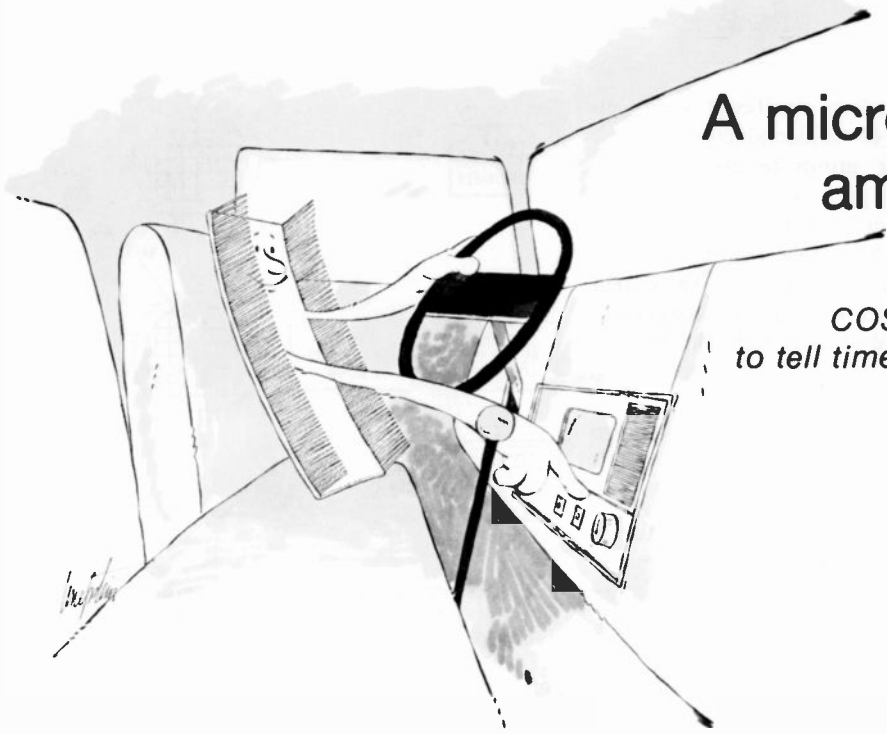
would be used for reticle generation, but multiple-projection printing on the wafer may be cheaper than direct 1X E-beam writing on the wafer. In addition, complex reticles can be made on MEBES much cheaper and more accurately than by conventional optical pattern generators.

These methods are available to RCA research engineers to aid RCA and help maintain our competitive posture in the semiconductor field.

Bob Geshner has been working in microlithography for most of the 18 years he has been with RCA. During his first years in Camden, he worked on microelectronic packaging and printed wiring standardization and later developed the first automated large-scale artwork system using a Gerber numerically controlled plotter. When his Microimage Technology group was moved to Somerville in 1973, he became the Engineering Leader of the Solid State Technology Center's QTA photomask facility. He was responsible for the development of the new MEBES facility and presently directs all SSTC photomask activities.

Contact him at:
**Solid State Technology Center
RCA Laboratories
Somerville, N.J.
Ext. 6514**





A microprocessor-controlled am/fm automobile radio

COSMAC has been used in this auto radio to tell time and to control and display frequency. The specific application may, however, have broader significance for communication systems designers.

K. Karstad

Designers of communications systems are using microprocessors as economical "component blocks." In many communications systems, for example, real-time clocks (system timing) are coordinated with frequency-measurement circuits. This paper shows one such application: a system¹ that uses a COSMAC microprocessor^{2,3} to generate timing functions automatically and to control the measurement and display of frequency.

A display for time and frequency

This auto radio was designed to give priority to a clock display. Frequency is displayed whenever the local oscillator is tuned. After a preprogrammed period (e.g., 5 seconds), the clock-time is displayed again. The system (Fig. 1) consists of a 3½-digit multiplexed LED display programmed to display channel-frequency for an a.m. or fm radio, a 12-hour elapsed-time counter, a 12-hour clock, or a four-year calendar. The hardware includes a central processing unit (CPU) with memory, a section for measuring and writing frequency information into memory, and a section for outputting stored and processed information to the LED display.

Three pushbutton switches allow on-demand display of frequency, elapsed time, or calendar. The clock is set by simultaneously depressing the pushbuttons for elapsed-time reset and calendar-control. After these two pushbuttons are

released, the programming sequence starts displaying the roll-call of months automatically at a two-month-per-second rate. When the calendar-control pushbutton is again depressed, the month display is "frozen" and the display automatically starts advancing the date in a manner similar to that used for months. When all the buffers have been updated, the colon in the display starts flashing at a rapid rate to indicate that the clock is set, but not yet running. One final push of the calendar-control button resets the seconds counter and starts the clock.

The detailed review of the circuit in Fig. 1 is beyond the scope of this paper; interested readers are referred to pertinent literature.^{1, 2, 3} It is, however, instructive to review the highlights of circuit functions since they are generally applicable in communications systems.

Measuring time with COSMAC is simple.

There are two basic approaches to timekeeping with a microprocessor. The first is by using external logic through a dedicated clock chip; i.e., a hardware approach in which the microprocessor only reads the data and controls its display. A variant of this approach involves interrupted operation of the microprocessor at fixed intervals, e.g., every 10 ms; externally generated logic interrupts the microprocessor operation and increments a software register. The second method of timekeeping with a microprocessor is a software approach in which timing loops are generated in software.

The disadvantage of the first method is the cost of a dedicated auxiliary clock chip. The restrictions that accompany use of the second method require a compromise in requirements, i.e., the rate of interruption must be high enough to provide good time resolution but not sufficiently high to burden the processor. Although a purely software approach does have an advantage in that no external hardware is required, its use markedly complicates the programming. Additionally, the provision of equal-length basic timing intervals requires care, particularly with a processor having variable-length instruction times. Finally, the processor cannot perform any other function while it is in a timekeeping loop.

The architecture of the eight-bit COSMAC microprocessor used in this circuit is inherently good for timing events accurately. The time base is generated automatically in the CPU, as any program is being run, by invoking the direct-memory access (DMA) feature. Software updating of time buffers in the random-access memory (RAM) can be executed at a convenient rate, e.g., as slowly as half-second periodicity. The COSMAC processor contains sixteen 16-bit registers. In the DMA mode, the first register, R(0), is automatically activated as a "DMA pointer" and incremented once as each byte is read from or written into the RAM. This feature is of primary importance in implementing the application shown in Fig. 1. Since every DMA increments the register R(0) in the CPU, a mechanism is provided to increment a counter automatically at a fixed, known

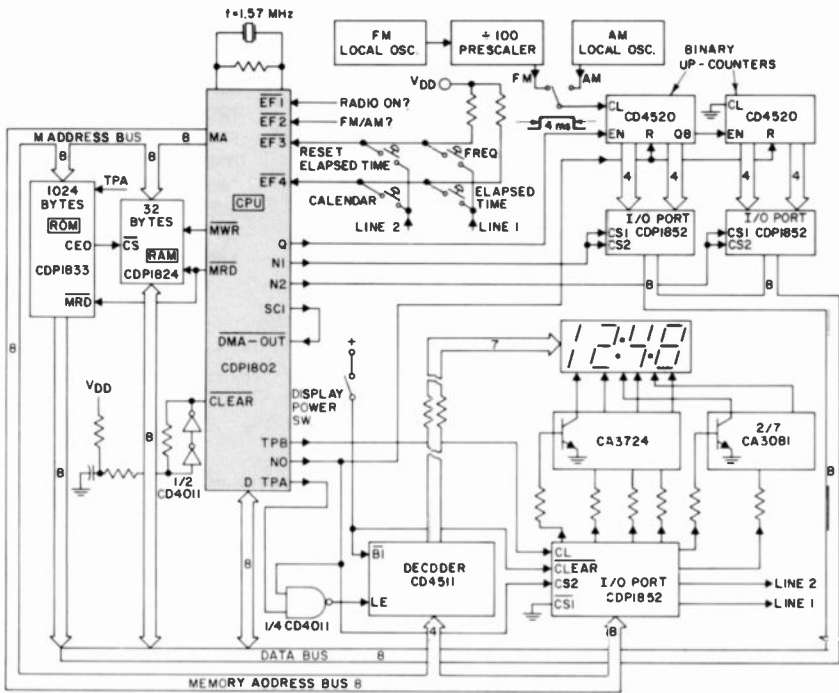


Fig. 1
COSMAC-controlled display for time and frequency information. The program runs in 1k bytes of ROM. A binary counter measures and reads a.m. or fm local-oscillator frequency. Display data, time, or frequency are multiplexed in a 3½ digit LED display. Display modes are controlled on demand by pushbuttons. Use of CMOS circuitry permits standby operation (display disabled) with current consumption of less than 5 mA.

rate as the program is running—without regard to instruction types and program structures. Conventional programming is used to control the flow of this information into an auxiliary counter, provided as a low-order byte in a CPU scratchpad register. The only restriction is the need to avoid three machine-cycle instructions (opcodes CN), not a great sacrifice since more than 80% of all COSMAC instructions are of the two-cycle variety.

It should now be apparent that timekeeping with the COSMAC CPU is comparatively simple; it merely involves monitoring the most significant bit of register R(0), which may simultaneously be doing fetch-and-execute machine cycles unrelated to timekeeping. Following is an explanation of the modified fetch-and-execute cycle used in the system shown in Fig. 2 in which the state-code line (SCI) is hardwired to the DMA-OUT pin.

Since SCI is low during fetch and execute, the CPU samples a DMA-OUT request and responds with a DMA cycle. During DMA, state-code SCI goes high, and effectively resets the DMA so that the

processor reverts to the normal, next fetch-and-execute pair. Thus, the normal sequence of fetch-execute is modified to an iterated sequence of fetch-execute-DMA instructions. The systems designer is free to choose a convenient time increment to fill the register in the CPU; e.g., one second. The crystal-oscillator frequency required

for the CPU under these conditions can now be calculated as follows:

$$\text{Since } \frac{8 \times 3 \times 2^{16}}{f} = 1 \text{ second}$$

then $f = 1.572864 \text{ MHz.}$

Note that:

- 1) Eight clock pulses are required per machine cycle in the COSMAC CPU.
- 2) The CPU operates with *three-cycle* instruction: fetch-execute-DMA.
- 3) Register R(0), which increments a timing-counter, must count to 2^{16} pulses to change state.

The four digits of a 12-hour clock display are stored in four bytes of RAM, and the low-order byte of a scratchpad register in the CPU is allocated as a seconds counter. The clock buffers in the RAM are updated each time the seconds counter overflows. In summary, the accuracy of the time base is limited only by the accuracy of the crystal clock used with the CPU.

Measuring frequency is a tradeoff between accuracy and processing time.

The frequency to which an a.m. or fm radio is tuned is determined indirectly by measuring the appropriate local-oscillator frequency and using the CPU to subtract the appropriate intermediate-frequency (i.f.) of the superheterodyne receiver. In auto radios, for example, the local oscillator is typically offset 262 kHz above the carrier frequency; thus, if the a.m. radio is tuned over the range from 540 to 1600 kHz, the local oscillator frequency to be measured varies over the range from 802 to

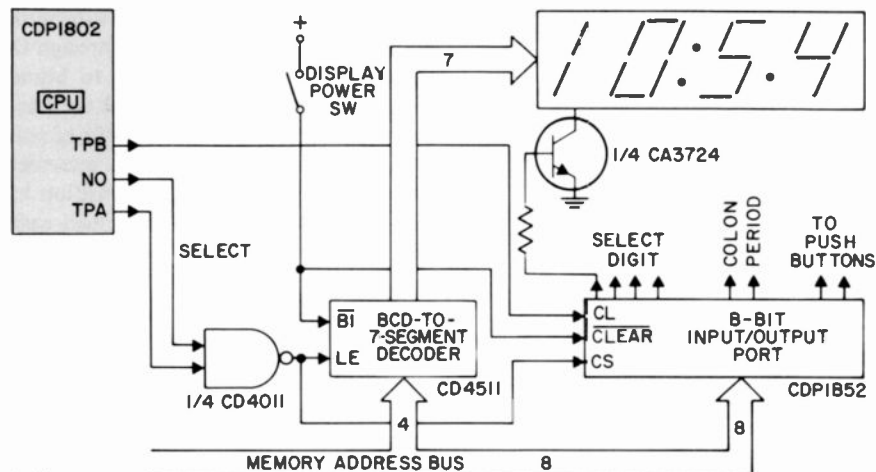


Fig. 2
Display circuit used in system shown in Fig. 1. Multiplexing of the display is software controlled. The eight-bit COSMAC processor also makes available a 16-bit data format with only one output instruction.

1862 kHz. In the case of an fm receiver, the local oscillator is typically offset 10.7 MHz above the fm carrier frequency; thus, if the fm radio is tuned over the range from 88 to 108 MHz, the local oscillator frequency varies over the range from 98.7 to 118.7 MHz. A divide-by-100 prescaler stage in the fm mode reduces the frequency to be measured into the range from 987 to 1187 kHz.

The pulse train generated by the appropriate local oscillator is counted in a 16-bit counter composed of two cascaded type CD4250 binary up-counters, enabled by a timing gate generated in the CPU. Upon request of the program, the low- and high-order bytes of the result are read into a scratchpad register and stored for further processing (e.g., subtraction of the particular intermediate frequency mentioned above). The inherent uncertainty (± 1 pulse) when counting pulses within a timing gate can be reduced with a comparatively long timing-gate period. On the other hand, a very long timing-gate period interferes with processing. Furthermore, if the timing-gate is generated by software, as is the case in this application, an integral number of instructions must be used. A timing-gate period of four milliseconds is a good compromise for the system under discussion. Recalling that a time-period of one-second (2^{16} instructions) is required to generate a full count in the aforementioned R(0) register of the CPU, the ideal number of instructions for a 4-ms timing-gate is calculated as follows:

$$4 \times 10^{-3} \times 2^{16} = 262.144 \text{ instructions.}$$

This value for the timing loop is rounded off to 262 instructions. The total error resulting from the round-off and the ± 1 -pulse uncertainty is approximately 0.02% (worst case), a value that is well within the channel spacing of a.m. and fm broadcast stations. The largest number of pulses that must be counted during a 4-ms timing-gate period occurs when the a.m. radio is tuned at the high-end of the band (the local oscillator tuned to 1862 kHz). Dividing the 4-ms timing-gate period by the periodicity ($1/f$) of the local oscillator reveals that 7448 pulses must be counted in this case. Thirteen bits from a binary counter can, therefore, provide adequate data over the full range of frequencies to be measured in this particular case.

Software controls the information display.

The COSMAC is an 8-bit processor; in conventional use, one of seven output

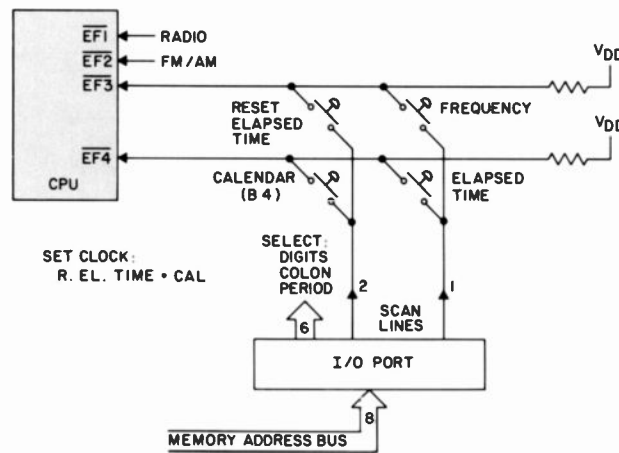


Fig. 3 Pushbutton control system for CPU. Of the four flag lines available for sensing external events, two are used in a 2 X 2 matrix to scan four demand pushbuttons. The "set clock" function is activated by pushing two of the buttons simultaneously.

instructions outputs one byte:

$$M(R(X)) - \text{BUS} : R(X) + 1$$

Another useful architectural feature of COSMAC is its capability to output 16 bits of information from any of the 16 scratchpad registers in the CPU with only one output instruction. For example, one output instruction causes the 16 bits in a register N to be output over the address bus, provided X is previously set equal to N . The higher-order byte appears first and is latched in an input-output (I/O) port by timing-pulse A (TPA). The lower-order byte, following later in the same machine cycle, is latched in another I/O port by timing-pulse B (TPB). Fig. 2 illustrates this sequence. Software controls the multiplexing of the display.

A knowledge of COSMAC architecture and programming procedures is needed to understand the software used in this circuit. Therefore, we will skip the details and simply note that the main program is short and consists of calls to various subroutines, which are nested and follow the COSMAC convention for unlimited subroutine nesting capability. Each pass through the program may vary according to branch conditions. The CPU must check the 0-to-1 transition of B_{15} in register R(0) at least every half-second, and it must increment the seconds counter if the transition has occurred. This check is performed easily since, even with the CPU multiplexing the LED display digits at a 100-Hz rate, a period of 10 ms is the maximum time for which the CPU is diverted to operation in timing loops.

For purposes of understanding the display-control sequences, assume that the RAM buffers for timing and frequency data have been updated; a synopsis of buffer-update procedures is presented below. Before data

from the RAM buffers are outputted to the multiplexed LED display, the status of the four pushbuttons is tested; Fig. 3 shows a simplified schematic diagram of the pushbutton control system. Each scan line emanating from the I/O port is individually activated, and the two pushbuttons associated with each line are tested serially for status by branch instructions in the program. If there are no closed pushbuttons, the program proceeds to the display section of the routine and outputs the hours and minutes data; this is the normal display mode. However, for example, should the elapsed-time pushbutton be closed, the RAM pointer will move to the elapsed-time buffers and display the elapsed time data for a predetermined period. Following a typical delay of 5 s, the program reverts to the display of real-clock-time data. The program reverts similarly following the pushbutton demand and display of either frequency or calendar data.

The details of driving and multiplexing the LED display can be studied by referring to Fig. 2. Each digit in the display is driven by a transistor in the CA3724 four-transistor IC array; the colon and period are each driven by a transistor in the CA3081 transistor-array IC; both of the transistor arrays are controlled by an I/O port (also shown in Fig. 1). The segments of the LED display are driven by a CD4511 BCD-to-7-segment decoder, which derives its memory-address data from a common bus that feeds similar data to the I/O port. Multiplexing is accomplished by providing coordinated data to the decoder and I/O port.

Figs. 1 and 2 show a separate display-control power switch. When this switch is open, the CPU and clock continue to run. The use of CMOS circuitry in the system

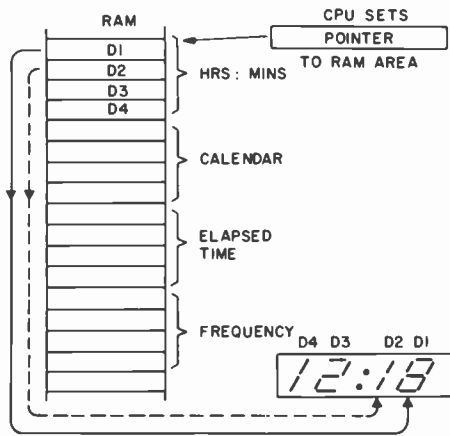


Fig. 4
Memory map of RAM buffers to be updated in circuit of Fig. 1. A CPU display pointer selects the correct buffer.

keeps this standby power below 5 mA. This is an important advantage in vehicular applications; power drain on the battery is minimized if the vehicle is idle for extended periods.

Updating the RAM buffers for time—one minute to four years, and everything in-between.

The memory map of the RAM buffers to be updated is shown in Fig. 4. Updating starts when the main program calls up a subroutine that assigns a half-second flagbit to follow the 0-to-1 transition of the bit B₁₅ (previously discussed in connection with the DMA counter in the CPU). In essence, the flagbit controls the seconds count and the exit from the subroutine to the main program following seconds update. The lower six bits of register R(1) in the CPU are assigned as a seconds counter. The seconds counter is incremented, and the program checks for a count of 60 or greater, which would mean that a minute has passed. If a minute has passed, the 60-s counter is reset to zero and the four RAM locations (D1 through D4) are stored with the updated hours and minutes values. In summary, there is an update every minute.

The lower byte of another register is allocated as an elapsed-time seconds counter. This register is checked for overflow, and if overflow has occurred, the four elapsed-time RAM buffers are updated. The update subroutine may be called twice from the main program. On the first call, it updates the RAM buffers for hours/minutes and month/date; on the second call, if one minute has elapsed, it updates the elapsed-time RAM buffers.

A four-year calendar is also included, i.e., the correct number of days for each month is indicated automatically. This feature is made possible by pointing the value of the current month to a lookup table stored in ROM. If the current date is less than the table entry, no action is required; if the current date is greater than the table entry, 01 is entered into the date buffers. The same subroutine, with minor modification, is used to update the elapsed time buffers for the 12-hour clock.

With a 12-hour clock and calendar display, it is also necessary to distinguish between morning and afternoon (am and pm). A separate flagbit (equal to zero) is defined as am. The second half of the particular update routine is entered only once every 12 hours (noon and midnight), and the flag is examined at that time. If the flag is 0, the stored flagbit is complemented and there is a return to the main program. If the flag reads 1, the 24-hour transition point has been passed and the program updates the month and date.

Updating the frequency buffers—a.m. or fm, that is the question.

The design shown in Fig. 1 requires that the channel frequencies be displayed whenever the radio is being tuned and for approximately five seconds thereafter. Following the buffer-update for time information, as just described, the program tests the operational status of the radio. If it is off, the frequency update function is bypassed and the normal display subroutine is called. If the radio is on, the frequency is measured by means of a software-generated 4-ms timing-gate, as previously described. The most recently measured value of frequency is compared with any previously stored value. If a frequency change is verified, the new value is stored in the RAM buffers in readiness for display. Verification of a frequency change also prompts a program test to determine whether the mode of operation is a.m. or fm. In the case of a.m. reception, the local-oscillator offset (i.e., the 262-kHz i.f.-signal value) is subtracted to determine the actual channel frequency being received; the result is converted from binary to bcd data. Before these digits are stored in the RAM, the least-significant digit is rounded-off to the nearest zero; the channel spacing for a.m. is 10 kHz.

The update procedure is essentially similar in the case of fm reception, except that the channel spacing is 0.2 MHz and the least

significant digit is always odd. Program provision is also made for turning on the period (decimal point) when fm information is displayed; likewise, the colon must be activated when time information is displayed.

Conclusion

The COSMAC microprocessor permits a software generated clock to be attained at low cost and high accuracy. This is a classic example of the usefulness of microcomputers for real-time clocks and for frequency measurement—one more example of the pervasiveness of the microprocessor in communications applications.

References

1. Karstad, K.: "A Microprocessor-Controlled Automotive AM/FM Radio," *Proc of SAE Congress and Exposition*, Detroit, Mich. (Feb-Mar 1978).
2. "User Manual for the CDPI802 COSMAC Microprocessor," Publication No. MPM-2013, RCA Solid State Division, Somerville, N.J.
3. "Register-Based Output Function for RCA COSMAC Microprocessors," ICAN-6562, RCA Solid State Division, Somerville, N.J.

Reprint RE-24-3-1

Final manuscript received June 6, 1978.



Kaare Karstad has worked in the microprocessor field since the product group was formed in the Solid State Division. His work has covered applications, engineering, and marketing support. He is presently doing microcomputer system designs in the areas of consumer applications and support systems. His earlier background includes CMOS applications and computer-oriented research at the RCA Laboratories.

Contact him at:
MOS Microcomputer Systems Support
Solid State Division
Somerville, N.J.
Ext. 6041

Using pulse radar data to reconstruct missile reentry trajectories

J.J. O'Connor

Often, because of radar unavailability or poor tracking geometry, a complete missile trajectory may be impossible to obtain. RCA has developed a method of determining these trajectories by using the available data and the equations of motion.

A missile test range is frequently required to provide, on a post-test basis (i.e., after the missile flight), the position and velocity components of the center of gravity of the missile at frequent and regular time points along the trajectory from pierce-point to impact. Pierce-point is considered to be the location of the missile when it pierces the "top" of the atmosphere, presently defined as 400,000 ft altitude. At this altitude, the air density is roughly 10^{-8} of the air density at sea level and, consequently, is negligible.

At the Air Force Eastern Test Range (ETR) the first step in fulfilling this requirement is to obtain C-band* pulse radar track data over as much of the region of interest as possible. Fortunately, the dense ionization plasma in the region of 100,000 ft altitude is not an insuperable barrier for C-band radiation, and, therefore, uninterrupted track throughout reentry is possible when a nearby radar is available.

Limitations in tracking coverage are due primarily to poor geometry or non-availability of a radar. For example, some regions of the trajectory may be over the horizon for the nearest radar, or the radar may be assigned to track another object. The radars may be the AN/FPQ-13, -14, or -15, FPS-16, or FPQ-6. Either echo or beacon tracking may be encountered.

Computational approach to describing missile motion

It is easier to reference trajectories to Earth geometry when they are expressed in Cartesian coordinates. A simple coordinate transformation of radar track-

ing data will not normally satisfy present accuracy requirements for target position. Such a procedure also will not provide any velocity information. Furthermore, there are frequently important intervals (particularly near impact) for which no track data exist. Therefore, something more sophisticated than simple coordinate transformation is required.

The method used at RCA's Missile Test Project (MTP) makes use of equations of motion in a differential-correction, least-squares adjustment process in which all available data are included. The available data may include: 1) multiple-radar track of the equipment section at the time of missile deployment; 2) multiple-radar reentry track; 3) on-board accelerometer or altimeter data during reentry; 4) time and location of impact, as determined by some sort of marine transponder array; and 5) environmental information. All tracking data, as well as weather data, impact data, and accelerometer or altitude data transmitted by telemetry from the reentry vehicle to ground receivers, are sent by communication links to the central computer facility uprange for the post-test analysis.

Two methods usually are used in trajectory reconstruction: point-by-point averaging and equations of motion.

In the point-by-point approach¹, position and velocity data from various sources at each time point are "averaged" in a weighted least-squares exercise, in which a large number of additional parameters, such as radar biases, are simultaneously estimated. This point-by-point approach is

always used in the powered-flight stages of a missile trajectory, because the missile motion is quite complex in the region and there are no adequate equations of motion.

There is no reason why the point-by-point approach cannot also be used for reentry. However, in the reentry region, the accelerations usually can be described by equations of motion; under these circumstances, the resulting reconstructed trajectory is much more accurate simply because there are far fewer parameters to be estimated than would be required by the point-by-point method. A complete mathematical description of the use of equations of motion is outside the scope of this paper. Instead, it will treat the missile behavior described by the equations of motion and indicate the accuracy achieved under some typical conditions.

A three-degree-of-freedom treatment of missile motion takes into account not only gravity and drag but also precession and nutation effects.

With the data usually available, the test range is limited to a three-degree-of-freedom description of missile motion—these three degrees being simply the rectangular coordinates of the center of gravity of the missile. A three-degree-of-freedom treatment, however, does not imply a simple point mass affected only by drag and gravity. Rather, it includes the effects of the full missile motion upon the motion of the center of gravity of the missile. For example, a three-degree-of-freedom treatment considers the spiral motion of a spinning missile traversing the atmosphere with a non-zero angle of attack—this angle being defined as the angle between the roll axis of the missile

* 3.90-6.20 GHz

¹ Welsh, C.W.; "Finding the best estimate of trajectory with the weighted least squares technique," *this issue*.

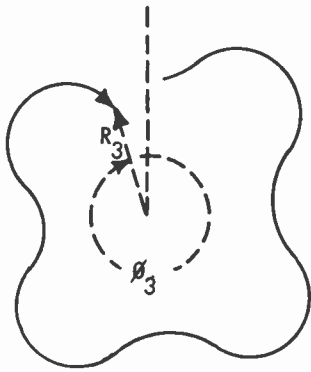


Fig. 1
Variation of angle of attack and its orientation angle (demonstrating the resultant effect of precession and nutation around the missile axis).

and the velocity vector of the center of gravity.

Simplifying somewhat, we may say that the effect of the aerodynamic forces on the missile motion is the same as the effect of a single resultant force acting at a specific point on the missile, called *the center of pressure*. The center of pressure normally lies on the axis of the missile and moves slightly forward or backward in conformity with changes in the air-flow regime. If the center of pressure lies behind the center of gravity, the aerodynamic forces tend to keep the missile flying "point-on", and the missile is said to be statically stable. Missiles are designed to have the center of pressure behind the center of gravity at three to five percent of the total body length.

Even when static stability exists, the performance of a missile is significantly improved by giving it a spin of one to two revolutions per second about its longitudinal, or roll, axis at deployment. This spin provides gyroscopic stability above the atmosphere and controls the angle of attack at the pierce-point.

During reentry, the spin causes a desirable precessional and nutational motion, which minimizes unpredictable deflections of the missile trajectory associated with aerodynamic forces.

We may visualize this precessional-nutational motion by assuming the trajec-

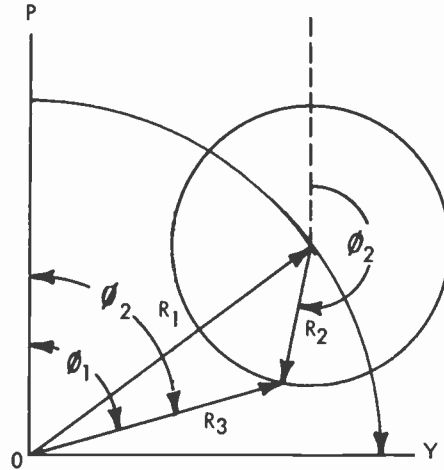


Fig. 2
Epicyclic motion of the missile axis (demonstrating separate effects of precession and nutation).

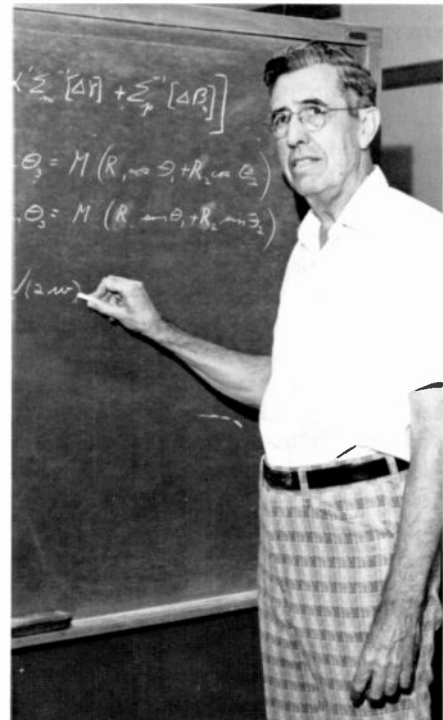
tory to be an imaginary wire on which the center of gravity of the missile is sliding. Let the missile push ahead of it a card through the center of which the wire passes perpendicularly. Let the point of the missile be equipped with a writing pen. An example of a pattern drawn by the point of the missile upon the card under these conditions is shown in Fig. 1 (on the assumption, of course, that the wire and the card have no effect on missile motion). The vector R_3 from the center of the figure to some instantaneous point on the pattern has a magnitude proportional to the sine of the instantaneous angle of attack. The angle ϕ_3 , between some reference line and R_3 , represents the orientation of the angle of attack.

The somewhat irregular motion depicted in Fig. 1 can be mathematically described by an epicyclic treatment. A diagram depicting the epicyclic nature of the precession/nutation is shown in Fig. 2. The plane of the orthogonal PY coordinate system lies perpendicular to the local tangent to the trajectory. The origin, O , lies on the local trajectory. The P coordinate axis lies in a vertical plane, directed so that it has a positive upward component.

The Y coordinate axis lies in the horizontal plane, positive to the right in terms of an observer looking along the trajectory in the direction the missile is flying. The vector R_1 , originating at O , relates to the instantaneous amplitude of precession. The vector R_2 , originating at the moving terminus

John O'Connor joined RCA's Missile Test Project in 1961 as a Senior Engineer. He is involved primarily with problems associated with missile and satellite trajectory computations. He has published in the *Physical Review* and is recognized as the discoverer of two radioactive isotopes.

Contact him at:
Radar Systems Analysis
Missile Test Project
RCA Service Co.
Patrick AFB, FL 32925
Phone: (305) 494-4252



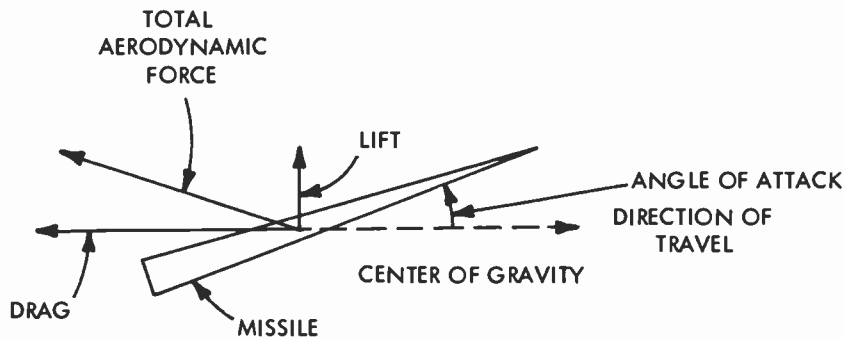


Fig. 3
Geometric relations of the aerodynamic forces acting on a missile.

of R_1 , relates to the instantaneous amplitude of nutation.

The orientation angles of R_1 and R_2 are shown by ϕ_1 and ϕ_2 , respectively. The magnitude of the vector R_3 , from O to the terminus of R_2 , is proportional to the sine of the instantaneous angle of attack; the angle ϕ_3 is the orientation angle of R_3 . The angle ϕ_1 progresses in a positive or negative direction; this is dictated by the direction of spin. The angle ϕ_2 progresses in a positive or negative direction; this is dictated generally by local disturbances at payload deployment or missile reentry.

As the missile penetrates the atmosphere, the rates at which ϕ_1 and ϕ_2 progress generally accelerate in absolute value; R_1 progressively diminishes and approaches zero some seconds before impact; R_2 may increase in the early stages of reentry but also diminishes and approaches zero some seconds before impact. The spin, or roll, rate generally declines slightly because of air friction.

In a three-degree-of-freedom description of missile motion, it is convenient to break down the instantaneous resultant aerodynamic force acting at the center of pressure into a drag component and lift component. Drag is a force acting along the trajectory. Lift is a force directed perpendicular to the trajectory and in a direction defined by the orientation angle measured in a clockwise-positive direction from a reference line in the vertical plane. "Clockwise" is defined in terms of an observer looking along the trajectory in the direction in which the missile is flying. Lift acts in a plane determined by the roll axis of the missile and the local velocity vector. Hence, the same orientation angle, ϕ_3 ,

applies to the lift vector and the angle of attack.

A sketch of the geometry in the plane determined by the roll axis of the missile and local velocity vector is shown in Fig. 3. The terms "direction of travel," "direction of the local velocity vector," and "direction of the tangent to the trajectory" are used synonymously. In a three-degree-of-freedom situation, the drag and lift are assumed to apply at the center of gravity.

For small angles of attack, the lift is proportional to the sine of the angle of attack and, therefore, has a magnitude proportional to the magnitude of the vector R_3 in Figs. 1 and 2, and a direction identical to the vector R_3 . Hence—although, in a three-degree-of-freedom description, the epicyclic treatment of the vector R_3 is of no direct interest—the very close geometrical relationship between R_3 and the lift vector suggests an epicyclic treatment of the lift vector itself. As a result, the trajectory reconstruction exercise may involve estimating the parameters corresponding to R_1 , ϕ_1 , R_2 , and ϕ_2 , where each of these is described in terms of a low-order polynomial in time.

Drag forces tend to reduce the missile's forward velocity.

These forces eventually counteract the gravity forces tending to increase the forward velocity of a descending missile. In fact, in the final stages of reentry, the drag forces are many times larger than the gravity forces. A reentering missile may, for example, reach maximum tangential velocity at an altitude of about 100,000 ft. Drag may be estimated in terms of a low-order time polynomial.

Contrary to popular belief, lift forces have a significant effect on missile impact position.

An interesting missile motion is associated with the lift forces. The statement is frequently made that, because of the high precessional rate (of the order of one revolution per second), the lift forces average out to zero. This statement is very nearly true; but the usual inference—that the net displacement caused by the lift forces is zero—is false. Integration of the lift-acceleration equations develops some non-zero constants which result in net displacements. In fact, the lift forces result in a trajectory diverging significantly from the no-lift trajectory. This divergence normally results in an impact position displaced somewhere between 50 and 300 ft from the no-lift situation, all other conditions being the same.

Actually, all other conditions are never the same. Lift forces are usually associated with non-zero angles of attack. Non-zero angles of attack inevitably result in drag forces larger than those existing with zero angles of attack. Consequently—and somewhat indirectly—lift forces are associated with increased drag forces, which will tend to make the missile fall short: an effect superimposed upon the divergence directly connected with lift forces.

A second misconception is that the effect of the lift forces can be described in terms of a significant helical or "corkscrew" motion of the center of gravity about the no-lift trajectory. In fact this helical motion, though present, is normally quite negligible in magnitude (less than 3 ft in radius) and takes place around the diverging trajectory.

The lift and drag forces and their effects cannot be predicted to a high degree of accuracy before the missile test and, hence, are determined from pulse radar data taken during the test.

Other trajectory perturbations

Other types of trajectory deviations that are evaluated from radar data include:

- *Guidance errors.* These errors constitute a major cause of unsatisfactory missile performance. Guidance errors, in the form of velocity components just before payload deployment, can usually be

measured by the test range to an accuracy of 0.2 ft/s. Biases and slow drifts in the guidance system can be evaluated.

- **Deployment impulse errors.** The missile velocity components just after payload deployment usually can be measured by the test range to an accuracy of 0.2 ft/s. Differencing these with the velocity components just before deployment gives computed deployment impulses to an accuracy of about $0.3 (= 0.2\sqrt{2})$ ft/s.

- **Roll lock-in.** This is a serious abnormality, represented by resonance between roll rate and precession rate in the presence of mass asymmetry in the missile. It results in a diverging angle of attack, increased drag, high lateral loads, and possible missile breakup.

Even if breakup does not occur, the missile may impact short by perhaps 500 ft, with a smaller cross-range component. This catastrophe most probably will occur below a 125,000 ft altitude and can be evaluated by a tracking radar.

- **Spin-through-zero.** The missile behavior is variable and can be serious. Typically, it is characterized by a rapid reduction in spin, leading to some spiraling outward of the trajectory from its normally negligible helical path, spinning through zero, and spinning up in the opposite direction with a reversal in the precession direction.

This phenomenon is associated with mass asymmetry in the missile and a roll torque caused by some deformity. Impact errors caused by the accompanying large lift forces may be as large as 4,000 ft in any direction, even if the missile does not break up. This catastrophe generally occurs below 125,000 ft and can be evaluated by a tracking radar.

- **Maneuvers.** Recently, planned maneuvers have been introduced into some reentering missiles as an evasive characteristic. The magnitude of these maneuvers is far greater than the magnitude of the disturbances just discussed. Maneuvers test to the limit the dynamic capability of the radar tracker. Furthermore, the complexity of the maneuvers not only obsoletes the analytical equations of motion but even obsoletes the concept of using analytical equations of motion for missiles of this type. Consequently, a preprocessing procedure applied to carefully corrected radar track data is followed in order to prepare tables of lift and drag, which are

then introduced into the trajectory determination programs.

Validation of MTP's method

Standard error propagation techniques are used to arrive at error estimates in computed reentry trajectories. In two cases with real data, comparisons were possible between independently computed trajectories. One trajectory was computed by the missile contractor, using all available information, including detailed on-board sensor data; the other trajectory was computed by RCA's Missile Test Project, using only radar data. These comparisons validated both the concepts of error analyses and the use of only radar data in computation of reentry trajectories.

The uncertainties in computed trajectories result primarily from errors in radar data or from incomplete radar data.

Approximations in the equations of motion are responsible for only a negligible portion of the error in the computed trajectories for non-maneuvering missiles. In support of this last statement, a test case was run in which a missile contractor supplied a smooth missile reentry trajectory generated by a six-degree-of-freedom program from 400,000 ft altitude to impact. Even though the angle of attack at reentry was about 60 deg and thus corresponded to large lift perturbations, simulated tracking data derived from the generated trajectory and fitted with the equations of motion resulted in root-mean-square (rms) residuals of only 6 ft. This figure of 6 ft represents the rms of the distances between computed and theoretical position points at corresponding time points. The largest residual was 10 ft. A similar test case with a maneuvering-missile trajectory and aerodynamic tables derived from the simulated track data gave similar agreement. When aerodynamic tables are derived from track data prior to the final least-squares estimation, the analytical equations used in the final computation are much simpler.

Rationale for the use of the equations of motion

The question may well be asked: Why not use the simpler equations of motion and prior aerodynamic tables, even for non-maneuvering missiles?

There are three reasons for preferring the

full analytical equations of motion in the case of non-maneuvering missiles.

- There is less data-processing effort involved in using the full analytical equations than in the alternative procedure.

- The computed trajectory is less likely to be led astray by undetected radar aberrations when full analytical equations are used. In fact, the trajectory obtained from derived aerodynamic tables is essentially the same as one obtains from ordinary digital filtering of the radar data.

- The full analytical equations are more amenable to interpolation and extrapolation in regions of missing or poor quality radar data.

Accuracy of reconstructed trajectories

Three examples of some typical missile test support conditions with the associated error analysis are given to show the improved precision obtained from the method used by the MTP.

Example 1. Data from a land-based radar within 50 mi of impact typically resulted in position errors of less than 50 ft and velocity errors of less than 10 ft/s in each of three orthogonal coordinates throughout reentry.

Example 2. Multiple-radar data at the time of deployment and data from a land-based radar within 50 mi of impact typically resulted in position errors of less than 50 ft and velocity errors trending from 0.1 ft/s at reentry to 10 ft/s at impact.

Example 3. (A broad ocean area situation.) Data were received from: 1) land-based radar track at time of deployment; 2) land-based radar track in descending trajectory down to 1.5 million ft altitude; 3) ship radar track during reentry; and 4) a marine transponder array at the time of impact. These resulted in a horizontal position error of 200 ft and a vertical position error of 80 ft at reentry, trending downward to a horizontal error of 50 ft and a vertical error of 15 ft at impact. The velocity error at reentry is 0.25 ft/s in each coordinate, trending upward to 30 ft/s at impact.

Finding the best estimate of trajectory with the weighted least squares technique

C.W. Welsh

When a number of sensors of differing accuracies track a missile, ship, or satellite, the weighted least squares technique gives the best estimate of position and velocity.

One of the prime functions of the Eastern Test Range is to provide the Range user with accurate trajectory position, velocity, and acceleration data for the User's missile at a selected data rate of between 2 and 10 points per second. Corrected data are available from individual radar trackers in real time. However, the real-time data are limited in accuracy by 1) the limits of the calibration and 2) the limits of the random error.

Postflight combination of all tracker data and minimization of the weighted squares of the residuals produces a "Best Estimate of Trajectory" (BET), with greatly improved accuracies over a single tracker. In this article, the fundamentals of Weighted Least Squares Estimation (WLSE) of data to produce our Best Estimate of Trajectory are reviewed, and a specific application is

described. The details of the mathematics will be found in the references and bibliography. Only enough mathematics is presented to enable the reader to grasp the concepts. Although the fundamental results of least squares theory are credited to Gauss, the application of WLSE theory to the BET at the Eastern Test Range was initiated and developed by RCA personnel.

The model

The mathematical model of the WLSE process can be expressed in the form

$$DEL = (P^T WP)^{-1} PWE,$$

where

DEL is the correction applied to the current estimate of the estimated parameter,

P is the partial derivative of the measurement with respect to the estimated quantity,

W is the weight matrix, composed of the inverse of the variances of the measurements, and

E is the differences between the current estimate of the measurement and the actual measurement.

The significant developments of the WLSE process were:

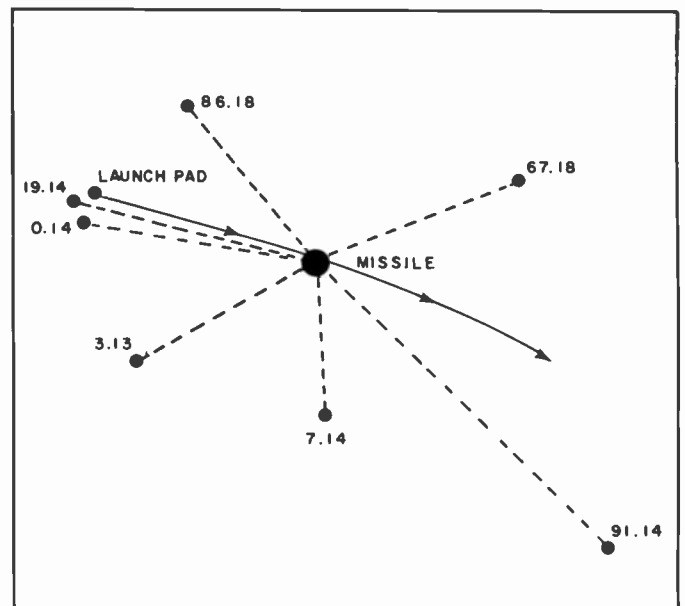
- The methods used to construct and invert the matrix $(P^T WP)$

Reprint RE-24-3-14
Final manuscript received June 22, 1978.

Table I
Observations used in the weighted least squares estimation for the best estimate of trajectory at the Eastern Test Range.

System	Observation
Ballistic camera	X, Y plate coordinates
Inertial guidance	X, Y, Z (Cartesian)
LORAC (Long range accuracy position system)	Latitude, longitude
Missile Impact Location System	Latitude, longitude, time
Radar	Range, azimuth, elevation
SRN9 (Satellite navigation system)	Range rate
TDMM (Telemetry doppler metric measurement)	Range differences
Tracking camera	Azimuth, elevation
Underwater acoustics system	Range
Ship inertial navigation system	Latitude, longitude

Fig. 1
Tracking radar identifications and relative locations with respect to a missile trajectory.



- Computation of the differences, E , in the measurement domain.
- Addition of the error model terms for the measurements.
- Allowing the weight matrix, W , to be input with each measurement sample, permitting dynamic weighting according to the dynamic quality of the data.

An application of Weighted Least Squares Estimation at ETR

Least Squares theory has been in use at the ETR by RCA for more than two decades. Weighted Least Squares Estimation was formulated in 1957, and the first Best Estimate of Trajectory was published in July 1961. The application techniques have been steadily improved and, today, Weighted Least Squares Estimation is primarily used to produce high-quality positions and velocities of missiles, ships and satellites. WLSE permits the combination of many sensors, each with its own degree of accuracy. Modeled errors are reduced and, when given adequate geometry and a good mix of sensors, the random errors are reduced and a single "best" trajectory, or set of locations, is produced. The specifics of the mechanics of the estimation process can be found in Refs. 1 and 2. Summarized, the process begins with estimates and standard deviations of the estimated quantities, the observations and their standard deviations, partial derivatives of the measurements, and appropriate transformation and differencing equations to produce residuals. Iterations (usually two or three) of the estimation parameter corrections produce new estimates of the parameters. The broad spectrum of the types of observations used in WLSE processes at ETR are listed in Table I. We will choose an illustrative subset of the observations as examples of how the WLSE process operates.

First, we will consider one of the modernized radars (an FPQ-14, designated as 19.14) on Merritt Island, Florida, near the launch facilities of Cape Canaveral. During track of a typical missile at a particular time during the flight, the radar is looking at an azimuth of 104 deg clockwise from north, at an elevation of 35 deg above the local tangent plane; the object of interest is at a distance of 4.1 million ft from the radar. Estimates of total

error of the radar data at this point were 0.0027 deg in azimuth, 0.0035 deg in elevation and 22 ft in range. These, when propagated into a Cartesian right-handed coordinate system referenced to the launch pad, with X downrange and Z uprange, become 145 ft in X , 156 ft in Y and 205 ft in Z . At this same time, there are six other radars viewing the missile from their locations, as indicated in Fig. 1.

It can be shown that range is the most significant contributor to a WLSE of the trajectory at these range distances, particularly when the tracking systems are distributed as indicated in Fig. 1. The uncertainty of the WLSE of X , Y and Z for this particular point is 7.8, 17.7 and 7.8 ft, respectively,—a significant improvement in accuracy over that obtained from a single sensor.

A graphic representation of the improvement in trajectory accuracy achieved by the Best Estimate of Trajectory is shown in Fig. 2. The solid line is the trace of the root-sum-square of the one-sigma uncertainties (σ_{Prss}) of a single radar trajectory of a typical launch. The trace is that of the 19.14 and 91.14 radars, located as shown in Fig. 1. The 91.14 radar is on the island of Antigua, in the East Caribbean. Of the six radars available, 19.14 is representative of the best radar track available (on a single-station basis) from launch until 400 s, at

Charles Welsh joined the Data Processing Group of RCA's Missile Test Project in 1960. He is responsible for the design, analysis, and analytical support of scientific data reduction computer programs.

Contact him at:

Missile Test Project, RCA Service Company, Patrick AFB, FL 32925 (305) 494-4314

Charlie Welsh at a remote data terminal.

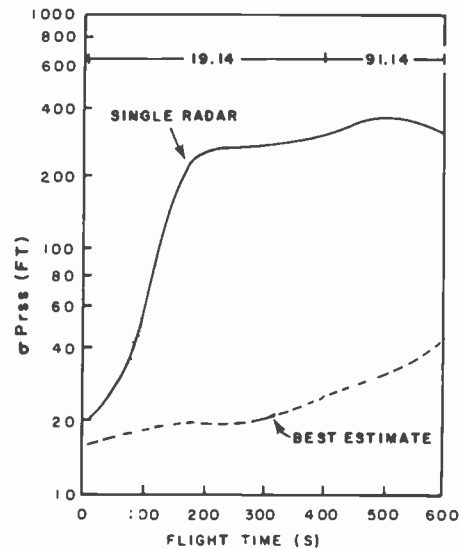
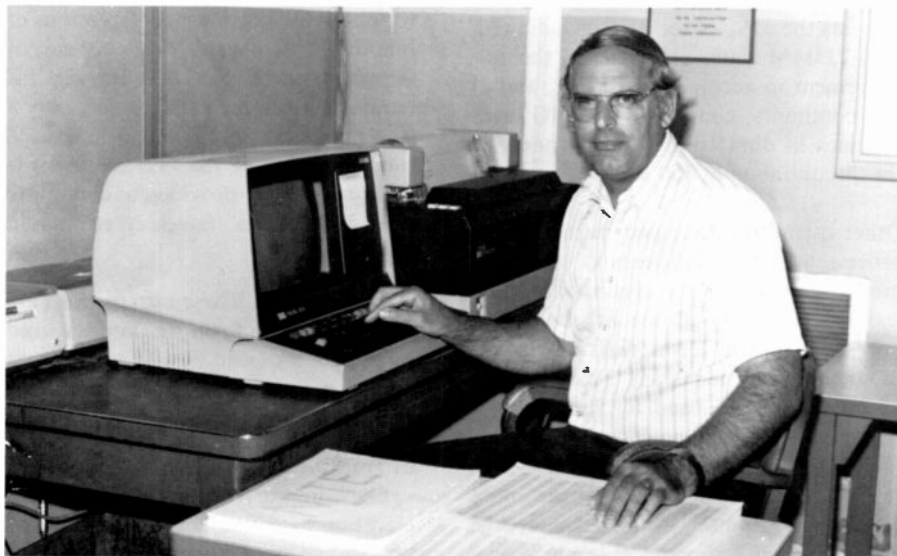


Fig. 2 One-sigma trajectory position estimates for a missile show the improvement in accuracy achieved by the use of Weighted Least Squares Estimation.

which time the target is sufficiently close to the 91.14 radar that its trajectory uncertainties are lower than those of 19.14. The lower trace in Fig. 2 depicts the root-sum-square of one-sigma uncertainties of the combined radar least-squares estimate of the trajectory, using all available radars. Comparison of the two traces in Fig. 2 shows that, after 200 s, the combined radar BET provides an improvement in accuracy

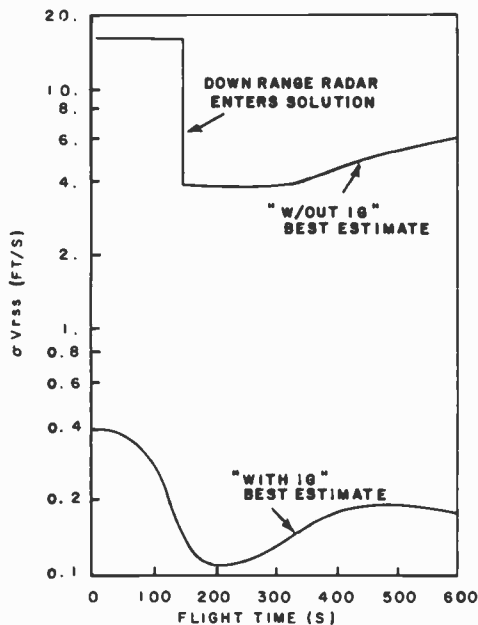


Fig. 3
One-sigma trajectory velocity estimates for a missile show the improvement in accuracy as additional sensor data is processed.

ranging from 10-to-1 to 30-to-1 over the single-station accuracy.

Adding Telemetry Doppler Metric Measurement (TDMM) data and Inertial Guidance (IG) data to the BET improves the *position* accuracy over the radar-only BET by a ratio of less than 2 to 1. However, the *velocity* accuracy is dramatically improved, as demonstrated in Fig. 3. The upper trace is the root-sum-square of the one-sigma uncertainties in velocity of the radar BET. The sharp improvement at 150s demonstrates the greatly improved geometry as the downrange stations enter the solution—particularly the 67.18 radar located at Bermuda. The lower trace presents the σV_{rss} of the BET including IG and TDMM data, showing: 1) the improvement in accuracy of 30-to-1, and 2) the continuity constraint that IG data provides in diminishing the sharpness of the discontinuity at 150 s.

Other quantities estimated in the WLSE process are the coefficients of the error models assigned to the observations. Unless the residuals indicate otherwise, the only error-model terms assigned to the radar data are constant biases in the observations A, E, and R. Since the estimated error-model coefficients are common to all of the observations for a sensor, the WLSE theory requires that the entire set of observations be evaluated before the coefficients are estimated. It can be shown

that the precision of the WLSE of the error-model coefficients is greatly influenced by the partial derivative of the error-model coefficient with respect to the Cartesian X , Y and Z . That is to say, a good estimate of the error model coefficient can be achieved if the observation experiences a significant change as X , Y and Z change. This function is enhanced by selective placement of the sensors with respect to the trajectory. Ref. 3 provides a periodic review of the random and systematic errors in the sensors used at ETR.

Improvements in the uncertainties of the estimated trajectory Cartesian velocities (VX , VY , VZ) are accomplished by adding a trajectory system that has very small high-frequency random-noise content; i.e., Inertial Guidance. The IG observations are integrated and transformed to a Cartesian coordinate system X , Y , Z , VX , VY , and VZ . Although the IG data high-frequency errors are very low, there are significant trends in the data. These low-frequency trends in the IG data are removed in the WLSE process by estimating coefficients of a third-degree polynomial in a time-error model on the IG observations. Adding IG data to the radar BET improves the velocity uncertainties at the point of interest from 2.3, 2.8 and 1.9 ft/s in VX , VY and VZ to 0.08, 0.1 and 1. ft/s.

Other contributors to the BET and their characteristics are:

- a) *The position of the missile on the launch pad.* This data set contributes to the resolution of the IG error-model coefficient values at launch.
- b) *Free-fall constraints.* The trajectory is constrained (during non-powered flight) to follow the gravitational equations of motion. This means that, instead of estimating the X , Y , Z , VX , VY , and VZ parameters for each time point, only a single point of X , Y , Z , VX , VY , and VZ (the beginning of the free-fall span) is estimated. This provides a continuity constraint to the trajectory estimation process.
- c) *Impact point.* These observations are usually in the form of latitude and longitude, provided by a Missile Impact Location System. The data provide a terminal trajectory input.
- d) *Tracking camera data.* These observations in the form of azimuth and elevation have small random-error content and no error model; they contribute

significantly to the early launch portion, particularly when placed at strategic locations around the launch site to give good geometry.

e) *Ballistic camera.* These observations are in the form of plate coordinates. The random errors are low, and no error model is required. The ballistic camera data are significant contributors to reentry accuracies.

f) *Drag and lift characteristics of the reentry body.* These parameters are usually provided by the Range user or are measured by a reentry tracking system. From these data, reentry accelerations due to the effects of the atmosphere can be estimated and permit extension of the free-fall equations of motion through the atmosphere to impact. Error models are necessary, usually on the coefficients of drag and lift, to account for:

- The deviations of the true atmosphere from the model being used,
- The departure of the true coefficients of drag and lift from the model, and
- The deviation of the reentry velocity from that used in the model.

Conclusions

The abundance of tracking sensors at ETR presented an excellent opportunity to develop the application of the Least Squares Theory to the Weighted Least Squares Estimation of trajectories and sensor-error models. Significant improvements of accuracy are realized by making use of the strong points of each sensor and, where possible, modeling the weak points.

References

1. Graybill, Franklin A.: *An Introduction to Linear Statistical Models*, McGraw-Hill Book Co., New York, 1961.
2. Williams, B.J., and Cummings, C.S.: "The Estimation of Trajectory and Error Model Parameters: Powered Flight," *Private communication*.
3. RCA Technical Analysis, "Quarterly Accuracy Report," *Private communication*.

Bibliography

1. Brown, D.C.: "A Treatment of Analytical Photogrammetry with Emphasis on Ballistic Camera Applications." *Private communication*.
2. Kendall, M.G., and Stuart, A.: *The Advanced Theory of Statistics*, Vol. 2, *Inference and Relationship*, Hafner Publishing Co., New York, 1973.
3. Welsh, C.W., and Bost, G.W.: "NITE—N-Interval Trajectory Estimation," *Private communication*.
4. Welsh, C.W.: "An Evaluation of the Usage of Telemetric Metric Angle Data and ITEK Angle Data in the Best Estimate of Trajectory," *Private communication*.

Identifying radar targets with automatic pattern recognition

D.L. Anderson

Since radar targets have distinctive "signatures," it is possible to automatically identify tracked objects by processing selected data from the returned radar signal.

Rapid, near-real-time target identification and classification is a crucial requirement for military radar networks, such as NORAD's Spacetrack system. Conventional means of target identification include the use of experienced signature analysts at remote radar sites. However, limitations inherent in the use of human analysts for near-real-time work are significant.

One solution to this problem is the application of computerized automatic pattern recognition (APR) techniques to the classification task. However, this has been done to various radars with a reasonable degree of success. Application has generally been to the lower-frequency (UHF and L-band) radars, and little effort has been made toward optimizing these techniques for narrow-band, non-coherent, C-band radars.

The intent of this brief paper is to introduce some of the basics of pattern recognition as applied to tracking radars for target classification. The subject is developed by considering a series of "spaces," as depicted in Fig. 1. Each of these spaces represents a means of identifying the target, with the individual elements being unique target descriptors.

The physical space

The physical space contains the target itself and includes an almost limitless number of descriptive elements. Some of these are: weight, size (dimensions), shape, material composition, motion dynamics, orientation, color, odor, and surface texture. If we had easy and economical access to this space, we would have all the information needed to identify and classify the target. Unfortunately, access to this space general-

ly is obtained only through remote sensors, such as a radar. The output of the radar sensor constitutes the second "space" for our consideration: the pattern space.

The pattern space

The pattern space contains the ordered collection of discrete measurements made by the sensor in the physical space. For the present application, these measurements consist of successive receiver output signal-to-noise ratios, which are converted by means of the radar range equation to "cross-section." Radar cross-section is the apparent size of the target, as seen by the radar, and is a function of many variables, such as target size, shape, and orientation; radar wavelength; and viewing (aspect) angle. The mapping of target signal-to-noise ratio (S/N) to radar cross-section is simply:

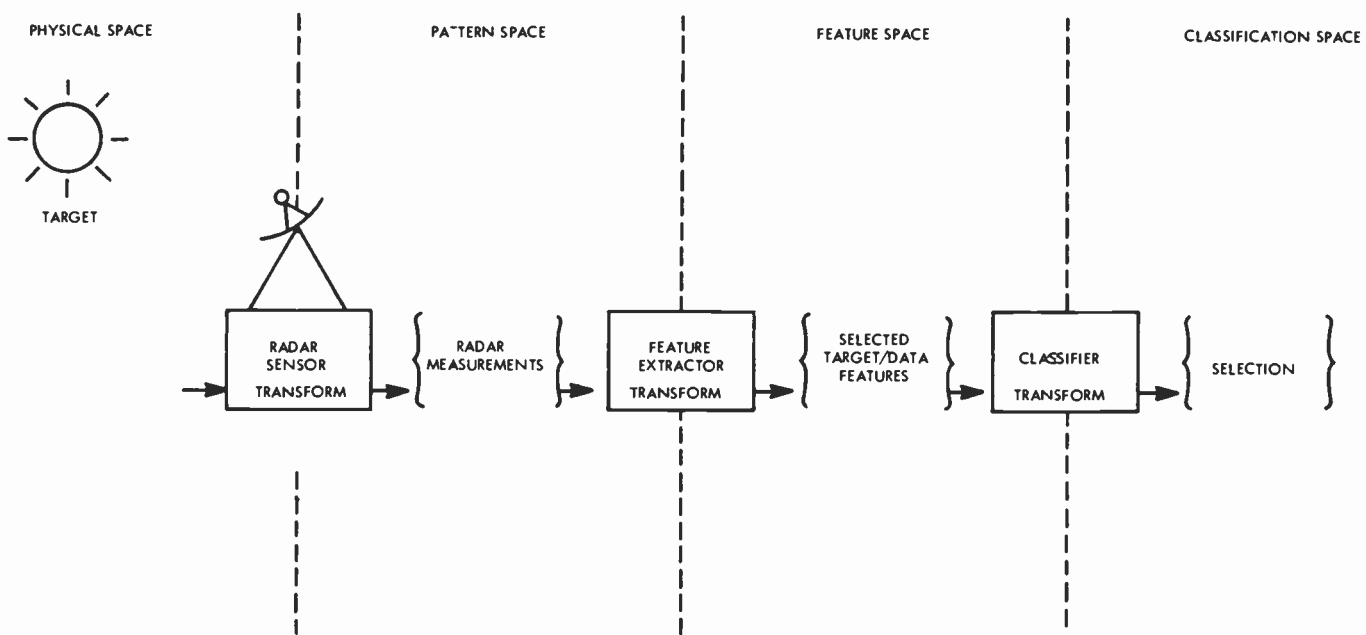


Fig. 1
How objects are identified. The radar target, in "physical space," reflects radar waves back to the radar sensor, giving a waveform in "pattern space." By taking selected information from the waveform (such as peak pulse heights and periodicity), a more descriptive "feature space" is produced. Finally, the features of the target object are compared with the features of known objects, identifying the object in "classification space."

$$\sigma = S/N \left(\frac{R^4}{K} \right)$$

where:

σ is the radar cross-section (usually in m^2)

S/N is the target signal-to-noise ratio at the radar receiver output

R is the target range from the radar (in m)

K is the radar loop gain constant (in m^2)

Radar cross-section often is expressed in decibel form as dB_{m^2} , where:

$$dB_{m^2} = 10 \log_{10} (\sigma_{m^2} / 1m^2)$$

and is the number of decibels above or below a reference area of one square meter. It usually is determined by:

$$dB_{m^2} = S/N_{dB} + 40 \log_{10} R - K_{dB}$$

Attempting target classification directly from the data in the pattern space immediately introduces a significant computational problem. A typical satellite track of five minutes duration with a radar pulse-repetition-frequency of 160 Hz will produce 48,000 cross-section values. This constitutes a pattern vector of 48,000 dimensions as denoted by:

$$P = P_1, P_2, \dots P_k,$$

where k in this case would be 48,000.

The large dimension of this vector, coupled with noise contamination and nonlinearity, as well as target motion/orientation-induced variations and target/radar-site pass-geometry-induced variations, creates a computational nightmare for target classification directly from P .

The solution to this problem is twofold. First, the measurements constituting P are processed to minimize noise effects and to normalize the data for system nonlinearities and pass-geometry-induced variations. Normalization might include a transformation of the data from a time base to an aspect-angle (target-viewing-angle) base for earth or inertially stable objects or, to a rotational-period-interval time base for rotating objects. This "front end" processing is very important to the final classification decision process.

Second, the dimension problem is minimized through separation of selected data or information features from the pattern space. Feature selection is one of the most critical elements of the pattern

recognition process. Typical features from the pattern space range from simple statistical parameters, such as means, maximum values, measures of dispersion, skews, and higher moments, to the results of more sophisticated transformations such as the Fourier, Z, Bhattacharyya, and other linear and non-linear transformations. Crucial to the whole process is the selection of features possessing characteristics that strongly discriminate between the expected radar target types.

In summary, the processed pattern vector may now be represented as:

$$PN = [P_1, P_2, \dots P_k] \begin{bmatrix} n_1 \\ n_2 \\ \vdots \\ n_k \end{bmatrix}$$

where N is the radar sensor data normalizing processing function.

The feature space

The feature space is the ordered collection of those n features obtained by suitable transformations from the pattern space. The n features comprise the elements of the n -dimension feature vector. Desirable feature vector characteristics include:

- *Orthogonality*, such that the inner product of any two elements of the feature vector is zero. This characteristic normally results in minimizing the computational complexities of the classification algorithm or process.
- *The condition that the elements of the feature vector form a basis vector for the desired feature space*. That is, the feature vector elements should be linearly independent. This quality strengthens the classification process and again minimizes the required computations.
- *Normalization of the vector*. Even though the vector elements may be "apples and oranges", each should be

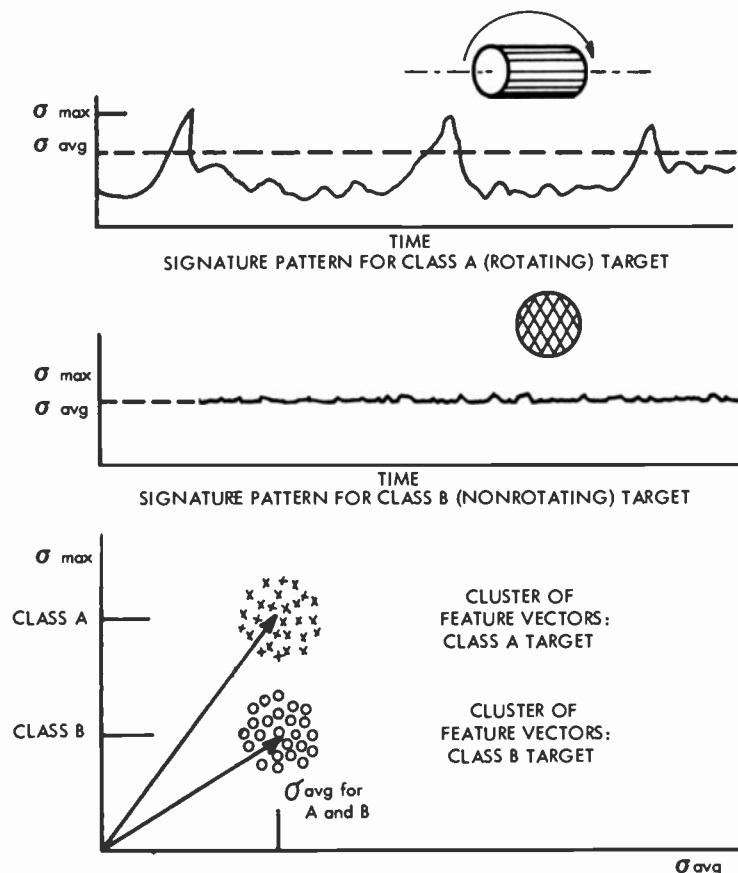


Fig. 2 Feature-space data is different for these two satellites, one tumbling and one rotating. Although their average radar cross-sections are essentially the same, the tumbling target has a higher peak cross-section and so can be differentiated from the rotating target.

given value ranges such that they contribute essentially equal weight to the selection process. This requirement may be altered, however, if the individual features are known to have different strengths or weights. Weighting considerations are discussed later in this article.

The optimum feature vector is that vector whose elements (features) are the fewest in number, and have distinct and non-overlapping value ranges between target classes. Consider the example in Fig. 2, which illustrates just two features: average cross-section, (σ_{avg}), and peak cross-section, (σ_{max}), for two target classes.

Clearly, a distinctive difference is seen in the peak cross-section values (σ_{max}) for the two classes, but, essentially, no difference is seen between the average (σ_{avg}) values. In this case, the use of σ_{avg} in the classification process would be of little value. If anything, its use would de-weight the strength of σ_{max} .

Often, the available features do have significantly different strengths, insofar as discrimination between target classes is concerned. This situation requires consideration of a weighting matrix, W , which weights the particular features according to their individual merits before the classification process. The feature vector, F , is the product of the pattern vector and the features-transformation function, X , where each column of X represents the function to extract 1 of n data features. With weighting, W , applied, the final feature vector becomes $F = PN\bar{X}W =$

$$[P_1, P_2, \dots, P_k] \cdot \begin{bmatrix} n_1 \\ n_2 \\ \vdots \\ n_k \end{bmatrix}$$

$$\begin{bmatrix} x_{11} & x_{12} & \dots & x_{1n} \\ x_{21} & x_{22} & & \\ \vdots & & & \\ x_{k1} & \dots & \dots & x_{kn} \end{bmatrix} \cdot \begin{bmatrix} w_1 \\ w_2 \\ \vdots \\ w_n \end{bmatrix}$$

The classification space

The classification space consists of that function which provides the final class

selection, based on the classification algorithm and supplied feature vector, and a collection of target-class types (prototypes), as selection candidates. Several methods are available to "choose" the correct target class with an acceptable degree of accuracy. Two of the more common methods are the *nearest neighbor* method and the *partition* method.

In the nearest neighbor approach, the individual Euclidian distances between the unknown target's feature vector and a collection of known (prototype) vectors are determined. The target class associated with the prototype nearest the target vector (shortest distance) is then chosen as the correct target type. The distance measurement, however, must be in some meaningful units, as often the individual components of the feature vector are different (apples and oranges). A useful and statistically sound measurement unit is the standard deviation (or other appropriate statistical parameter for the distribution of concern). The standard deviation unit is determined for each feature of the vector from the distribution of each feature. The distribution is obtained from a sufficiently large sample of feature vectors for each target class. The mean feature vector from the large sample comprises the prototype for that particular class.

In the partition method, the classification space is divided into a set of $r-1$ discriminating surfaces (hyperplanes), where r is the number of prototypes in the classification space. The target classification is then accomplished simply by determining which "cell" or partition in the classification the unknown target feature vector falls within.

The prototype array may be represented by the following $n \times r$ matrix, where column entries 1 through n are the elements of the individual prototype vectors (assuming the nearest neighbor approach).

$$C = \begin{bmatrix} C_{11} & C_{12} & \dots & C_{1r} \\ C_{21} & C_{22} & & \vdots \\ \vdots & & & \vdots \\ C_{n1} & & & C_{nr} \end{bmatrix}$$

The final target classification now becomes simply:

$$\text{Target choice} = PN\bar{X}W \left\{ \begin{array}{l} \text{classification} \\ \text{operator} \end{array} \right\} C$$

Methods are available to provide a credence estimate of the final target choice. With the nearest neighbor method, for example, the magnitude of the distance between the target vector and the chosen prototype is itself a good indicator of the choice validity.

Future effort

It is the author's hope that this somewhat brief introduction to Automatic Pattern Recognition will provoke further work toward improving APR in its application to narrow-band, non-coherent, C-band radar target identification. The task is interesting, in that the APR schemes implemented must of necessity be simple and computationally fast to fit in the real-time operational environment. This fact greatly reduces the usefulness of many of the more powerful mathematical methods often employed with pattern recognition. Many innovative and effective schemes remain to be explored.

Reprint RE-24-3-17
Final manuscript received June 22, 1978.

Dave Anderson has been with RCA's Missile Test Project for more than 20 years, working in the fields of radar, instrumentation, and optical signatures. His last assignment at ETR was Software Analyst, assigned to the Range Measurements Laboratory, where he was responsible for the development of support and data processing software for on-axis radar, optical, and laser instrumentation. He is currently assigned to the RCA GEODSS (Ground-based Electro-optical Deep Space Surveillance System).

Contact him at:
RCA GEODSS
2323 Teller Road
Newbury Park, CA 91320
Phone: (805) 499-1921



Digital filtering for radar antenna servo drives

M. Coomer|R. Pepple

A general tracking-loop digital-filter algorithm, readily adaptable to many radars and missions, is developed for a China Lake radar modification.

Many tracking radars now have digital computers that perform operations previously accomplished by analog functions under the control of site personnel. One of the more challenging control applications is the radar track loop. The capacity and speed of presently available digital computers offer the possibilities of comprehensive, flexible track management not previously available to the radar console operator. Such a control algorithm was developed recently for application to a Nike Hercules radar at China Lake, California, that was being modified by RCA. Programmed in FORTRAN, on the Eclipse S/200 Computer, the algorithm uses about 15 percent of the available cycle time in 100 pps tasking. In this paper, the design considerations and some of the features of this program are discussed.

Problem definition

A digital filter is more effective than analog types in separating target-position information from noise. By converting the radar's analog input to digital, such a filter can be incorporated into the system.

The trajectory of a target, such as an aircraft or missile, can be determined by making a time series of three-dimensional position vector measurements. The type of radar discussed in this article measures at a constant sample rate two angles (azimuth and elevation) that define a line of sight and the distance along the line of sight to the target (slant range). The angles are obtained by employing a single, highly directive, electromechanically steered antenna. A pulsed signal provides measurement of range in terms of propagation time delay. Since the same antenna is used for both transmission and reception of the pulses, the receiver is only turned on (gated) for the brief periods when the pulse return (echo) is expected. The timing of the

gate and steering of the antenna are accomplished by servomechanisms. A servomechanism is a control device in which the difference between a reference signal and some function of the controlled variable supplies a drive signal to the control elements that tends to reduce the difference (error) to zero. In the case of the angle drives, the reference is the center of the antenna beam; for range, the reference is the midpoint of the time the receiver is gated. A monopulse radar develops position errors in all three coordinates from each received pulse; the servos drive the antenna and range gate so that the errors from the next received pulse will be smaller than the preceding set. Since the drive is always toward a future position, each servo must develop an estimate of target motion, in order to predict where the target will be. If just the velocity of the target is used, the servo is referred to as a type-1 system; if target velocity and acceleration are used, the servo is known as a type-2 system. A type-1 system will maintain a constant position error for a constant target velocity. A type-2 system will have no position error for constant target velocity and a constant position error for constant target acceleration.

The period of time that a servo requires to determine target motion is inversely proportional to its bandwidth. A wide-bandwidth system will respond more quickly to changes in target motion than will a narrow-band system; unfortunately, a wide-band system will also respond more quickly to measurement noise. Another consideration is the ability of the device being driven by the servo to respond to changes in motion. The large mass of a radar antenna limits its response to motion changes to a bandwidth of about 3 Hz. The angle drive servos should not, therefore, have a bandwidth of more than 3 Hz. The range gate servo, being an electronic timing device with essentially no inertia, can have

bandwidths that approach the information bandwidth of the radar. A radar that has a pulse repetition rate of 160 pulses per second, for example, will have an information bandwidth of 80 Hz.

Target motion is rarely limited to constant velocity, particularly in radar coordinates, so a servo of type-3 or even type-4 characteristics would seem to be indicated. A type-3 system will have no position error for constant target acceleration. Even changing target acceleration can be considered to be made up of short intervals of constant acceleration so, if the bandwidth of the system is wide enough, a type-3 system is adequate. Stability considerations, however, limit electromechanical servo designs to no higher than type-2. Digital servos can be designed for higher type response and, when used in combination with the electromechanical system, can raise the mount response by one order. That is, by knowing the response characteristics of a type-2 antenna drive, the error signals fed to the mount servo can be modified by digital calculations to produce the response equivalent of a type-3 system.

In a conventional radar, the angle and range receivers develop voltages that are proportional to position errors in each coordinate and these voltages are then input to the angle and range drive servos. In the digital drive modification discussed in this article, the error voltages are converted to digital form (A/D) and processed by the computer in combination with the radar mount parameters (azimuth, elevation, and range) to produce an estimate of present and future target position. This future position is differenced with the present mount position to determine where the mount should be driven. Since the electromechanical servos have known drive limitations, an overdrive ("push function") is added to the differences. These

combined signals are converted to analog voltages (D/A) and input to the mount servos. If the mount servos are type-2, the push function will be proportional to target acceleration.

Target motion is usually rather complicated in radar (i.e., polar) coordinates; for example, an airplane flying at constant velocity past a radar will create large-angle tracking accelerations. This not only produces servo errors (in a type-2 system) but makes target motion prediction difficult in the computer if the prediction equations are in azimuth and elevation. The solution is to do the digital processing in Cartesian (East, North and Up) coordinates and then convert the predicted target position to radar coordinates for the drive function.

Design goals

The digital filter must pass a polynomial that approximates trajectory motion while minimizing noise. The design goal was to develop a vector that contains the best estimate of present and future target positions.

The primary mission of a tracking radar is to provide accurate trajectory data during the entire period that the target is within the signal-sensitivity capabilities of the radar. This requires that the radar be precisely calibrated, capable of rapid target acquisition, and able to handle any target dynamics. Further, since the radar is a position-sensing device, and target velocity and acceleration are necessary parts of target trajectory requirements, the radar must not only minimize position errors but must also provide smooth track, so that velocity and acceleration can be derived from the basic data gathered. Some data enhancement can be achieved by post-test data processing, but the best data comes from the best real-time radar operation.

As far as the computer program is concerned, the ultimate limit for target dynamics is the radar mount; the goal of this program was to fully exploit the mount capability. The radar hardware would be operated in its widest bandwidth settings, and the computer would provide an effective bandwidth that matched the dynamics of the target.

The basic track and data loop is shown in Fig. 1. The radar measurements are azimuth, elevation, and range from the encoders and their associated error

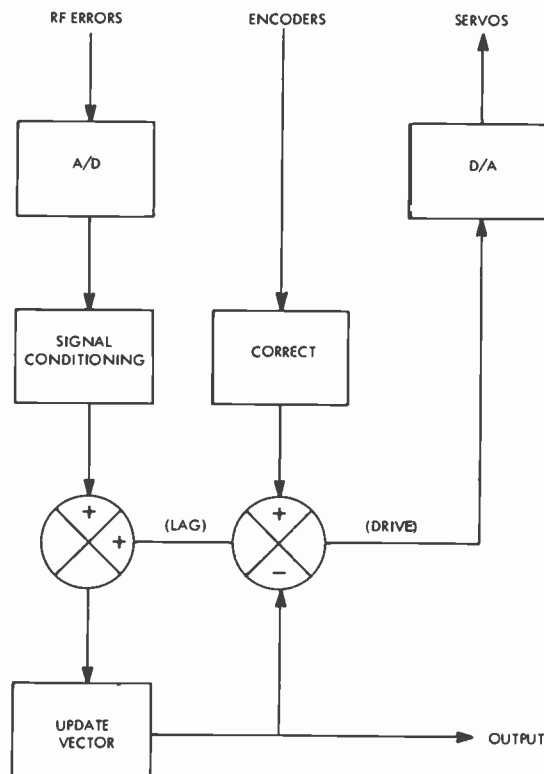


Fig. 1
The basic track and data loop of the China Lake modified radar. Note the conversion of RF error signals from analog to digital for processing, the intercession of the update vector, and the reconversion to analog to drive the servos.

voltages plus signal strength from the receiver. The error voltages are digitized at the monopulse rate and passed through a signal-conditioning algorithm. The signal conditioning will convert the voltages to angle and range error units by using receiver calibration information, edit and filter them to a bandwidth compatible with the drive-loop requirements. The encoder data are corrected for various nonlinearities, such as mount non-orthogonality and droop. The signal conditioning and correction algorithms must be specifically tailored for each radar installation and will not be discussed in any detail in this paper.

The vector containing the best estimate of present and future target positions is compared with the corrected encoder data to provide mount-drive error (lag) and mount drive to the future position. The mount lag is combined with the conditioned error signals (which represent target position relative to the mount) to obtain the vector error. The vector is then corrected and the loops are closed. The vector is also output for recording and remote site usage.

The vector development algorithm presents the major challenge in the drive loop design and is the primary subject of this paper. The vector algorithm must be able to quickly establish an accurate estimate of present target position and be able to predict the next target position with these estimates isolated from measurement noise. Trajectory motion is primarily a low-frequency effect, and measurement noise is usually distributed throughout the frequency spectrum. Since the digital filter must pass a polynomial that approximates trajectory motion and minimizes measurement noise, a low-pass filter is indicated. A conventional means of describing a low-pass filter is in terms of its 3dB bandwidth; that is, the frequency at which its power response is one-half of its response at zero frequency. The response of the filter at zero frequency (position) must be unity.

A practical trajectory filter need only pass a second-degree polynomial in time (without position error for constant acceleration) and be restricted to an effective time span during which target acceleration is essentially constant. All of the filters used in a real-time operation are end-point filters;

that is, they contain only present and past trajectory information and are required to output a smoothed value equivalent in time to the most recent measurement. End-point filters can be either moving arc (convolution) or recursive. The moving arc filter utilizes a finite set of data points to produce a smoothed output; as each new measurement is read in, the oldest measurement is dropped out. This filter has the advantage of possessing a finite memory of past tracking disturbances or dynamics, but it is storage and computationally expensive. This is especially so if low bandwidths are desired, since bandwidth is inversely proportional to span length. Further, bandwidth variation is possible only if many sets of data multipliers are either stored or computed.

A recursive filter requires only the smoothed outputs from the previous point plus the present measurement to produce a new set of smoothed outputs. Very little storage and only a few computations are required, and bandwidth can be varied with almost no additional computations. However, since past smoothed data is used, the filter retains a memory of all past data (good and bad). This infinite memory can be modified by deweighting past data, however, so that results virtually identical to a moving arc filter can be obtained recursively. The deweighting factor employed in the China Lake filter is B , where B is positive and less than one, and i increases backward in time from zero for the present point.

Filter derivation

A quadratic polynomial filter with exponentially decaying memory was developed, using the least-squares criterion.

The quantity to be minimized is:

$$R = \sum_{i=0}^n B^i (\bar{X}_n - iT\dot{\bar{X}}_n + \frac{1}{2}i^2T^2\ddot{\bar{X}}_n - X_{n-i})^2$$

where:

B is the exponential decay factor and must be between 0 and 1,

\bar{X}_n is the current smoothed position estimate,

$\dot{\bar{X}}_n$ is the current smoothed velocity estimate,

$\ddot{\bar{X}}_n$ is the current smoothed acceleration estimate,

T is the time between data points, and

X_{n-i} are the measured data points; X_n being the current point, X_{n-1} being the previous point, etc.

The solution for a recursive filter starts off the same as for a standard least-squares derivation by taking the partials of R with respect to \bar{X}_n , $\dot{\bar{X}}_n$, and $\ddot{\bar{X}}_n$ and setting the partials equal to zero. Before solving these three equations for the three unknowns, though, we substitute values from the previous $(n-1)$ recursion to obtain a recursive filter. This procedure gives us a solution for \bar{X}_n , $\dot{\bar{X}}_n$, and $\ddot{\bar{X}}_n$ expressed in terms of \bar{X}_{n-1} , $\dot{\bar{X}}_{n-1}$, $\ddot{\bar{X}}_{n-1}$, X_n , T , and various summations of B . In other words, all that we need for a recursion of the filter is the results from the previous recursion and the latest data point. Since we are only working with one data point at a time, we normally drop the subscripts from our notation. In addition, we simplify summation notation by letting:

$$S_0 = \sum_{i=0}^n B^i, \quad S_1 = \sum_{i=0}^n iB^i,$$

$$S_2 = \sum_{i=0}^n i^2B^i, \quad S_3 = \sum_{i=0}^n i^3B^i$$

and $S_4 = \sum_{i=0}^n i^4B^i$

Using these simplifications of the notation, we can then express our filter in algorithm form as follows:

1. Update the summations

$$S_4 = B[S_4 + 4S_3 + 6S_2 + 4S_1 + S_0]$$

$$S_3 = B[S_3 + 3S_2 + 3S_1 + S_0]$$

$$S_2 = B[S_2 + 2S_1 + S_0]$$

$$S_1 = B[S_1 + S_0]$$

$$S_0 = 1 + BS_0$$

2. Take the determinant of the summation matrix

$$C_1 = S_2S_4 - S_3^2$$

$$C_2 = S_1S_4 - S_2S_3$$

$$C_3 = S_1S_3 - S_2^2$$

$$D = C_1S_0 - C_2S_1 + C_3S_2$$

3. Calculate the smoothing coefficients

$$\alpha = \frac{C_1}{D}$$

$$\beta = \frac{C_2}{D}$$

$$\gamma = \frac{C_3}{D}$$

4. Difference the latest data point with the predicted value from the previous recursion.

$$\Delta X = X - X_p$$

5. Compute the new smoothed estimates

$$X = X_p + \alpha \Delta X$$

$$\dot{\bar{X}} = \dot{X}_p + \beta \frac{\Delta X}{T}$$

$$\ddot{\bar{X}} = \ddot{X}_p + 2\gamma \frac{\Delta X}{T^2}$$

6. Predict the values for the next recursion

$$X_p = \bar{X} + T\dot{\bar{X}} + \frac{1}{2}T^2\ddot{\bar{X}}$$

$$\dot{X}_p = \dot{\bar{X}} + T\ddot{\bar{X}}$$

$$\ddot{X}_p = \ddot{\bar{X}}$$

We then have a filter which is computationally fairly simple, requiring only 23 additions or subtractions, 30 multiplies, and 5 divides for a single recursion. This means that the filter can be used at a high sampling rate. How high a rate it can sustain is, of course, dependent upon the speed of the computer upon which it is implemented and the computational load imposed by the rest of the program.

Since this is a recursive filter, there are several variables which must be initialized prior to the first recursion. The summations (S_0 through S_4) are normally initialized based upon built-in values which reflect the chosen B -number and starting value of n . (The filter is never started from $n=0$ when used in a closed loop, in order to avoid instabilities.) Although n itself does not appear in the final algorithm, it normally is maintained as a counter and displayed as an indication of the current state of the filter. The predicted vector (X_p , \dot{X}_p and \ddot{X}_p) must be initialized in real time from actual data preceding the first recursion of the filter. When the program itself has information which it uses to place the process in an initial state, this same information should be used to initialize the filter. When the program merely "finds" the process in some state, a single data point can be used to initialize X_p and first and second differences to initialize \dot{X}_p and \ddot{X}_p .

Two special cases are discussed to further an understanding of the filter action.

The full derivation of the filter is quite complicated and has been reduced here, for space considerations, to a listing of the necessary steps in the solution. In a way, this is unfortunate, because the development of two special cases is not evident from the mathematics shown. So let us merely say that the following can be shown:

If $B = 1$

$$\alpha = 3(3n^2 + 3n + 2) / (n+1)(n+2)(n+3)$$

$$\beta = 18(2n+1) / (n+1)(n+2)(n+3)$$

$$\gamma = (30 / (n+1)(n+2)(n+3))$$

If $B < 1$ and $n \rightarrow \infty (B^n \rightarrow 0)$

$$\alpha = 1 - B^3$$

$$\beta = (3/2)(1 - B)^2(1 + B)$$

$$\gamma = (1/2)(1 - B)^3$$

The ($B=1$) case represents the recursive least-squares solution to a second-degree polynomial of n equally weighted data points and is often called an *expanding memory* filter. This filter has optimum starting characteristics, requiring only three data points to obtain initial position, velocity, and acceleration values. It is unsatisfactory as a tracking filter, however, because the span of points processed after initialization will soon exceed the span of points over which the constant acceleration assumption is valid. The bandwidth of this filter is approximately $(1.9/nT)$ Hz.

The ($B^n \rightarrow 0$) case represents a steady-state filter that is independent of the number of points processed (after initialization). The bandwidth of this filter is approximately $[0.62(1-B)/T]$ Hz. This filter is computationally convenient and is in use in a number of computerized radars, including those at the Air Force Eastern Test Range. Although it is a good steady-state filter, it suffers from starting problems, even if the bandwidth is widened by making B a fairly small number. This is a serious problem, because starting conditions are required not just at target acquisition but anytime the target motion has discontinuities in velocity or acceleration. For cases such as missile staging, the second-degree polynomial assumption is not valid, and the filter must either reinitialize quickly or the target will be lost.

The China Lake filter has the acquisition capabilities of the expanding memory filter

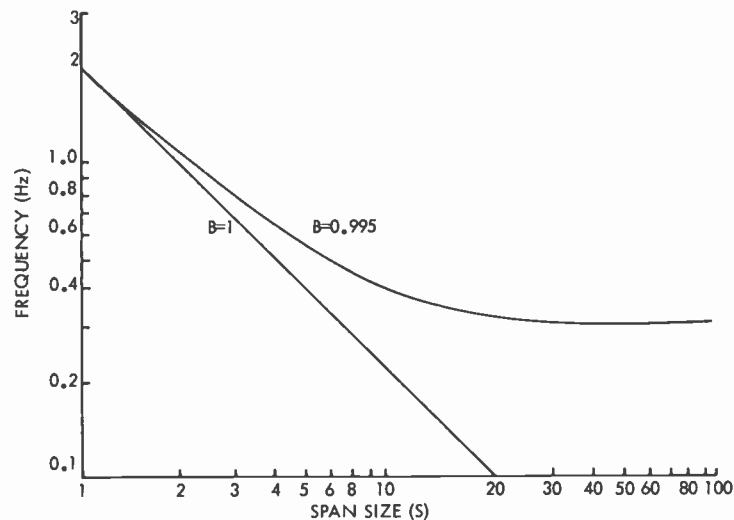


Fig. 2 Half-power (-3dB) frequency of an expanding memory filter ($B=1$) and an exponentially weighted filter with $B=0.995$ for a 100 pps sample rate.

when B^n is large and steady-state response when B^n is small, coupled with a smooth transition between these states. Bandwidth variation as a function of time after acquisition is shown in Fig. 2 for a ($B=1$) filter and the ($B=0.995$) China Lake filter, both for a 100 pps sample rate. Anytime a trajectory discontinuity is encountered, the filter is returned to its acquisition bandwidth. (This will be discussed again later.)

Filter parameters

Since the China Lake filter can assume any response characteristic desired, parameters were selected to make it compatible with the limitations of the radar mount and the tracking mission.

The parameters selected are the filter update rate, T , maximum bandwidth (starting value of n) and minimum bandwidth (B). Ideally, the filter update rate should be the same as the mount drive rate. A high drive rate (usually 100 pps) is required to insure that there is a smooth digital-to-analog conversion; the same considerations apply to the filter update rate; i.e., changes in each successive filter output should be small. If computer cycle time is a problem, the filter update rate can be less than the drive rate but must be at least four times the mount servo bandwidth. The Eclipse S/200 Computer used at China Lake allowed use of 100 pps update rate.

The starting value of n (maximum bandwidth) must be selected based on the mount servo bandwidth. Drive instability will occur if the filter bandwidth is wider than the servo bandwidth. A maximum

filter bandwidth of about one-half the servo bandwidth is recommended, since both the filter and the servo have frequencies where their response is greater than unity. Having selected a maximum bandwidth, the expanding memory bandwidth formula will give the desired value of n . The China Lake servos have a bandwidth of about 3 Hz, so a starting value of $n=150$ (1.5s) was chosen.

Assuming that an effective test for change of acceleration within a filter span is used so that the filter will reinitialize, the minimum bandwidth is somewhat immaterial and subject only to the desire for maximum smoothing. However, repeated reinitializations are not desirable, so bandwidths that are too narrow are to be avoided. The ($B^n \rightarrow 0$) formula will yield the value of B . For China Lake, primarily concerned with aircraft tracking, the value $B=0.995$ (0.31 Hz bandwidth) was found to be most satisfactory. For other applications, such as satellite tracking, minimum bandwidths of less than 0.1 Hz are feasible.

Response curves for various values of nT for the China Lake case are shown in Figs. 3 and 4.

Filter control

Tracking errors must be monitored continuously to guard against trajectory events that the filter cannot handle. However, the filter must be prevented from resetting due to tracking noise.

In the China Lake program, a separate low-pass filter (2-Hz bandwidth) was used

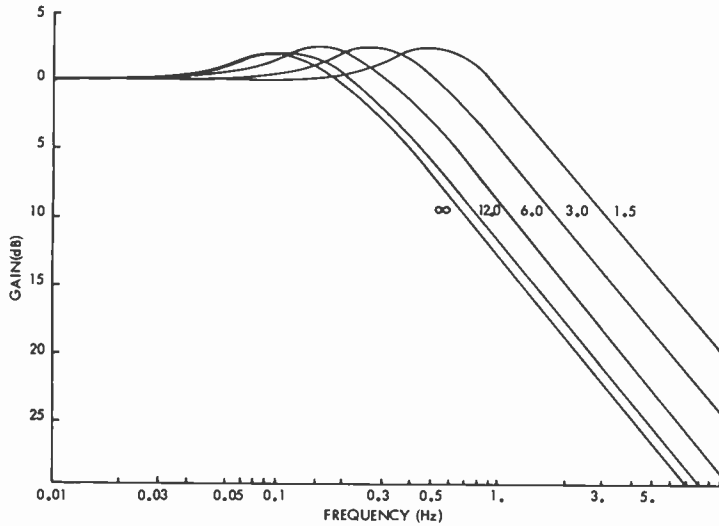


Fig. 3
Amplitude response of a second-degree, exponentially weighted filter (100 pps, $B=0.995$) for various span sizes.

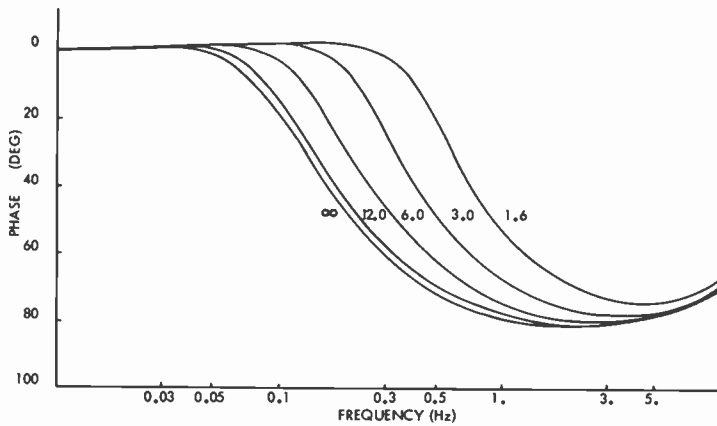


Fig. 4
Phase response of a second-degree, exponentially weighted filter (100 pps, $B=0.995$) for various span sizes.

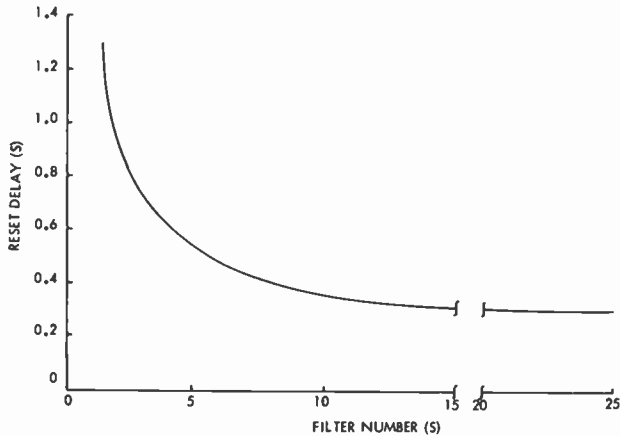


Fig. 5
Delay time before filter reset.

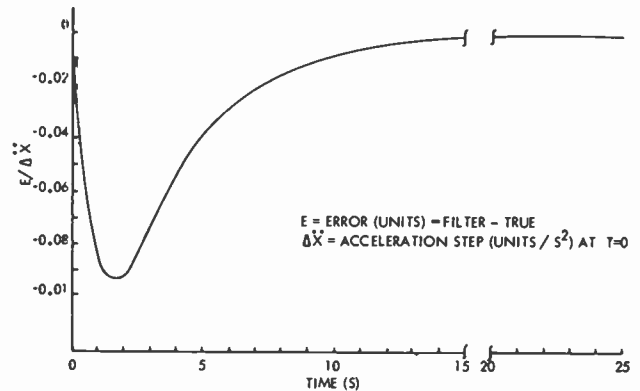


Fig. 6
Normalized position error of the exponentially weighted filter (100 pps, $B=0.995$) to an acceleration step from a reset memory of 1.5 seconds.

for the tracking error signals to establish an error trend. This trend is compared against a noise estimate obtained from the signal conditioning algorithm. When the trend exceeds the noise level, an error counter is started. When this count exceeds a value that is a function of the main filter bandwidth, the main filter is reset to its acquisition bandwidth.

The most serious tracking problem occurs when there is a trajectory acceleration change. When this happens, the rate of position-error buildup is inversely proportional to the bandwidth of the main filter. Consequently, the critical error count is proportional to bandwidth. The critical count in terms of seconds is shown in Fig. 5. The function used is 20α (seconds), because α is proportional to bandwidth and has already been computed.

Recovery of the China Lake filter after reset following an acceleration step is shown in Fig. 6. Final recovery is relatively slow, because the filter bandwidth is continuously narrowing. This is somewhat deceptive because the error counter is not reset until recovery is within the noise level. So, if the acceleration step was large, more than one reset will occur and significant error magnitudes will be reduced faster than shown.

Vector calculations

The drive function requires the development of a three-dimensional vector.

To this point, the filter discussion has been limited to separate parameters. The three-

dimensional trajectory vector is formed in Cartesian coordinates because these coordinates have the best-behaved derivatives and the filter introduces errors if derivatives higher than the second are present in the trajectory. However, the radar measurements are polar, and each coordinate may have different bandwidth requirements.

The solution chosen has three separate filters (one for each radar coordinate) applied to Cartesian error components obtained by transforming polar errors. The three polar errors produce nine Cartesian errors. These components are multiplied by the corresponding filter coefficients and then combined to produce the new vector.

The calculations are as follows:

$$\begin{aligned} r &= R \cos E \\ x &= r \sin A \\ y &= r \cos A \\ z &= R \sin E \end{aligned}$$

$$\begin{bmatrix} \Delta X_A & \Delta X_E & \Delta X_R \\ \Delta Y_A & \Delta Y_E & \Delta Y_R \\ \Delta Z_A & \Delta Z_E & \Delta Z_R \end{bmatrix} =$$

$$\begin{bmatrix} Y & -XZ/r & X/R \\ -X & -YZ/r & Y/R \\ 0 & r & Z/R \end{bmatrix} \cdot \begin{bmatrix} \Delta A & 0 & 0 \\ 0 & \Delta E & 0 \\ 0 & 0 & \Delta R \end{bmatrix}$$

$$\begin{bmatrix} \bar{X} & \dot{\bar{X}} & \ddot{\bar{X}} \\ \bar{Y} & \dot{\bar{Y}} & \ddot{\bar{Y}} \\ \bar{Z} & \dot{\bar{Z}} & \ddot{\bar{Z}} \end{bmatrix} = \begin{bmatrix} X_p & \dot{X}_p & \ddot{X}_p \\ Y_p & \dot{Y}_p & \ddot{Y}_p \\ Z_p & \dot{Z}_p & \ddot{Z}_p \end{bmatrix} +$$

$$\begin{bmatrix} \Delta X_A & \Delta X_E & \Delta X_R \\ \Delta Y_A & \Delta Y_E & \Delta Y_R \\ \Delta Z_A & \Delta Z_E & \Delta Z_R \end{bmatrix} \cdot$$

$$\begin{bmatrix} \alpha_A & \beta_{A/T} & 2\gamma_{A/T^2} \\ \alpha_E & \beta_{E/T} & 2\gamma_{E/T^2} \\ \alpha_R & \beta_{R/T} & 2\gamma_{R/T^2} \end{bmatrix}$$

where:

A, E, R are the radar measurements

$\Delta A, \Delta E, \Delta R$ are the radar errors

$\alpha_A, \beta_A, \gamma_A$ are the azimuth filter coefficients

$\alpha_E, \beta_E, \gamma_E$ are the elevation filter coefficients

$\alpha_R, \beta_R, \gamma_R$ are the range filter coefficients

Filtering in this manner allows the bandwidth characteristics to be maintained in polar coordinates but achieves the low-distortion characteristics of Cartesian filtering.

Marie Coomer joined the RCA Missile Test Project in 1964. She was the first woman assigned on a permanent status to a down-range station on the ETR. She participated in the development of several tracking radars and in 1972, at Cape Canaveral, she performed the original analysis for a recursive, exponentially weighted, expanding memory, real-time filter. In 1976, she installed this filter as part of the modification of the China Lake Tower 9 Northwest radar. She presently is the Staff Software Specialist for the Test Operations Support Section of the MTP.

Contact her at:
Missile Test Project
RCA Service Co.
Patrick AFB, FL 32925
Phone: (305) 494-4718

Marie Coomer and Royal Pepple at radar controller's console.



Bibliography

1. Barton, D.K.: "Radar System Analysis," Prentice-Hall, 1964.
2. Ehling, E.H.: (Editor and Principal Author), "Range Instrumentation," Prentice-Hall, 1967.
3. Morrison, N.: "Introduction to Sequential Smoothing and Prediction," McGraw-Hill Book Co., 1969.

Reprint RE-24-3-7

Final manuscript received June 22, 1978.

This work was performed by RCA for the U.S. Naval Weapons Center at China Lake, CA, under Contract No. N60530-77-C-0011.

Royal Pepple has been involved in data processing at RCA's Missile Test Project since 1958. He is primarily concerned with developing data-processing and systems-analysis techniques for electronic trajectory-measuring systems.

Contact him at:
Missile Test Project
RCA Service Co.
Patrick AFB, FL 32925
Phone: (305) 494-2814

Dates and Deadlines

Upcoming meetings

Ed. Note: Meetings are listed chronologically. Listed after the meeting title (in bold type) are the sponsor(s), the location, and the person to contact for more information.

JAN 23-25, 1979—Automated Testing for Electronics Manufacturing Los Angeles Marriott, Los Angeles, CA **Prog Info:** ATE Seminar/Exhibit, 1050 Commonwealth Ave., Boston, MA 02215

JAN 23-25, 1979—Reliability and Maintainability (IEEE) Shoreham Americana, Washington, DC **Prog Info:** D.F. Barber, POB 1401, Branch PO, Griffiss AFB, NY 13441

JAN 30-FEB 1, 1979—Communications Networks 79 Conf. and Expo; Sheraton Park Hotel, Washington, DC **Prog Info:** Ed Halsted, The Conference Company, 60 Austin St., Newton, MA 02160

FEB 2-3, 1979—SMPTE Television Conf. (SMPTE) San Francisco, CA **Prog Info:** SMPTE Headquarters, 862 Scarsdale Ave., Scarsdale, NY 10583

FEB 6-8, 1979—Aerospace & Electronic Systems Winter Conf. (WINCON) (IEEE) Los Angeles, CA **Prog Info:** Sheldon Jones, Aerojet ElectroSystems, P.O. Box 296, Azusa, CA 91702

FEB 15-17, 1979—Intl. Solid State Circuits Conf. (IEEE) Sheraton Hotel, Philadelphia, PA **Prog Info:** Lew Winner, 301 Almeria Ave., P.O. Box 343788, Coral Gables, FL 33134

MAR 6-8, 1979—Optical Fiber Communication (IEEE, OSA) Shoreham Americana Hotel, Washington, DC **Prog Info:** Optical Soc. of America, 2000 L Street, N.W., Suite 620, Washington, DC 20036

MAR 13-16, 1979—Audio Engrg. Soc. 62nd Technical Mtg. and Exhibit, Sheraton, Brussels, Belgium **Prog Info:** Donald J. Plunkett, AES, 60 E. 42nd St., New York, NY 10017

MAR 14-16, 1979—Simulation Symposium (IEEE) Tampa, FL **Prog Info:** Dr. Joe Clema, Simulation Tech., 4124 Linden Ave., Dayton, OH 45432

MAR 19-21, 1979—Fourth Annual Control of Power Systems Conf. (IEEE) Texas A&M U., College Sta., TX **Prog Info:** B. Don Russell, Electric Power Institute, Dept. of Elect. Engr., Texas A&M, College Sta., TX 77843

MAR 25-28, 1979—Natl. Association of Broadcasters Conv., Dallas, TX **Prog Info:** NAB, 1771 N St., N.W., Washington, DC 20036

MAR 27-30, 1979—Vehicular Technology (IEEE) Arlington Heights, Chicago, IL **Prog Info:** Al Goldstein, Natl. Mgr. Field Engr., Motorola, Inc., 1301 E. Algonquin Road, Schaumburg, IL 60196

APR 2-4, 1979—Acoustics, Speech & Signal Processing (IEEE) Intl. Inn, Washington, DC **Prog Info:** Anthony Eller, Naval Research Laboratory, Washington, DC 20375

APR 3-5, 1979—Space Instrumentation for Atmospheric Observation (IEEE) El Paso Civic Center, El Paso, TX **Prog Info:** Dr. Joseph H. Pierluissi, Dept. of Elect. Engrg., U. of Texas at El Paso, El Paso, TX 79968

APR 23-25, 1979—Intl. Symp. on Computer Architecture (IEEE) Marriott Hotel, Philadelphia, PA **Prog Info:** Dr. Barry Borgerson, Sperry Univac, P.O. Box 500, Blue Bell, PA 19424 (215-542-2013)

APR 24-26, 1979—ELECTRO (IEEE) Coliseum, New York, NY **Prog Info:** W.C. Weber, Jr., Program Chairman, ELECTRO, 999 N. Sepulveda Blvd., El Segundo, CA 90245 (213-772-2965)

APR 24-26, 1979—Reliability Physics Symp. (IEEE) Airport Hilton, San Francisco, CA **Prog Info:** Dr. Frank B. Micheletti, Rockwell International, 3370 Miraloma Ave., Anaheim, CA 92803

APR 25-27, 1979—Conf. on Modeling and Simulation, Univ. of Pittsburgh, Pittsburgh, PA **Prog Info:** W.G. Vogt, Modeling and Simulation Conf., 348 Benedum Engineering Hall, U. of Pittsburgh, Pittsburgh, PA 15261

APR 30-MAY 2, 1979—Intl. Microwave Symp. (IEEE) Sheraton Twin Towers, Orlando, FL **Prog Info:** R. E. Henning, College of Engr., University of South Florida, Tampa, FL 33620 (813-974-2581)

MAY 14-17, 1979—Industrial and Commercial Power Systems Conf. (IEEE) Washington Plaza, Seattle, WA **Prog Info:** T.E. Sparling, T.E. Sparling & Assoc., 1920 Eastlake Ave., Seattle, WA 98102 (206-325-7770)

MAY 15-17, 1979—National Aerospace & Electronics Conf. (NAECON) (IEEE) Dayton Convention Ctr., Dayton, OH **Prog Info:** NAECON, 140 E. Monument Ave., Dayton, OH 45402 (513-255-3627)

MAY 15-17, 1979—Electrical & Electronic Measurement & Test Instrument Conf. (IEEE) Ottawa, Ont. **Prog Info:** Harry Ashworth, Bell Northern Research, P.O. Box 3511, Station C, Ottawa, Ont. K1Y 2H7

JUNE 4-7, 1979—National Computer Conf. (AFIPS, IEEE) New York, NY **Prog Info:** Thomas C. White, American Federation of Information Processing Societies, 210 Summit Ave., Montvale, NJ 07645 (201-391-9810)

JUNE 11-13, 1979—Intl Conf. on Communications (IEEE) Sheraton Hotel, Boston, MA **Prog Info:** Richard C. Stiles, Director Telecommunications Planning, GTE Labs. Inc., 40 Sylvan Road, Waltham, MA 02154 (617-890-8460 ext. 301) or Duane Mattisen (617-862-5500 ext. 5400)

JUNE 12-14, 1979—Intl. Pulsed Power Conf. (IEEE) South Park Inn, Lubbock, TX **Prog Info:** Dr. M. Kristiansen, Texas Tech. U., Box 4439, Lubbock, TX 79409 (806-742-3533)

JUNE 18-22, 1979—Intl. IEEE/AP Symp. & USNC/URSI Mtg Seattle, WA **Prog Info:** I. Peden, Dept. of Elect. Engr., U. of Washington, Seattle, WA 98195 (206-543-0340)

JUNE 19-21, 1979—Power Electronics Specialists Conf. (IEEE) San Diego, CA **Prog Info:** Jerrold Foutz, code 9234, Naval Ocean Systems, San Diego, CA 92152 (714-225-2752)

JUNE 25-27, 1979—Design Automation Conf. (IEEE) Cherry Hill, N.J. **Prog Info:** Harry Hayman, P.O. Box 639, Silver Springs, MD 20901 (301-981-0060)

Calls for papers

Ed. Note: Calls are listed chronologically by meeting date. Listed after the meeting (in bold type) are the sponsor(s), the location, and deadline information for submittals.

JUN 4-7, 1979—National Computer Conf. (AFIPS) New York Colosseum, New York, NY **Deadline Info:** 150-word abs. to Dr. Richard E. Merwin, Box 32222, Washington, DC 20007

Pen and Podium

Recent RCA technical papers and presentations

To obtain copies of papers, check your library or contact the author or his divisional Technical Publications Administrator (listed on back cover) for a reprint. For additional assistance in locating RCA technical literature, contact RCA Technical Communications, Bldg. 204-2, Cherry Hill, N.J., extension 4256.

Advanced Technology Laboratories

J.E. Saultz|S.E. Ozga
W.A. Helbit|A. Feller

SOS technology for real-time signal processor—SPIE's 22nd Annual Tech. Symp.

H.W. Kaiser|J.I. Pridgen|L.J. Palkuti

Ultra-high upset megarad-hard Si-gate CMOS/SOS code generator—1978 IEEE Annual Conf. on Nuclear and Space Radiation Effects

Automated Systems

L. Arlan

Investigation of fast scan performance of SIT camera tube—Range Commanders Council, Edwards AFB (9/78)

G.T. Burton

ESSWACS—electronic solid state wide angle camera systems—Electro-Optical Systems Design Conf., Boston, MA (9/78)

Government

Communications Systems

L. Ferber

Recent advances in magnetic tape recording—Acoustical Soc. of America, Philadelphia, PA (5/16/78)

Laboratories

K. Ametani

Compositional analysis of single crystals of flux-grown magnetic garnets by atomic absorption spectrophotometry—*Talanta*, Vol. 25, pp. 317-323

A.E. Bell|F.W. Spong

Antireflection structures for optical recording—*IEEE J. Quantum Electronics*, Vol. QE-14, No. 7 (7/78)

W.J. Burke|M. Ettenberg|H. Kressel

Optical feedback effects in cw injection lasers—*Applied Optics*, Vol. 17 (7/15/78) p. 2233

W.H. Fonger|C.W. Struck

Unified model of energy transfer for arbitrary Franck-Condon offset and temperature—*J. Luminescence*, Vol. 17 (1978) pp. 241-261

W.E. Ham

Yield-area analysis: Part 1—a diagnostic tool for fundamental integrated-circuit process problems—*RCA Review*, Vol. 39 (6/78)

K.G. Hernqvist

Effects of glass electrolysis on electrical breakdown in high vacuum—25th Int. Field Emission Symp., Albuquerque, NM (9/17-22/78)

K.G. Hernqvist

The hydrogen dissociator—*IEEE Trans. on Plasma Sci.*, Vol. PS-6, No. 3 (1978), pp. 238-243

K.G. Hernqvist

Improved mercury arc lamps—*Proc. IEEE*, Vol. 66, No. 9 (1978) pp. 1098-1099

S.A. Keneman|J. Bordogna|J.N. Zemel

Evaporated films of arsenic trisulfide: physical model of effects of light exposure and heat cycling—*J. Appl. Phys.* Vol. 49, No. 9 (9/78)

W. Kern

Chemical etching of silicon, germanium, gallium arsenide, and gallium phosphide—*RCA Review*, Vol. 39 (6/78)

P. Kuczer|H.O. Hook|A.M. Goodman

A versatile high-voltage bias supply for extended range MIS C(V) and G(V) measurements—*RCA Review*, Vol. 39 (6/78)

D. Meyerhofer

Characteristics of resist films produced by spinning—*J. Appl. Phys.*, Vol. 49, No. 7 (7/78)

H.W. Lehmann|R. Widmer

Profile control by reactive sputter etching—*J. Vac. Sci. Technol.*, Vol. 15, No. 2 (3-4/78)

C.J. Nuese

Advance in heterojunction lasers for fiber optics applications—*SPIE*, Vol. 139, *Guided Wave Optical Systems and Devices* (1978)

G.H. Olsen|A.V. Cafiero

Single-crystal growth of mixed (La, Eu, Y, Ce, Ba, Cs) hexaborides for thermionic emission—*J. Crystal Growth*, Vol. 44 (1978) pp. 287-290

D. Redfield

Cost criterion for low efficiency solar cells to make system power cost competitive with that of high efficiency cells—*Proc. 13th Photovoltaic Specialists Conf.*, Washington DC (6/5-8/78)

D. Redfield

Theory and applications for optimization of every part of a photovoltaic system—*Solar Energy*, Vol. 21, pp. 107-112

A. Rosen|G.A. Swartz

F.C. Duigon|A.M. Gombár

Simple method of fabricating and passivating high power pin diodes—*J. Electrochemical Soc.*, Vol. 125, No. 4 (4/78)

O.H. Schade, Jr.

Advances in BiMOS integrated circuits—*RCA Review* Vol. 39, No. 2 (6/78)

M.L. Tarnig

Carrier transport in oxygen-rich polycrystalline-silicon films—*J. Appl. Phys.*, Vol. 49, No. 7 (7/78)

E.K. Sichel|J.I. Gittleman|B. Abeles

Optical properties of granular magnesium films—*Thin Solid Films*, Vol. 51 (1978) pp. 89-92

R. Widmer

Simple water-sensitive detector (emergency switch)—*J. Vac. Sci. Technol.*, Vol. 15, No. 3 (5-6/78)

C.E. Weitzel

CMOS/SIS—using selective SF₆ etching of (1102) sapphire—*IEEE Trans. Electron Devices*, Vol. ED-25, No. 8 (8/78)

Missile and Surface Radar

D.F. Bowman

A frequency scanned subarray for a radar phased array—*Proc. EASCON '78*, Washington, DC (9/24-27/78)

P.N. Bronecke|J. Darby

Test procedures for high yield, high reliability electronic assemblies utilizing hermetic chip carriers—Ninth Annual NEPCON Central '78, Rosemont, IL (9/26-28/78)

J.H. Chisholm|S.I. Newburg|R. Greene

Analysis of objects associated with COSMOS 921, 956, and 972—Tenth Annual NORAD Spacecraft Identification Conf., Colorado Springs, CO (8/1-3/78)

B.A. Francis

Motion determination of Skylab using wide-band imaging—Tenth Annual NORAD Spacecraft Identification Conf., Colorado Springs, CO (8/1-3/78)

K.F. Kinnard|D.J. Dempsey|R.D. Mitchell

Laser ranging and tracking—*Proc. Tenth Annual Electro-Optics Conf. and Exposition*, Boston, MA (9/19-21/78)

R.L. Schelhorn

Attaching leadless hermetic packages to printed wiring boards with the capability of withstanding severe thermal shock environments—Ninth Annual NEPCON Central '78, Rosemont, IL (9/26-28/78)

L. Weinberg|A. Ruvin

Digital multiple beamforming techniques for radar—*Proc. EASCON '78*, Washington, DC (9/24-27/78)

Patents

Advanced Technology Laboratories

C.W. Reno|D.G. Herzog
On-axis film scanner with reflected illumination—4105926

Astro-Electronics

W.L. Cable|D.S. Binge|R.F. Korosec
Adjustment device—4108407

E.R. Ganssle|R.J. Williams|R.R. Scott
Mounting structure—4116263 (Assigned to U.S. Government)

L. Muhlfelder|R.B. Hogan
Magnetic torquing system for changing the spin rate of an orbiting satellite—4114841 (Assigned to U.S. Government)

Automated Systems

B.R. Clay|D.A. Gore
Deflection-type modulator of laser beam for communications—4105915

B.R. Clay|G.T. Gurton
Double modulation holographic recording technique—4116526

Avionics Systems

C.A. Clark, Jr.|K.C. Adam
Clamping circuit—4109166

K. Katagi
Polar to rectangular coordinate converter—4106021

Broadcast Systems

R.A. Dischert|J.M. Walter
Clock generator for video signal processing—4110785

Consumer Electronics

W.W. Evans
Lockup inhibiting arrangement for a phase locked loop tuning system—4110693

R.P. Parker
Combined blacking level and kinescope bias clamp for a television signal processing system—4110787

R.L. Shanley, II
Set-up arrangement for a color television receiver—4118729

J.L. Smith
Static convergence device including magnetic corrector apparatus—4117433

D.H. Willis
Inrush current start-up circuit for a television receiver including a start-up decoupling circuit—4112365

D.H. Willis
High voltage protection circuit having predictable firing point—4114072

Distributor and Special Products Div.

J.D. Callaghan
Rotator with remote indicator and self-synchronization—4109191

Government Communications Systems

H.H. Chapman, Jr.
Electronic mail box—4106060

A.T. Crowley
Pulse wave phase and frequency detector—4105947

G.W. Hunka
Optical cursor tracking correction system—4114034 (Assigned to U.S. Government)

G. Katz
Method of assembling components on printed circuit boards—4113524

Edward J. Nossen
Frequency synthesizer—4114110 (Assigned to U.S. Government)

M. Packer
Organic welding flux composition—4115157

Government Systems Division Staff

W.G. Anderson
Quiescent biasing of R-F power transistors for other than class A operation—4105944

Laboratories

A. Bloom|L.K. Hung
Liquid crystalline 4-cyano-or 4-nitro-bensylidene-4' (N,N-dialkylamino)-1-aminoazabenzene dyes—4105654

D.E. Carlson|C.R. Wronski
Amorphous silicon photovoltaic device having an insulating layer—4117506

J.A. Castellano|M.T. McCaffrey
Liquid crystal cell—4108793

C.A. Catanese|S.A. Keneman|J.G. Endriz
Electron multiplier with switchable beam confinement structure—4109178

C.A. Catanese|N.L. Lindburg
J.B. Harrison, Jr.
Electron multiplier with high energy electron filter—4115719

D.J. Channin
Matrix address system using erase operation—4109242

L.S. Cosentino|G.F. Stockdale
J.G. Endriz
Electrical connection between conductors on spaced plates—4109299

W.R. Curtice
Triggered burst generator—4114051 (Assigned to U.S. Government)

R.V. D'Aiello
Photovoltaic device having an extended pn junction—4112457

W. Denhollander
Transformer arrangement for synchronous-ly switched vertical deflection system—4117380

R. Destephanis
Record support and alignment apparatus for a video disc player—4113262

A.G. Dingwall
Voltage controlled oscillator (VCO) employing nested oscillating loops—4105950

J.G. Endriz
Electron beam oscillation compensation method—4115724

M.T. Gale|J. Kane
Fabrication of diffractive subtractive filter embossing master—4108660

R.A. Geshner|J. Mitchell, Jr.
Method for removing defects from chromium and chromium oxide photo-masks—4105468

J. Goel|I. Drukier|S.Y. Narayan
Method of making a submicrometer aperture in a substrate—4117301

A.M. Goodman
MIS readout device with dielectric storage medium—4106107

J.G. Henderson|C.M. Wine
Phase locked loop television tuning system—4106059

G.B. Herzog
Position encoder employing charge transfer circuit—4114035

W. Hinn
Video amplifier with suppressed radio frequency radiation—4118731

M.D. Holbrook|R.P. Fillmore
Voltage multiplier circuit—4106086

R.J. Hollingsworth
Unbalanced sense circuit—4114055

R.S. Hopkins, Jr. |A.J. Banks
R.A. Dischert
Memory read/write organization for a television signal processor—4109276

E.A. James|P. Kuznetsov
Method of depositing or repairing a patterned metal layer on a substrate—4107351

H.C. Johnson
FM-CW radar ranging system—4106020

G.S. Kaplan
Digitally processed radar speed sensor—4107680

G.S. Kaplan
Clutter free communications radar—4109247

E.O. Keizer
Method for forming keel-tipped stylus for video disc system—4104832

T.F. Lenihan
Single wire transmission of multiple switch operations—4118700

A.W. Levine|G. Kaganowicz|P. Datta
Electro-optic devices—4105298

J.J. Risko|L.S. Napoli
Amplitude modulated impatt diode oscillator and a low cost communication system using same—4118598

J.D. Levine
Device having thermionic cathode heated by field-emitted electrons—4115720

S.G. Liu
Fast-switching pulse modulation—4115708

F.J. Marlowe|C.H. Anderson
Modular type guided beam flat display device—4117368

N.F. Maxemchuk
Digital sampling rate conversion of color tv signal—4106053

N.F. Maxemchuk
Error detection and correction—4110735

R.W. Nosker
Smooth groove formation method employing spin coating of negative replica of inscribed disc—4113897

G.H. Olsen|C.J. Buiocchi
T.J. Zamerowski
Vapor phase growth technique of III-V compounds utilizing a preheating step—4116733

J.I. Pankove
Amorphous-silicon—amorphous-silicon-carbide photovoltaic device—4109271

J.I. Pankove|M.A. Lampert
Method of passivating a semiconductor device by treatment with atomic hydrogen—4113514

J.I. Pankove|F.J. Marlowe
Solid state oscilloscope—4114095

S. Ponczak|J.A. Olmstead
Method of forming a curved implanted region in a semiconductor body—4113516

R.M. Rast
Frequency counter for a television tuning system—4109283

J.J. Risko
Method for making Schottky barrier diodes—4110488

A. Rosen|E. Mykietyn
Electronically tunable microwave frequency FET discrimination—4110700 (Assigned to U.S. Government)

E.K. Sichel
Electrochromic cermet material and device including the same—4110259 (Assigned to U.S. Government)

R.G. Stewart|S.S. Eaton, Jr.
Sense circuit employing complementary field effect transistors—4107556

H.J. Wolkstein
Frequency synthesizer with rapidly changeable frequency—4105948

Missile and Surface Radar

E. Jellinek
System for automatic vehicle location—4107689

V. Stachijko
Amplitude balanced diode phase shifter—4105959 (Assigned to U.S. Government)

Mobile Communications

B.M. Pradal
Audio signal processor—4110692

Picture Tube Division

R.J. D'Amato
Process of fabricating a cathode ray tube—4112562

R.H. Godfrey|A.M. Morrell
Cathode-ray tube having apertured mask—4109177

RCA Ltd., Canada

C.M. Kudsia|H.J. Moody|L.A. Keyes
Traffic switching in communications satellites—4109202

RCA Service Co.

E.L. Crosby, Jr.
Variable lift inflatable airfoil for tethered balloons—4102519 (Assigned to U.S. Government)

SelectaVision Project

J.G. Amery|T.W. Burrus
Noise reduction apparatus—4110784

C.A. Elliott|L.D. Huff
Package actuated record extracting mechanism for a video disc player—4109919

Solid State Division

A.A. Ahmed
Ground fault detecting apparatus including current-responsive threshold detection circuitry—4114089

A.A. Ahmed
Switchable current amplifiers—4117417

O.H. Bismarck
Pulse staggering circuit—4109209

R.R. Brooks
GTO ignition circuit—4109632

J.J. Chinery
Method of testing semiconductor devices—4114096

W.F. Dietz
North-south pincushion distortion correction circuit—4118656

R.D. Faulkner
Electron discharge tube having a cup-shaped secondary electron emissive electrode—4112325

R.D. Faulkner
Non-uniform dynode mesh for an electron discharge tube—4112326

N.F. Gubitose|R.A. James
Machine for straightening the wire leads of a device—4106532

M.V. Hoover

Bridge amplifiers employing complementary transistors—4117415

L.A. Jacobus, Jr.

Method of making an insulated gate field effect transistor by implanted double counterdoping—4108686

M.A. Kalfus|D.M. Baugher

Transistor switching circuit—4117351

M.A. Kalfus

Circuit for single-line control of GTO controlled rectifier conduction—4115707

M.A. Kalfus|H.W. Becke

Switching circuit—4117350

H. Khajezadeh

Integrated circuit protection device comprising diode having large contact area in shunt with protected bipolar transistor—4106048

A.J. Leidich

Monostable circuit—4105901

O.H. Schade, Jr.

Current mirror amplifiers with programmable current gains—4117416

R.C. Shambelan|C.W. Lindsley

Machine for changing the spacing of a plurality of wafers—4108323

S. Shwartzman|A. Mayer

Transducer assembly for megasonic cleaning—4118649

Geverd new editor of *RCA Engineer*



Mike Geverd is now Editor of the *RCA Engineer*, and also Administrator, Technical Communication Programs. He succeeds John Phillips, who is now Manager, Proposals and Publicity, at GSD's Automated Systems activity in Burlington.

Mr. Geverd began his more than 20-year-long career in printed communications with the RCA Service Company and Astro Electronics as a technical writer. He then served as Editor of TREND before joining Sperry Univac and Philco Ford, where he managed several technical publications programs.

Most recently he was president of Brian Advertising, an agency specializing in advertising and press relations for technical and industrial clients.

Mausler is new EdRep at NBC



Robert Mausler has been appointed an Editorial Representative for the National Broadcasting Company in New York City. He is a Senior Engineer, Technical Development, responsible for evaluating new broadcast-related equipment, and for liaison with industry and other broadcasters.

Bob has published a number of papers in the *RCA Engineer*, and currently represents NBC on various SMPTE, IEEE, EIA, and Television Academy committees.

As EdRep, Bob will assist other NBC engineers in preparing papers for the *RCA Engineer* and will keep the *Engineer* informed of new developments, professional activities, awards, publications, and promotions in his area.

Promotions

Alascom

G. Bartley, from Senior Engineer to Manager, Configuration Management.

Astro-Electronics

R. Ciuna, from Engineer to Manager, Specialty Engineering.

R. Kallan, from Project Engineer to Manager, Equipment Engineering for NOVA Program.

R. Mancuso, from Engineer to Manager, Thermal Engineering.

M. Markulec, from Engineer to Manager, Equipment Engineering for Defense Meteorological Satellite Program.

T. Murphy, from Senior Engineer to Manager, Specialty Engineering.

Missile and Surface Radar

W. Mulqueen, from Senior Member, Engineering Staff, to Unit Manager, Design & Development.

W. Beckett, from Senior Member, Engineering Staff to Unit Manager, Engineering Systems Project.

Engineering News and Highlights

Bill Howard, NBC EdRep, retires



Bill Howard, an engineer with NBC for 32 years, retires in November.

He joined RCA-NBC Labs in 1946, working on the development of live and film television camera chains. He then put WNBK-TV, Cleveland, on the air in late 1948. Bill held a number of technical-supervision positions at NBC stations before returning to the NBC Engineering Development Group in 1960.

Bill's contributions to the *Engineer* have been numerous—he was an EdRep for 17 years, more than two-thirds of the *Engineer's* existence. When NBC celebrated its fiftieth anniversary, Bill collected technical history and many interesting photographs of the early days of radio and tv at NBC and created a well-received two-part article "NBC Engineering—a fifty-year history" (Jun|Jul and Aug|Sep 1977).

C. Falcon, from Senior Member, Engineering Staff to Unit Manager, Engineering Systems Project.

G. Lonkevich, from Senior Member, Engineering Staff to Unit Manager, Engineering Systems Project.

R. Sharp, from Senior Member, Engineering Staff to Unit Manager, Engineering Systems Project.

J. Jarsma, from Senior Member, Engineering Staff to Unit Manager, Engineering Systems Project.

E. Butterfoss, from Principal Member,

Engineering Staff to Unit Manager, Engineering Systems Project.

A. Conn, from Senior Member, Engineering Staff to Unit Manager, Engineering Systems Project.

R. Becker, from Unit Manager, ESP to Manager, Configuration Management.

J. Cole, from Unit Manager, ESP to Manager, Test Operations.

J. Frattura, from Senior Member, Engineering Staff to Unit Manager, ESP.

E. Hathaway, from Unit Manager, ESP to Manager, ORTS Project.

R. Kooperstein, from Senior Member, Engineering Staff to Unit Manager, ESP.

A. Kornbluth, from Unit Manager, ESP to Manager, Combat Systems Configuration.

L. Troutman, from Senior Member, Engineering Staff to Unit Manager, Systems.

R. Van Olst, from Principal Member, Engineering Staff to Unit Manager, ESP.

F. Wuebker, from Unit Manager, ESP to Manager, Integration Projects.

Solid State Division

R. Dawson, from Leader, Technical Staff (Solid State Technology Center) to Manager, New Technology Applications Research (RCA Laboratories, Somerville).

G. Deneky, from Associate Member, Technical Staff to Leader, Technical Staff.

L. Rosenberg, from Leader, Technical Staff to Manager, Design Automation of LSI Systems and Design Laboratory.

E. Schnable, from Member, Technical Staff to Leader, Technical Staff.

F. Thomas, from Member, Technical Staff to Leader, Technical Staff.

H. Wittlinger, from Senior Member, Technical Staff to Leader, Technical Staff in IC Applications Engineering and Test Group.

Government Engineering

G. Claffie, from Unit Manager to Manager, Marketing Development, Advanced Technology Laboratory Marketing.

A. Stromback, from Senior Member, Engineering Staff to Unit Manager, Microsystem Equipment Design.

Picture Tube Division

M. Adams, from Member, Technical Staff to Engineering Leader—Equipment Development.

Advanced Technology Laboratory

A.D. Stromback, from Senior Member, Engineering Staff to Unit Manager, Microsystem Equipment Design.

Laboratories

Robert Geshner, from Senior Member, Technical Staff to Leader, Photomask Operations, Solid State Technology Center.

Professional Activities

Sheby Named Meeting Co-Chairman

Dr. David Sheby of Government Communications Systems Engineering will be a co-chairman at the Society of Photo-Optical Instrumentation Engineers' Technical Symposium East scheduled for April 1979. Dr. Sheby's specific area of interest is Smart Sensors.

Hittinger is life trustee

William C. Hittinger, Executive Vice President, Research and Engineering, has been elected a life corporate member of the Lehigh University board of trustees. He had been an alumnus trustee since 1972.

Richter an IEEE reviewer

Ed Richter, Automated Systems, was recently appointed a reviewer for microwave papers submitted for publication in the *IEEE Transactions on Instruments and Measurements*.

Licensed engineers

When you receive a professional license, send your name, PE number (and state in which registered), RCA division, location, and telephone number to *RCA Engineer*, Bldg. 204-2, RCA, Cherry Hill, N.J. New listings (and corrections or changes to previous listings) will be published in each issue.

Missile and Surface Radar

Caplan, L.A., Moorestown; CA-QU-4393
Corn, J.D., Moorestown; PA-027570-E

technical excellence



Barthel



Berkowitz



Cohen



Corn



Cox



Detoro



Gross



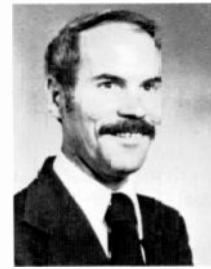
Kalata



Kramarenko



Lonkevich



Paterson



Sartell



Schelhorn



Shaw



Smith



Thomson (l)
Urkowitz (r)



Moorestown lists first- and second-quarter TE Award winners

A total of seventeen Technical Excellence Awards were presented to Missile and Surface Radar personnel during the first six months of 1978. The award winners and a brief summary of each citation are given below.

Daniel L. Barthel—for innovative application of advanced software design techniques to achieve design goals and schedule deadlines for the AEGIS ORTS Data Base Generator Program.

Harold Berkowitz—for development of a self-contained, packaged Cooling Water Unit (CWU) for demineralized water cooling of transmitters and associated electronics in Navy ships.

Albert Cohen—for his outstanding contributions to the successful integration and checkout of the AN/TPQ-27 functional computer program.

Joseph D. Corn—for successful modification of the basic 250-kW, X-band Nike Hercules transmitter to provide 500-kW capability for the NIDIR Program.

Herbert C. Cox—for significant enhancement of the AEGIS dynamic simulator (SPECTRM) capabilities through addition of ECM environment modeling.

Melvin T. Detoro—for his technical leadership, commitment, and personal drive that resulted in integration of the AN/SPY-1A radar equipment units into an operational system in record time.

Samuel D. Gross—for his outstanding systems engineering concepts, analysis, and technical leadership on the COBRA JUDY Program.

Paul R. Kalata—for his critical analysis of radar tracking and missile guidance filters that led to a consolidated AEGIS/SM-2 control filter system with improved stability and more favorable transient response in several operational scenarios.

Peter Kramarenko—for his practical, carefully implemented approach in developing the Element Test Function (ETF) concept and associated computer program definition for the AN/SPY-1A radar.

George T. Lonkevich—for special contributions to the design and implementation of the real-time skeleton portion of the AEGIS Interface Simulator System (ISS) to support AN/SPY-1A computer program testing.

William J. Paterson—for innovations in the computer/software system design for COBRA JUDY Contract Definition.

Telford B. Sartell—for his outstanding technical achievement in the adaptation and use of the AEGIS Tactical Executive System (ATES) in the development of the Interface Simulator System (ISS).

Robert L. Schelhorn—for technical contributions to microelectronics technology and packaging that have elevated RCA to a

preeminent position in leadless-carrier packaging, copper-based metallization systems, and porcelainized-metal substrates.

Douglas R. Shaw—for design, development, factory-follow, and test of the Signal Processor Logic Unit (SPLU) and the MTI and Sweep Integrator, all for the HR-76 Fire Control Radar.

Edward J. Smith—for technical leadership in formulating, developing, and coordinating the electrical-cable interconnection requirements for the CSED Site, the first AEGIS destroyer, and the first AEGIS cruiser.

Don Thomson—for outstanding work during integration, acceptance testing, and sell-off of the first HR-76 Fire Control Radar System.

Harry Urkowitz—for outstanding performance, technical leadership, and enhancement of RCA's capability and reputation in a highly specialized data-processing application.

Kaplan cited for work on Distributed Data Network

Don Kaplan, center, has received the Government Communications Systems' Technical Excellence Award for his work on the basic hardware design of a Distributed Data Network. The network, which is the common interconnection point for a large-scale computer communications system, represents a significant advance in the state of the art for this technology. Pictured with Don are **J.B. Howe** (left), Chief Engineer; and **Joseph Springer**, Unit Manager.



July Technical Excellence Award Goes to Signal Distribution Network Team

NMIC Development and Support Program Team Gains Technical Excellence Award



Automated Systems' Technical Excellence Award for July went to the Signal Distribution Network Team. The team was cited for their performance in developing and delivering the hardware and software that comprise the Government's Signal Distribution Network. Pictured from left to right are: **Harry J. Woll**, Div. VP and General Manager; **Al Dirsra**, Manager Design Engineering; team members **Bill Clark**, **Manny Tashman**, **Leo Kaye**, **Stu Warren**, and **Nick Meliones**; **Tony Amato**, Manager Product Engineering; **Walt Wadden**, Manager Systems Analysis and Projects; and **Gene Stockton**, Chief Engineer.

Superior performance by the NMIC (National Military Information Center) Development and Support Program Team earned RCA a special citation from the Defense Intelligence Agency, and has earned the Team the August Technical Excellence Award from Automated Systems. Pictured from left to right are: **Harry J. Woll**, Div. VP and General Manager; team members **Ray Bitteker**, **Bob Lindley**, **Chris Kryzanowsky**, and **Skip Chaples**; **Walt Wadden**, team manager; team members **Dick Coulter, Jr.**, **Will Cleveland**, **Chuck McKusick**, and **Bob Monat**; and **Gene Stockton**, Chief Engineer.

Staff Announcements

Corporate Engineering

Donald S. McCoy has been appointed Staff Vice President, Electronic Systems Engineering, reporting to **Howard Rosenthal**, Staff Vice President, Engineering.

Laboratories

Robert H. Dawson has been appointed Manager, New Technology Applications Research, reporting to **David D. Holmes**, Director of the Television Research Laboratory.

Robert D. Lohman, Director, Display Systems Research Laboratory and **James L. Miller**, Director, Manufacturing Systems and Technology Research Laboratory, have announced the organization of the Technology Transfer Laboratory as follows: **Louis E. Potter**, Manager, Advanced Development—Manufacturing Technology; and **Franz Van Hekken**, Manager, Advanced Development—Electron Guns.

James L. Miller, Director Manufacturing Systems and Technology Research Laboratory, has announced the organization of Manufacturing Systems and Technology Research Laboratory as follows: **David P. Bortfeld**, Head, Manufacturing Systems and Process Control; **Luke Dillon, Jr.**, Head, Manufacturing Test and Control Systems; **Istvan Gorog**, Head, Manufacturing Research; **Karl G. Hernqvist**,

Fellow, Technical Staff; **Marvin A. Leedom**, Head, Mechanical and Instrumentation Technology; **William G. McGuffin**, Manager, Instrumentation; and **D. Alex Ross**, Staff Engineer.

Brown F. Williams, Director, Energy Systems Research Laboratory, has announced the organization of the Energy Systems Research Laboratory as follows: **David E. Carlson**, Head, Photovoltaic Device Research; **Richard Williams**, Fellow, Technical Staff; **Arthur H. Firester**, Head, Process and Applications Research; **Bernard Hershenov**, Head, Energy Systems Analysis; **David Richman**, Head, Semiconductor Materials Research; and **Joseph J. Hanak**, Fellow, Technical Staff.

Larry J. French has been appointed Director, LSI Systems and Design Laboratory, reporting to **Gerald B. Herzog**, Staff Vice President, Technology Centers.

Larry J. French, Director, LSI Systems and Design Laboratory, has announced the organization of LSI Systems and Design Laboratory as follows:

Richard H. Bergman, Manager, LSI Design and Photomask; **Larry J. French**, Acting, LSI Systems; **John W. Gaylord**, Manager, Process Monitoring and Control, and **Lawrence M. Rosenberg**, Manager, Design Automation.

David D. Holmes, Director, Television Research Laboratory, has announced the

organization of the Television Research Laboratory as follows: **Robert H. Dawson**, Manager, New Technology Applications Research; **David D. Holmes**, Acting, Signal Processing Research, and Acting, Electronic Packaging Research; **Stanley P. Knight**, Head, Signal Conversion Systems Research; and **Werner F. Wedam**, Head, TV Receiver Systems Research. Messrs. Dawson, Knight and Wedam will report to the Director, Television Research Laboratory.

Alfred H. Teger has been appointed Director, Advanced Systems Research Laboratory, reporting to **Nathan L. Gordon**, Staff Vice President, Systems Research.

Alfred H. Teger, Director, Advanced Systems Research Laboratory, has announced the organization of the Advanced Systems Research Laboratory as follows: **Allen J. Korenjak**, Head, Automation Systems Research; **Thomas M. Stiller**, Fellow, Technical Staff; **Eduard Luedicke**, Staff Scientist; **Richard H. Roth**, Head, System Architecture Research; **Allen H. Simon**, Fellow, Technical Staff; **Paul M. Russo**, Head, Microsystems Research; and **Charles M. Wine**, Fellow Technical Staff.

Daniel A. Walters has been appointed Director, Communication Systems Research Laboratory, reporting to **Kerns H. Powers**, Staff Vice President, Communications Research.

Daniel A. Walters, Director, Communications Systems Research Laboratory,

has announced the organization of Communication Systems Research Laboratory as follows: **Marvin Blecker**, Head, Systems Analysis Research; **Emilie M. Lengel**, Manager, Automation and Computing Services; **Leonard Schiff**, Head, Communication Analysis Research; and **Harold Staras**, Staff Scientist, Satellite Programs.

Bernard J. Lechner, Director, Video Systems Research Laboratory, has announced the organization of the Video Systems Research Laboratory as follows: **Jon K. Clemens**, Head, Signal Systems Research; **James J. Gibson**, Fellow, Technical Staff; **Eugene O. Keizer**, Head, Video Recording Research; **Charles B. Oakley**, Head, Broadcast Systems Research; **Robert E. Flory**, Fellow, Technical Staff, and **J. Guy Woodward**, Fellow, Technical Staff.

Robert D. Hohman, Director, Display Systems Research Laboratory, has announced the organization of the Display Systems Research Laboratory as follows: **Charles H. Anderson**, Head, Applied Mathematical and Physical Sciences; **Roger L. Crane**, Fellow, Technical Staff; **Ralph W. Klopfenstein**, Fellow, Technical Staff; **John A. van Raalte**, Head, Displays and Device Concepts Research; **Peter J. Wojtowicz**, Head, Electron Optics and Deflection

Research; **P. Niel Yocom**, Head, Display Materials and Processes Research, and **Simon Larach**, Fellow, Technical Staff.

Richard E. Quinn, Staff Vice President, Administration, Princeton, N.J., announced the appointment of **John L. Vossen, Jr.**, as Manager, Thin Film Technology.

Leonard H. Gibbons, Jr. has been appointed Manager, Reliability Engineering Laboratory, reporting to **Robert M. Cohen**, Director, Quality and Reliability Assurance.

John Kucker has been appointed Manager, Palm Beach Gardens Operations, reporting to **John E. Schaefer**, Manager, Domestic Integrated Circuit Manufacturing.

Solid State Division

Ben A. Jacoby, Division Vice President, Systems, Services and Strategic Planning has announced the Systems, Services and Strategic Planning organization as follows: **Anthony J. Bianculli**, Administrator, Strategic Planning; **Fred G. Block**, Manager, Central Engineering and Acting Manager, Engineering Standards; **Lloyd O. Brown**, Administrator, Industry Research; **Thomas L. Cambria**, Director, Management Information Systems; **Robert M. Lenz**, Administrator, Industry Statistics; **Parker T. Valentine**, Manager, Operations Support;

and **John D. Watkins**, Manager, Solid State Materials.

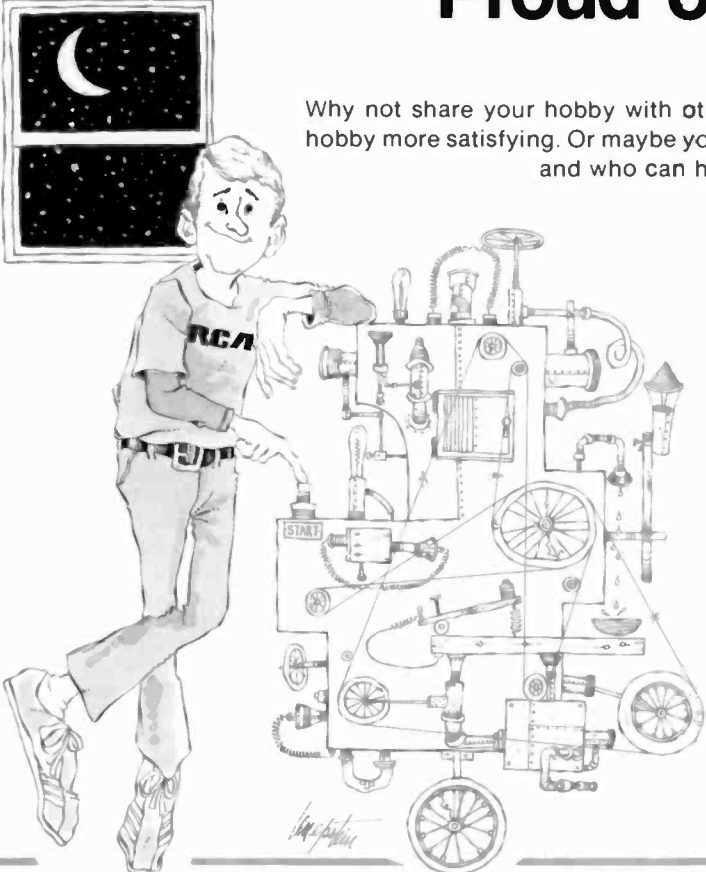
John E. Schaefer has been appointed Director, Government and HiReliability IC Products, reporting to **Carl R. Turner**, Division Vice President, Integrated Circuits.

Richard L. Sanquini, Director, IC Products, has appointed **Richard W. Ahrons**, Manager, Memory and Microprocessor Product Marketing and Support Engineering. His organization is announced as follows: **Michael V. D'Agostino**, Manager, Memory and Microprocessor Product Marketing; **Edwin M. Fulcher**, Leader, Technical Staff—Memory and Microprocessor Systems Development; **Al A. Key**, Leader, Technical Staff—Memory and Microprocessor Applications Engineering, and **Larry A. Solomon**, Leader, Technical Staff—Memory and Microprocessor Software.

Patent Operations

John V. Regan, Vice President, Patent Operations, has announced the following appointments in the Patent Operations organization: **Albert Russinoff**, Staff Vice President, Inter Parties Patent Matters; **Eugene M. Whitacre**, Staff Vice President, Patents—Consumer and Broadcast Equipments, and **Sharon K. Stepno**, Manager, Washington Patent Office.

Proud of your hobby?



Why not share your hobby with others? Perhaps their interest will make your hobby more satisfying. Or maybe you'll find others who already share your hobby and who can help make your own efforts more rewarding.

The *RCA Engineer* likes to give credit to engineers who use their technical knowledge away from the job. We've published articles about subjects as diverse as a satellite weather station, model aircraft and railroading, solar heating, and an electronic fish finder.

For more information on how you can participate in this feature of the *RCA Engineer*, call your local EdRep (listed on the inside back cover of the *Engineer*) or contact Frank Strobl (222-4220) or Bill Lauffer (222-4255) at the *RCA Engineer*.

Editorial Representatives

Contact your Editorial Representative, at the extensions listed here, to schedule technical papers and announce your professional activities.

Commercial Communications Systems Division

Broadcast Systems

BILL SEPICH* Camden, N.J. Ext. 2156
KRISHNA PRABA Gibbsboro, N.J. Ext. 3605
ANDREW BILLIE Meadow Lands, Pa. Ext. 6231

Mobile Communications Systems

KARL NEUMANN* Meadow Lands, Pa. Ext. 6444

Avionics Systems

STEWART METCHETTE* Van Nuys, Cal. Ext. 3806
JOHN McDONOUGH Van Nuys, Cal. Ext. 3353

Cablevision Systems

JOHN OVNICK* N. Hollywood, Cal. Ext. 241

Government Systems Division

Astro-Electronics

ED GOLDBERG* Hightstown, N.J. Ext. 2544

Automated Systems

KEN PALM* Burlington, Mass. Ext. 3797
AL SKAVICUS Burlington, Mass. Ext. 2582
LARRY SMITH Burlington, Mass. Ext. 2010

Government Communications Systems

DAN TANNENBAUM* Camden, N.J. Ext. 3081
HARRY KETCHAM Camden, N.J. Ext. 3913

Government Engineering

MERLE PIETZ* Camden, N.J. Ext. 2161

Missile and Surface Radar

DON HIGGS* Moorestown, N.J. Ext. 2836
JACK FRIEDMAN Moorestown, N.J. Ext. 2112

Solid State Division

JOHN SCHOEN* Somerville, N.J. Ext. 6467

Power Devices

HAROLD RONAN Mountaintop, Pa. Ext. 633-827
SY SILVERSTEIN Somerville, N.J. Ext. 6168

Integrated Circuits

FRED FOERSTER Somerville, N.J. Ext. 7452
JOHN YOUNG Findlay, Ohio Ext. 307

Electro-Optics and Devices

RALPH ENGSTROM Lancaster, Pa. Ext. 2503

Consumer Electronics

CLYDE HOYT* Indianapolis, Ind. Ext. 5208
FRANCIS HOLT Indianapolis, Ind. Ext. 5217
PAUL CROOKSHANKS Indianapolis, Ind. Ext. 5080
STEVE RACE Indianapolis, Ind. Ext. 5636
DON WILLIS Indianapolis, Ind. Ext. 5883

SelectaVision Project

ROBERT MOORE Indianapolis, Ind. Ext. 3313

RCA Service Company

JOE STEOGER* Cherry Hill, N.J. Ext. 5547
RAY MacWILLIAMS Cherry Hill, N.J. Ext. 5986
DICK DOMBROSKY Cherry Hill, N.J. Ext. 4414

Distributor and Special Products Division

CHARLES REARICK* Deptford, N.J. Ext. 2513

Picture Tube Division

ED MADENFORD* Lancaster, Pa. Ext. 3657
NICK MEENA Circleville, Ohio Ext. 228
JACK NUBANI Scranton, Pa. Ext. 499
J.R. REECE Marion, Ind. Ext. 5566

Alascom

PETE WEST* Anchorage, Alaska Ext. 7607

Americom

MURRAY ROSENTHAL* Kingsbridge Campus, N.J. Ext. 4363

Globcom

WALT LEIS* New York, N.Y. Ext. 3655

RCA Records

JOSEPH WELLS* Indianapolis, Ind. Ext. 6146

NBC

BOB MAUSLER* New York, N.Y. Ext. 3589

Patent Operations

JOSEPH TRIPOLI Princeton, N.J. Ext. 2992

Research and Engineering

Corporate Engineering

HANS JENNY* Cherry Hill, N.J. Ext. 4251

Laboratories

MAUCIE MILLER Princeton, N.J. Ext. 2322
LESLIE ADAMS Somerville, N.J. Ext. 7357

*Technical Publications Administrator, responsible for review and approval of papers and presentations.

RCA Engineer

A technical journal published by
Corporate Technical Communications
"by and for the RCA engineer"

Printed In USA

Form No RE-24-3

